

PHENOTYPIC CHARACTERIZATION OF ALLELIC VARIANTS OF THE
MECHANISTIC TARGET OF RAPAMYCIN (mTOR)

By

Joy Gary

A DISSERTATION

Submitted to
Michigan State University
in partial fulfillment of the requirements
for the degree of

Pathobiology - Doctor of Philosophy

2015

ABSTRACT

PHENOTYPIC CHARACTERIZATION OF ALLELIC VARIANTS OF THE MECHANISTIC TARGET OF RAPAMYCIN (mTOR)

By

Joy Gary

mTOR is a serine/threonine kinase at the hub of multiple signaling pathways, with roles in proliferation, translation, and growth. The PI3K/AKT/mTOR pathway is frequently hyperactivated in cancers and can be targeted pharmacologically. To better understand the role of mTOR in cancer treatment and in response to cell stressors, mouse models of decreased mTOR and of a single nucleotide polymorphism (SNP) in *Mtor* were evaluated. Specifically, mice with T-cell-specific, constitutively-active AKT (Lck-MyrAkt) that develop spontaneous thymic lymphomas were crossed to mice with genetically reduced mTOR expression (knock down, KD). Genetic mTOR reduction was associated with prolonged survival (24 weeks in KD mice versus 14 weeks in WT mice), though both eventually developed pre-T lymphoblastic leukemia/lymphoma (pre-T LBL). Transcriptional profiling of the murine pre-T LBL revealed that mTOR KD was associated with decreased expression of *Cdk6*, a critical proliferative control node in T-cell development and oncogenic transformation. The combination of a mTOR inhibitor (rapamycin) and a CDK4/6 inhibitor (PD-0332991, palbociclib) cooperatively decreased viability and signaling downstream of drug targets in murine thymic lymphoma cells and human T-cell acute lymphoblastic leukemia/lymphoma (T-ALL/LBL) cell lines. In addition, the role of mTOR in response to cell stressors was examined in the context of inflammatory, genotoxic, and oncogenic stress. In this study, a rare SNP in *Mtor* (C1977T, leading to the amino acid substitution R628C), found in BALB/c mice, was

linked to decreased DNA damage response (DDR) through gene expression profiling in an inflammatory environment. Mice with the SNP (628C KI) had significantly decreased survival post total body irradiation (TBI) compared to WT and heterozygous mice. Mouse embryonic fibroblasts (MEFs) and bone marrow from 628C KI mice were more sensitive to DNA damage and the DNA damage proteins FANCD2 and ATM were decreased in KI MEFs. Downstream targets of mTOR, most notably those phosphorylated by mTORC2, were also decreased in KI MEFs, especially the target PKC α . Proliferation was decreased by irradiation in WT MEFs, and was minimally affected by irradiation in KI MEFs. KI mice exposed to fractionated irradiation over several weeks developed thymic lymphomas more rapidly and had decreased survival compared to WT mice. Finally, to evaluate oncogenic stress, keratinocytes from KI mice were Ras-transformed and grafted onto nude mice, resulting in a higher rate of papilloma development than seen with keratinocytes from WT mice. The mTOR KD mouse model confirmed the importance of mTOR in T-cell leukemia/lymphoma, while the KI model highlighted the role of mTOR in response to cell stressors that put selective pressure on cancer cells. These findings emphasize the continued importance of research into therapies targeting mTOR and mTOR's role in cancer progression.

Copyright by
THE UNITED STATES GOVERNMENT
2015

This work is dedicated to the many people who supported me through the process of graduate school, including the members of the Mock laboratory, the Comparative Molecular Pathology laboratory and fellows, the Sally Rosen Kaplan Fellowship, the Pathobiology and Diagnostic Investigation Department at MSU, my loving husband, and my dear family. Thank you for your support and for believing in me.

ACKNOWLEDGEMENTS

Many thanks to the current and past members of the Mock Laboratory, the Laboratory of Cancer Biology and Genetics, and the Comparative Biomedical Scientist Training program (NCI) for support and advice, and to my graduate committee: Dr. Matti Kiupel (MSU major advisor), Dr. Beverly Mock (NCI major advisor), Dr. Joshua Webster, Dr. Vilma Yuzbasiyan-Gurkan, and Dr. Jennifer Thomas, as well as my program mentor Dr. Mark Simpson. Thanks also to our collaborator, Joseph Testa, at Fox Chase Cancer Center. Much gratitude to the many who offered suggestions and advice during experimental design and manuscript preparation, including Doug Lowy, Peter Aplan, James Mitchell, Urbain Weyemi, Andre Nussenzweig, Elsa Callen Moreu, Yves Pommier, Alexander Kovalchuk, Michelle Herrmann, Jinqi Chen, and Remy Bosselut. Also thanks to the above for their willingness to share insights, reagents, and technical expertise from their laboratories. We also thank Maudeline Etienne, Dena Tran, Zaw Phyo, Solomon Lynch, Kenneth Felsenstein, and Ben Gamache for insights and assistance with these studies. J.G. is a fellow in the NIH Comparative Biomedical Scientist Training Program supported by the National Cancer Institute in partnership with Michigan State University. This work was supported by the Intramural Research Program of the National Institutes of Health, National Cancer Institute, Center for Cancer Research. The contents of this publication do not necessarily reflect the views or policies of the Department of Health and Human Services, nor does the mention of trade names, commercial products, or organizations imply endorsement by the U.S. Government.

TABLE OF CONTENTS

LIST OF TABLES	x
LIST OF FIGURES	xi
KEY TO ABBREVIATIONS	xvi
CHAPTER 1: Introduction	1
mTOR: The signaling pathway, structure, and roles in the normal cell	1
mTOR in cancer.....	4
mTOR mutations.....	7
The BALB/c allele of mTOR is a susceptibility gene for plasmacytoma formation.....	7
Project goals	12
Hypotheses.....	13
CHAPTER 2: General Methods.....	14
Mice	14
Collection of cells and tissues	14
Flow cytometry and protein analysis	15
Genotyping	18
Microarray and RT-PCR	18
Glycolysis analysis	19
Statistical analysis	20
CHAPTER 3: Constitutive mTOR inhibition in mouse thymic pre-T LBL identifies <i>Cdk6</i> as a target for combination treatment of T-ALL/LBL.....	21
Abstract	22
Introduction	22
Methods	23
<i>Mice</i>	23
<i>Flow cytometry and protein analysis</i>	24
<i>Pre-T LBL clonality</i>	25
<i>Pre-T LBL cell culture and fluorescence in situ hybridization (FISH)</i>	26
<i>Microarray and RT-PCR</i>	26
<i>Drug treatment of murine pre-T LBL cells</i>	27
<i>Matrix dose response screen in human T-ALL/LBL cell lines</i>	27
Results.....	28
<i>Pre-tumor thymocytes from mTOR KD mice have decreased mTOR activity</i>	28
<i>Genetic and pharmacologic mTOR inhibition prolonged survival of Lck-Akt mice</i>	32

<i>CDK6 is decreased in KD thymic pre-T LBL</i>	39
<i>Murine pre-T LBL is sensitive to inhibition of mTOR and/or CDK4/6</i>	42
<i>The combination of CDK4/6 and mTOR inhibition is cooperative in human T-ALL/LBL cell lines</i>	46
Discussion	53
 CHAPTER 4: A rare, naturally occurring SNP in <i>Mtor</i> (C1977T) is associated with increased sensitivity to stress at the cellular and organismal level	57
Introduction	57
Materials and Methods	59
<i>Mice</i>	59
<i>Microarray and RT-PCR</i>	60
<i>Cell culture</i>	61
<i>Comet Assay</i>	63
<i>Immunoblotting, immunohistochemistry, and immunofluorescence</i>	63
<i>Flow cytometry and proliferation</i>	65
Results	66
<i>Characterization of 628C KI mice</i>	66
<i>Predicted effects of 628C allele</i>	67
<i>Transcriptional differences in cells exposed to inflammatory stress</i>	68
<i>Phenotypic changes associated with DNA damage</i>	72
<i>Assessing DNA damage by Comet Assay in bone marrow treated ex vivo</i>	75
<i>Assessing DNA damage by Comet Assay and micronuclei in mouse embryonic fibroblasts</i>	77
<i>Assessing DNA damage by colony formation in transformed MEFs</i>	79
<i>DNA damage response proteins following irradiation in MEFs</i>	81
<i>Downstream targets of mTOR following irradiation in MEFs</i>	81
<i>Proliferation</i>	85
<i>Irradiation-induced thymic lymphoma</i>	86
<i>Ras-transformed 628C KI keratinocytes form larger papillomas more rapidly than WT keratinocytes</i>	87
Discussion	89
 CHAPTER 5: Synthesis and Conclusions	93
 APPENDICES	98
APPENDIX A: Additional results from mTOR WT and 628C KI mice that are not significantly different by genotype	99
APPENDIX B: Levels of three miRNAs are differentially expressed between WT and 628C KI B220+ splenocytes by Nanostring; the magnitude of the differences by Real Time PCR were not significant	102

APPENDIX C: Glycolysis is similar in primary and transformed mTOR WT and 628C KI, and mTOR WT and KD mouse embryonic fibroblasts	104
APPENDIX D: Top Molecular and Cellular Functions identified by Ingenuity Pathway Analysis in genes from bone marrow of pristane-treated animals	106
APPENDIX E: Apoptosis and cell cycle in WT and 628C KI MEFs 3 hours and 18 hours post irradiation	114
REFERENCES	116

LIST OF TABLES

Table 1:	Antibodies used in this project, including company and catalog number	17
Table 2:	Top enriched molecular and cellular function networks in bone marrow from pristane-treated animals identified by Ingenuity Pathway Analysis	70
Table 3:	Differentially expressed genes associated with DNA damage response (z-score = 0.864, p-value of overlap = 0.002) identified by Ingenuity Pathway Analysis in bone marrow from pristane-treated mice	71
Table 4:	Cell Morphology-associated top molecular functions as identified by Ingenuity Pathway Analysis	105
Table 5:	Small Molecule Biochemistry-associated top molecular functions as identified by Ingenuity Pathway Analysis	107
Table 6:	DNA Replication, Recombination, and Repair-associated top molecular functions as identified by Ingenuity Pathway Analysis	109
Table 7:	Molecular Transport-associated top molecular functions as identified by Ingenuity Pathway Analysis	112
Table 8:	Gene Expression-associated top molecular functions as identified by Ingenuity Pathway Analysis	113

LIST OF FIGURES

Figure 1:	Simplified diagram of the mTOR pathway showing the components of mTORC1 and 2, mTOR inhibitors, and the main downstream mTOR targets	2
Figure 2:	Schematic of the mTOR protein with important domains highlighted	4
Figure 3:	Photomicrographs of a mesenteric oil granuloma (A,B) and a mesenteric plasma cell tumor (C,D) from pristane-primed mice	9
Figure 4:	Diagram illustrating the introduction of the SNP at nucleotide 1977 in <i>Mtor</i> , originally found in the BALB/c and NZB mice, onto a B6;129 background through homologous recombination, and the resulting amino acid substitution at 628	11
Figure 5:	Schematic summarizing the characteristics of the strains bred to produce the Lck-Akt/mTOR WT (WT) and Lck-Akt/mTOR KD (KD) mice	24
Figure 6A:	Digital bands from a capillary-based immunoassay assessing levels of downstream targets of mTOR in pre-tumor thymocytes (4 weeks) in two representative mice	29
Figure 6B:	Chemiluminescence peaks from a capillary-based immunoassay assessing levels of downstream targets of mTOR in pre-tumor thymocytes (4 weeks) in two representative mice	30
Figure 7:	Flow cytometry scatter plots for thymic CD4 and CD8 labeling (A), with bar graphs of absolute numbers (B) and percents (C) of each cell type	31
Figure 8:	Flow cytometry scatter plots (A) and bar graphs of absolute numbers (B) and percentages of cells (C) for CD44 and CD25-labeled, lineage-depleted T- lymphocytes from pre-tumor thymi	32
Figure 9:	Photomicrographs of thymic lymphomas from WT and KD mice...	33
Figure 10:	Survival curve for Lck-Akt/mTOR WT and Lck-Akt/mTOR KD mice	34

Figure 11A: Digital bands from a capillary-based immunoassay assessing levels of downstream targets of mTOR in pre-T LBL from two representative mice	34
Figure 11B: Chemiluminescence peaks from a capillary-based immunoassay assessing levels of downstream targets of mTOR in pre-T LBL from two representative mice	35
Figure 12: Flow cytometry scatter plots of CD4 and CD8-labeled populations in thymic pre-T LBL from WT and KD mice	36
Figure 13: Clonality of pre-T LBL assessed by nested PCR for T- cell receptor rearrangement	36
Figure 14: <i>TCRα/Myc</i> translocations in WT and KD mice	37
Figure 15: Proportions of <i>TCRα/Myc</i> translocations and MYC protein levels in WT and KD pre-T LBL	38
Figure 16: Survival curve from Lck-Akt mice treated with a mTOR inhibitor (everolimus)	39
Figure 17: Transcript and protein levels of CDK6 and protein expression of other cell cycle regulators in WT and KD thymic pre-T LBL	41
Figure 18: Protein and transcript levels of <i>Cdkn2a</i> (<i>p16</i>) in WT (n=4) and KD (n=3) tumors	42
Figure 19: Levels of CDKN1A (<i>p21</i>) and cyclin D1 protein in a representative KD tumor compared to a WT tumor	42
Figure 20: Viability and CDK6 protein levels from WT and KD thymic pre-T LBL cells treated with rapamycin	44
Figure 21: Viability of WT and KD pre-T LBL cells with increasing doses of a CDK4/6 inhibitor (PD-0332991)	44
Figure 22: Cell cycle and apoptosis were analyzed post treatment with a mTORi and a CDK4/6i in mTOR WT pre-T LBL cells	45
Figure 23: Percent viability of WT thymic pre-T LBL cells treated with a mTORi, a CDK4/6i, and a combination of the two inhibitors	46
Figure 24: Activity of the combination of a CDK4/6 inhibitor (PD-0332991) and a mTOR inhibitor (rapamycin) evaluated in human T-ALL/LBL cell lines	48

Figure 25:	Combination index of T-ALL/LBL cell lines treated with a mTORi (rapamycin), a CDK4/6i (PD-0332991), and a combination of the two agents	49
Figure 26:	Cell cycle proteins from six T-ALL/LBL cell lines treated with PD-0332991, rapamycin, and the combination of the two agents ..	50
Figure 27:	Downstream targets of mTOR, phospho-ribosomal S6 ^{S240/244} and phospho-AKT ^{S473} were evaluated in T-ALL/LBL cell lines treated with 1 nM rapamycin, 500 nM PD-0332991, and the combination of the two agents	51
Figure 28:	Four representative T-ALL/LBL cells lines treated with increasing doses of a dual mTOR inhibitor, PP242, or a mTORC1 inhibitor, rapamycin, in combination with increasing doses of a CDK4/6 inhibitor (PD-0332991) for 48 hours	52
Figure 29:	Immunoblot analysis of one T-ALL/LBL cell line (TIB-153), evaluating phospho-RB, RB, CDK6, cyclin D3, and phospho-AKT ^{S473} after treatment with the combination of PP242 (1.25 μM) and the CDK4/6 inhibitor (500 nM), as well as the combination of rapamycin (1 nM) and the CDK4/6i (500nM)	53
Figure 30:	Principal components analyses of genes from tissues of the non-pristane-treated animals (A), pristane-treated animals (B), and bone marrow of pristane-treated animals (C); the genes are most different in the pristane-treated bone marrow	69
Figure 31:	<i>Fancc2</i> , <i>Fancc</i> , and <i>Fanccg</i> transcripts are lower in bone marrow from pristane-treated KI mice by RT-PCR in samples from microarray analysis, but not in additional animals	72
Figure 32:	Kaplan-Meier survival curve for mTOR WT, heterozygous (Het), and 628C KI mice treated with 8 Gy gamma irradiation	73
Figure 33:	Severe bone marrow depletion (pancytopenia) in irradiated mice collected 18 days post 8 Gy total body irradiation (A), in comparison to untreated, aged-matched mice (B)	74
Figure 34:	Cleaved caspase 3 labeling in WT and KI bone marrow and small intestines, with quantification of labeling by color deconvolution (% positive pixels)	75
Figure 35A:	Representative comets from untreated and irradiated (6 Gy) WT and 628C KI bone marrow cells 2.5 hours post irradiation	76

Figure 35B: Comparison of the average tail moment from WT and KI irradiated bone marrow cells	77
Figure 36: Representative comets from untreated and treated WT and KI MEFs at 5 minutes and one hour after 4 Gy gamma irradiation, and comparison of average tail moment from WT and KI MEFs at these time points ..	78
Figure 37: Percent cells with micronuclei for WT and KI MEFs irradiated at 4 Gy and collected at time points post irradiation	79
Figure 38: Colony formation and surviving fraction of transformed WT and KI MEFs 10 days after 2, 4, 6, and 8 Gy gamma irradiation	80
Figure 39: Immunoblot of DDR proteins at 30 minutes, 1 hour, 3 hours, and 6 hours post 4 Gy gamma irradiation in mTOR WT and 628C KI primary MEFs	81
Figure 40: Downstream targets of mTORC1 and mTORC2 at time points post 4 Gy irradiation in WT and 628C KI MEFs	83
Figure 41: PKC α labeling in untreated and 4 Gy-irradiated WT and 628C KI MEFs 6 hours post irradiation	84
Figure 42: Labeling for F-actin in untreated WT and 628C KI MEFs, and in WT and KI MEFs 6 hours post 4 Gy irradiation	84
Figure 43: Proliferation based on percent confluence in untreated and irradiated WT and 628C KI MEFs	85
Figure 44: Survival curve of WT and 628C KI mice exposed to fractionated doses of 1.75 Gy, once weekly for 4 weeks, that developed thymic lymphomas	87
Figure 45: Papilloma volume from WT and 628C KI Ras-transformed keratinocytes grafted onto nude mice	88
Figure 46: Immunoblots of FANCD2 and phospho-PKC α (PRKCa) in WT and 628C KI keratinocytes, both untreated (Un) and Ras-transformed (ras)	88
Figure 47: Polymorphonuclear cells (PMNs) and lymphocytes from untreated (WT and KI) and pristane-treated (designated WTP and KIP) mTOR WT and 628C KI mice by CBC	99

Figure 48:	Average protein expression levels by quantification of western blot bands or by size-based, automated, capillary immunoassay system (peak area), showing levels of downstream targets of mTOR	101
Figure 49:	Spot intensity by Nanostring array for miR30a, miR101, and mir423-5P, and transcript levels by RT-PCR for each miR in WT and KI bone marrow cells	103
Figure 50:	Curves representing glycolytic function in SV40-transformed and primary mTOR WT, KI, and KD mouse embryonic fibroblasts	105
Figure 51:	Percent cells in early and late apoptosis 3 hours and 18 hours post 4 Gy irradiation in WT and KI MEFs by flow cytometry	114
Figure 52:	Cell cycle by flow cytometry in WT and KI MEFs 3 hours and 18 hours post 4 Gy irradiation	115

KEY TO ABBREVIATIONS

4E-BP1 – Eukaryotic translation initiation factor 4E-binding protein 1

AKT – V-Akt murine thymoma viral oncogene homolog

ATM – Ataxia telangiectasia mutated

CDK4 - Cyclin-dependent kinase 4

CDK6 - Cyclin-dependent kinase 6

CDKN1A (p21) – Cyclin-dependent kinase inhibitor 1A

CDKN1B (p27) – Cyclin-dependent kinase inhibitor 1B

CDKN2A (p16) – Cyclin-dependent kinase inhibitor 2A

DDR – DNA damage response

DEPTOR – DEP domain TOR-binding protein

DMEM – Dubecco's modified eagle medium

DNA-PK – DNA-dependent protein kinase

EIF4E – Eukaryotic translation initiation factor 4E

FANCD2 – Fanconi Anemia group D2 protein

FAT – FRAP, ATM, and TRRAP

FBS – Fetal bovine serum

FKBP12 – FKBP-rapamycin-associated protein 12

FRAP – FKBP-rapamycin associated protein

HEAT – Huntington, Elongation factor 3, PR65A, Tor

IMDM – Iscove's modified debecco's medium

KD – Knock down

KI – Knock in

LCK – Lymphocyte-specific protein kinase tyrosine kinase

MEF - Mouse embryonic fibroblast

mSIN1 – Mammalian stress-activated protein kinase interacting protein

MNDAL – Myeloid cell nuclear differentiation antigen-like

MSLT8 – Mammalian lethal with Sec-13 protein 8

mTOR – Mechanistic target of rapamycin

mTORC1 – Mechanistic target of rapamycin complex 1

mTORC2 – Mechanistic target of rapamycin complex 2

PBS – Phosphate buffered saline

PI3K – Phosphatidylinositol 3-Kinase

PKC α – Protein kinase C, alpha

PRAS40 – Proline-rich AKT substrate, 40 kDa

PROTOR – Protein observed with Rictor

PTEN – Phosphatase and tensin homolog

RAFT1 – Rapamycin and FKBP12 target

RAPT1 – Rapamycin target 1

Raptor – Regulatory associated protein of mTOR

RB – Retinoblastoma protein

Rictor – RPTOR independent companion of mTOR, complex 2

RPMI – Roswell Park Memorial Institute medium

P70SK6 (S6K) – Ribosomal protein S6 kinase, 70 kDa

RpS6 (S6) - Ribosomal protein S6

SGK – Serum- and glucocorticoid-induced kinase

SNP – Single nucleotide polymorphism

TSC1/2 – Tuberous sclerosis complex

TBS – Tris-buffered saline

WT – Wild-type

CHAPTER 1: Introduction

mTOR: The signaling pathway, structure, and roles in the normal cell

The mechanistic target of rapamycin (mTOR, formerly known as FRAP, RAPT1, or RAFT1) is a highly-conserved serine/threonine kinase (Brunn, Fadden et al. 1997) in the PI3K/AKT pathway (Sekulić, Hudson et al. 2000). mTOR is a central hub in the complex regulation of cell growth and metabolism, which functions by integrating environmental cues such as growth factors, insulin (Withers, Ouwens et al. 1997), oxygen, and amino acids (Jewell, Russell et al. 2013). mTOR phosphorylates downstream targets, initiating changes in transcription, translation, lipogenesis, and nutrient transport, as well as autophagy, mRNA degradation, and apoptosis [reviewed in (Hall 2008) and (Laplante and Sabatini 2009)]. *Mtor* is the mammalian homolog of the *Saccharomyces cerevisiae* gene products DDR/Tor1 and DDR/Tor2 (Alarcon, Cardenas et al. 1996); these yeast Tor proteins were identified as targets of the immunosuppressive macrolide compound, rapamycin, in an earlier mutation screen (Cafferkey, Young et al. 1993).

mTOR is active when incorporated in one of two different complexes: mTORC1 or mTORC2. mTORC1 is composed of mTOR, RAPTOR, PRAS40, MLST8 (GβL), and DEPTOR, while mTORC2 is composed of mTOR, RICTOR, PROTOR, mSIN1, MLST8 (GβL), and DEPTOR [(Loewith, Jacinto et al. 2002), (Jacinto, Loewith et al. 2004)], and reviewed in [(Roberto Zoncu 2011); Figure 1)]. In both complexes, DEPTOR negatively regulates mTOR activity (Peterson, Laplante et al. 2009); mTORC1 is also negatively regulated by the TSC1/TSC2 complex (Garami, Zwartkuis et al. 2003). The most extensively studied targets of mTORC1 are 4E-BP1 and S6K (Burnett, Barrow et al.

1998), which augment translation. When mTORC1 phosphorylates 4E-BP1, it releases EIF4E, which promotes cap-dependent translation (Richter and Sonenberg 2005); when mTOR activates S6K, it increases mRNA biogenesis, cap-dependent translation, and the translation of ribosomal proteins (Ma and Blenis 2009). The main targets for mTORC2 are AKT, PKC α , and SGK, which are involved in cytoskeleton rearrangements, proliferation, and cell survival [(Tchevkina and Komelkov 2012) (Jacinto, Loewith et al. 2004); Figure 1]. mTOR has many other targets, as the mTOR signaling pathway is extremely complex, with a variety of upstream signals and regulators and downstream targets and effectors as mapped by Caron et al. (Caron, Ghosh et al. 2010). Because of this complexity, knowledge about the targets and functions of mTOR is constantly growing.

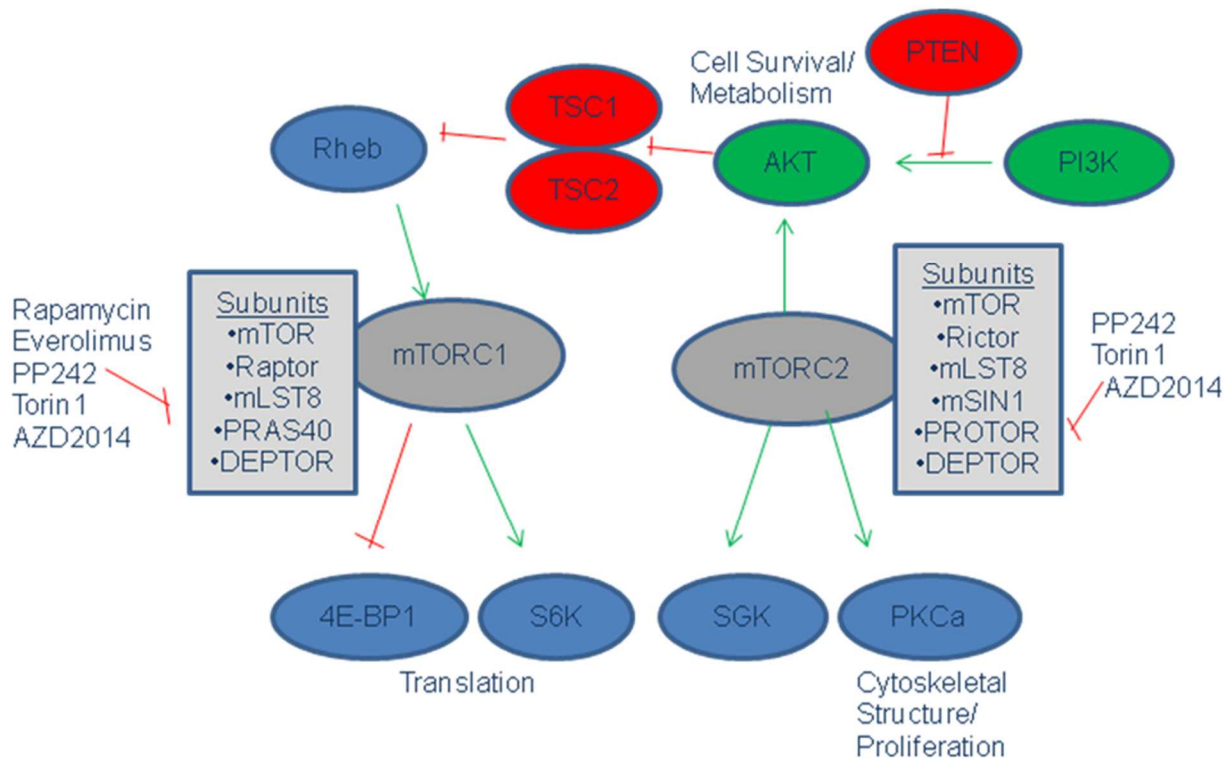


Figure 1: Simplified diagram of the mTOR pathway showing the components of mTORC1 and 2, mTOR inhibitors, and the main downstream mTOR targets. Figure adapted from (Guertin and Sabatini 2009, Zhang, Readinger et al. 2011).

Figure 1 (cont'd). Inhibitory signals are indicated by red lines with cross bars, while activating signals are shown with green arrows. Proteins represented by green ovals have been shown to be oncogenes, while those that are red have been shown to be tumor suppressors. The compounds shown next to the subunits in purple text are inhibitors that act on each mTOR complex.

mTOR is a large protein composed of 2549 amino acids (289 KDa) that is a member of the PI3K-related kinase (PIKK) family (Figure 2). The N-terminus of the protein contains numerous tandem-repeated domains composed of two antiparallel α -helices known as HEAT domains [(for **H**untington, **E**longation factor 3, **P**R65/**A** subunit of PP2A, and **T**or; orange rectangles in Figure 2 (Perry and Kleckner 2003), (Tchevkina and Komelkov 2012)]. These HEAT domains are sites of protein-protein interaction, and have not been well characterized in mTOR (Knutson 2010). Other, well characterized domains of the protein include the FAT domain (**F**RAP, **A**TM, **T**RAPP), the FRB domain [(**F**KBP12-**r**apamycin **b**inding domain, (Tchevkina and Komelkov 2012)], and the PI3K catalytic kinase domain, which is near the C-terminus of the protein. The kinase and FRB domains have been well studied, because of FKBP12's role in binding rapamycin, which results in inhibition of the kinase function of the protein [(Chen, Zheng et al. 1995),(Sabatini, Erdjument-Bromage et al. 1994)].

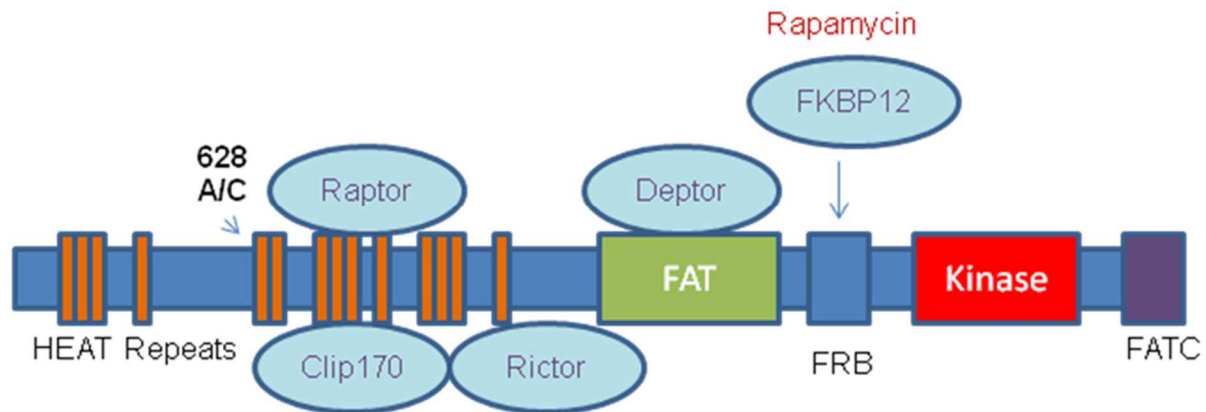


Figure 2: Schematic of the mTOR protein with important domains highlighted. Note that the thin, orange rectangles represent HEAT domains. Also shown is the amino acid substitution at aa628 produced by a single nucleotide polymorphism that is referred to throughout the manuscript. Light blue ovals show approximate binding sites of interacting proteins. Figure adapted from (Laplante and Sabatini 2012).

mTOR in cancer

The PI3K/AKT/mTOR pathway is often deregulated in cancer cells, usually through *Pi3k* or *Pten* mutations, receptor tyrosine kinase activation (Samuels, Wang et al. 2004, Hollander, Blumenthal et al. 2011), and *Akt* amplifications [reviewed in (Altomare and Testa 2005)]. Constitutive PI3K/AKT activation is found in 50% of de-novo acute myeloid leukemia samples (Tamburini, Elie et al. 2007), and mTORC1 activation was detected in almost all AML samples tested [(Xu, Thompson et al. 2005), (Tamburini, Green et al. 2009)]. In prostate cancer, deletions or mutations in the PI3K/AKT/ mTOR pathway inhibitor, *Pten*, are common genetic alterations (Ruscetti and Wu 2013). Elevated levels of phosphorylated downstream targets of mTOR, including phosphorylated 4E-BP1 and S6, are apparent in many cancers, including mammary carcinoma, colorectal carcinoma, endometrial cancers, glioblastoma, hepatocellular carcinoma, pulmonary adenocarcinomas, lymphoma, melanoma, ovarian carcinoma, prostate carcinomas, and renal cell carcinomas, indicating mTOR activation [reviewed

in (Menon and Manning 2009)]. Because of mTOR's role in integrating growth signals, which leads to protein translation and cell growth, it is not surprising that it is often activated in cancer cells.

Dysregulation of the PI3K/AKT/mTOR pathway in cancer has been reported to have a role in cancer initiation and progression through many of its downstream targets. In mouse models of prostate cancer with PTEN deletion, mTORC2 activity is required for both tumor formation and growth (Guertin, Stevens et al. 2009). In human prostate cancer cells with *PTEN* deletion, a study using ribosome profile mapping of targets translationally controlled by mTOR showed the affected cellular processes to be proliferation, metabolism, protein synthesis, and invasion (Hsieh, Liu et al. 2012). In multiple cancers, mTOR's role in inhibiting 4E-BP1, and thus promoting translation, allows the tumor cells to ramp up cell cycle activators, anti-apoptosis genes, and ribosome biogenesis, promoting cell growth [reviewed in (Hay and Sonenberg 2004, Sengupta, Peterson et al. 2010)]; mTOR also regulates HIF1 α in response to hypoxia, which is a major pressure experienced by neoplastic cells (Hudson, Liu et al. 2002). In addition, mTOR is a major regulator of autophagy, which is the process by which the cell degrades organelles and proteins in lysosomes to release intracellular nutrients as an adaptive response to nutrient stress, a strategy utilized by some cancer cells (Kroemer, Mariño et al. 2010). Finally, mTORC1 activates a protein SREBP1, which is involved in lipogenesis and the pentose phosphate pathway, which is increased in tumor cells (Porstmann, Santos et al. 2008). All of these roles of mTOR provide tumor cells with a growth advantage in the face of nutritional stress and promote the dysregulated growth that is a hallmark of cancer.

Because of its role in tumor growth, inhibition of mTOR has been found to be a promising treatment for some cancers. The first mTOR inhibitor to be discovered was rapamycin, which is a macrolide antibiotic originally discovered on Rapa Nui island in 1970. Rapamycin is secreted by the bacterial strain, *Streptomyces hygroscopicus* as an anti-fungal mechanism [(Vezina, Kudelski et al. 1975), and reviewed in (Tchevkina and Komelkov 2012)]. In yeast first, and then in human cells, rapamycin was found to have anti-proliferative properties, and was immunosuppressive in mammals [(Brown, Albers et al. 1994), reviewed in (Tchevkina and Komelkov 2012)]. Rapamycin acts by binding to the protein FKBP12, and inhibiting mTORC1 kinase activity (Chen, Zheng et al. 1995). Through this mechanism, rapamycin and other first generation mTOR inhibitors, such as everolimus, mostly inhibit mTORC1 and tend to inhibit mTORC2 only after long-term treatment (Sarbasov, Ali et al. 2006). However, when first generation inhibitors suppress mTORC1 activity, they dysregulate downstream negative feedback mechanisms, resulting in enhanced PI3K-AKT signaling (Wan, Harkavy et al. 2006). Newer, second generation mTOR inhibitors, such as PP242, AZD2014, and Torin1, inhibit both mTOR complexes 1 and 2 by binding to the catalytic site as ATP-competitive inhibitors [(Thoreen, Kang et al. 2009), (Feldman, Apsel et al. 2009)].

Rapamycin was found to suppress tumor growth in the early eighties (Eng, Sehgal et al. 1984) and has since been studied as a treatment for a variety of tumors. mTOR inhibitors are currently approved for renal cell carcinoma, Tuberous Sclerosis Complex (rare genetic disease leading to formation of multiple neoplasms caused by mutation in *Tsc1/2*), pancreatic neuroendocrine tumor, and subependymal giant cell

astrocytoma and are being tested in combination with other chemotherapeutic agents for a variety of cancer types (clinicaltrials.gov).

mTOR mutations

A less common mechanism of PI3K/AKT/mTOR dysregulation in cancers is a mutation in *Mtor* itself. A total number of 480 *Mtor* coding mutations are listed in the COSMIC database [Catalog of the Somatic Mutations In Cancer, <http://cancer.sanger.ac.uk/cancergenome/projects/cosmic/> (Forbes, Bindal et al. 2011)]. Some of these mutations (S2215Y and R2505P) confer hyperactivity to the protein, with increased phosphorylation of downstream targets (Sato, Nakashima et al. 2010) while other mutations are nonsense mutations, leading to an early termination of translation. Additional mutations are missense, leading to a single amino acid substitution, which can be silent or affect the structure and function of the protein. Single nucleotide polymorphisms (SNPs) in *Mtor* in humans have been associated with an increased risk of death in esophageal cancer patients (Hildebrandt, Yang et al. 2009), and an increased risk of developing microsatellite instability (MSI)¹ in colon tumors (Slattery, Herrick et al. 2010). However, only a few of the SNPs in *Mtor* have been characterized, and the relevance of mutations in *Mtor* to carcinogenesis is only beginning to be investigated.

The BALB/c allele of mTOR is a susceptibility gene for plasmacytoma formation

A naturally-occurring SNP in *Mtor* was discovered by our lab in BALB/c and NZB mice at an otherwise highly conserved site (C1977T). This SNP was uncovered by genetic mapping during positional cloning studies of alleles associated with susceptibility to plasma cell tumor formation (Bliskovsky, Ramsay et al. 2003).

BALB/cAnPt and NZB/BINJ mice are almost uniquely susceptible to mesenteric plasma cell tumor formation after intraperitoneal (IP) pristane (alkane oil that is a common component of many mineral oils; 2,6,10,14 tetramethylpentadecane) injections (priming); 60% of BALB/cAnPt and 30% of NZB/BINJ mice develop these mesenteric plasma cell tumors when given IP pristane [(Potter and Wiener 1992) Figure 3C,D]. The tumors form in sites of mixed granulomatous inflammation (Figure 3A,B) after pristane injections are given at day 0, 60, and 120 [0.5 ml IP, (Potter 1983, Potter and Wiener 1992)]. Mesenteric inflammation, referred to as oil granulomas, are composed of variable aggregates of macrophages that occasionally contain neutrophils, multinucleate giant cells, aggregates of lymphocytes and plasma cells, surround variably-sized clear vacuoles, and are occasionally associated with fibrosis and mineralization (Figure 3A,B). Tumors arise following a latency period of 200-300 days [(Morse 1980), (Potter 1983)]. These plasma cell tumors develop as sheets of neoplastic plasma cells within the granulomas, and can be classified by cellular morphologies into plasmacytic, plasmablastic, and anaplastic subgroups [(Qi, Zhou et al. 2007), Figure 3C,D], though the molecular and clinical consequences of each morphologic subgroup are unclear. The tumors require IL6 to grow and are accompanied by ascites (Hilbret 1995) and secretion of IgG or IgA antibodies (Potter and Wiener 1992). Immune system stimulation is also required for tumor formation, as specific pathogen free mice (SPF) mice do not develop plasma cell tumors [(McIntire and Princler 1969), (Byrd, McDonald et al. 1991)]. Interestingly, pristane injected into other locations does not stimulate tumor formation, except for rare subcutaneous sarcomas (Potter and Wiener 1992).

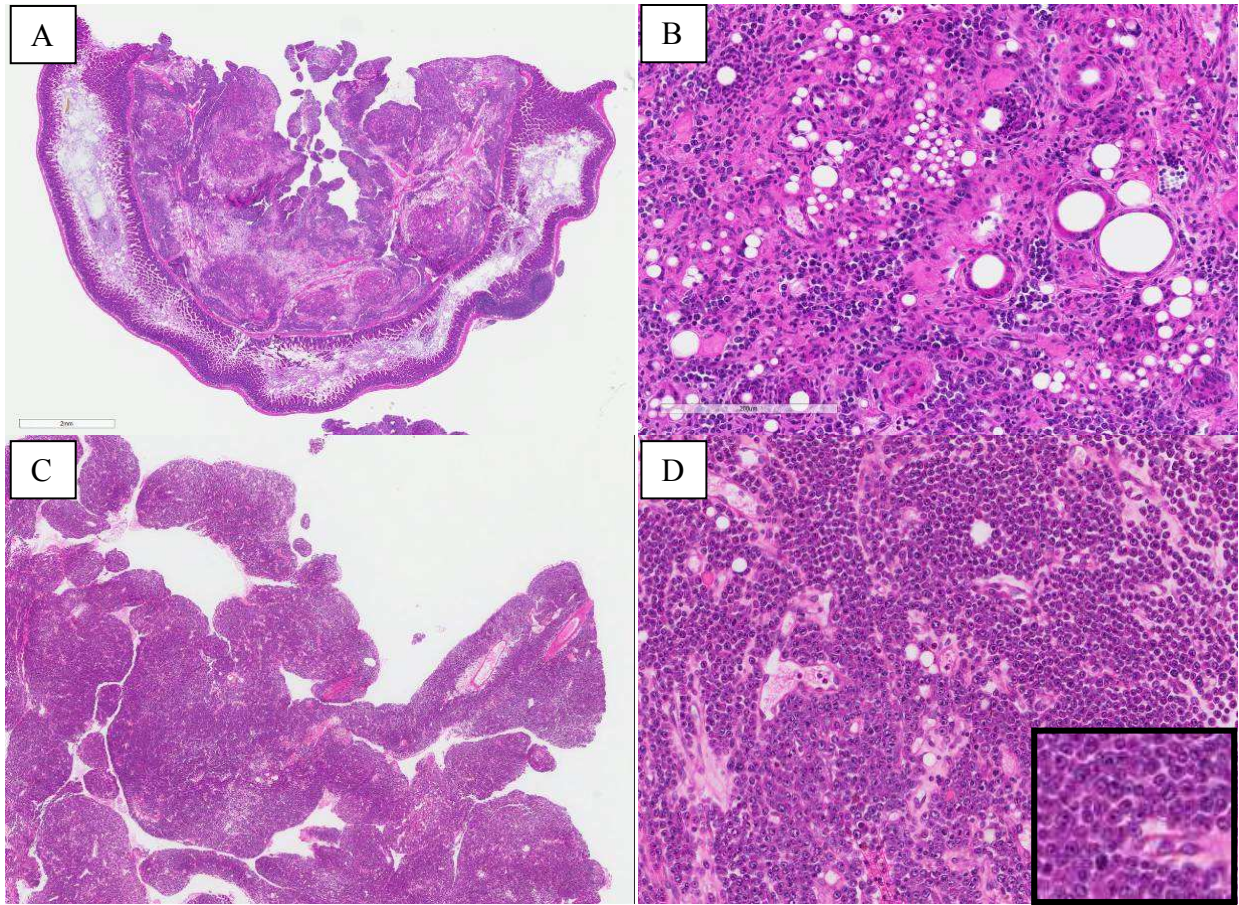


Figure 3: Photomicrographs of a mesenteric oil granuloma (A,B) and a mesenteric plasma cell tumor (C,D) from pristane-primed mice. Images taken at 2X (A,C), 20X (B,D), and 40X (inset D), Hematoxylin and eosin.

Through genetic linkage studies, our lab determined that 4 susceptibility alleles are linked with plasma cell tumor formation in BALB/cAnPt and NZB/BINJ mice (Mock, Krall et al. 1993), including alleles of *Cdkn2a* [p16; (Zhang, Ramsay et al. 1998, Zhang, DuBois et al. 2001)], *Mtor* [(Mock, Hartley et al. 1997, Bliskovsky, Ramsay et al. 2003)], a new gene named *Mndal* (Zhang, Kagan et al. 2009), and a remaining allelic variant which has not been linked to a gene. One of these susceptibility genes, *Mtor*, was found to have a polymorphism in susceptible mice at an otherwise highly conserved region of the gene. Specifically, BALB/cAnPt and NZB/BINJ mice have a rare single nucleotide polymorphism in *Mtor* (C1977T) in exon 12, which leads to a single amino

acid substitution (cysteine instead of arginine) at aa 628 (R628C). The consequences of this single amino acid substitution on the structure and function of the protein are unknown, and became one of our major research questions.

To specifically explore the consequences of the SNP in the BALB/c allele of *Mtor*, we created a knock in mouse through homologous recombination with the BALB/c allele of *Mtor* (C1977T) on a B6;129 background (as described in (Zhang, Readinger et al. 2011), Figure 4). In the initial construction of these mice, the neomycin cassette disrupted the transcription of *Mtor*, leading to significantly reduced levels of mTOR protein (approximately 70% decrease (Zhang, Readinger et al. 2011)). These mTOR knockdown mice (KD) are 25% smaller than wild-type (WT) and heterozygous (HET) littermates; they also have small spleens, smaller cell size, fewer thymic and splenic T-cells, and fewer splenic, lymph node, and bone marrow B220+ B-lymphocytes (Zhang, Readinger et al. 2011). Protein levels of Raptor and Rictor (components of mTORC1 and mTORC2), as well as downstream phospho-targets of mTOR, such as phospho-S6K, were lower in several tissues from these mice (Zhang, Readinger et al. 2011). The mTOR KD mice are more susceptible to mortality after inoculation with *Streptococcus pneumoniae*, likely due to a decreased ability to form germinal centers in lymphoid tissues and decreased immunoglobulin somatic hypermutation and class switch recombination in B-cells, processes required for high affinity antibody responses (Zhang, Pruitt et al. 2013). Interestingly, mTOR KD mice have been shown to have a longer life span than mTOR WT mice (Wu, Liu et al. 2013). These mTOR KD mice provide a unique model of decreased mTOR, as deletion of mTOR is embryonic lethal

(Gangloff, Mueller et al. 2004), and can be used as a model for the study of pharmacologic mTOR inhibition.

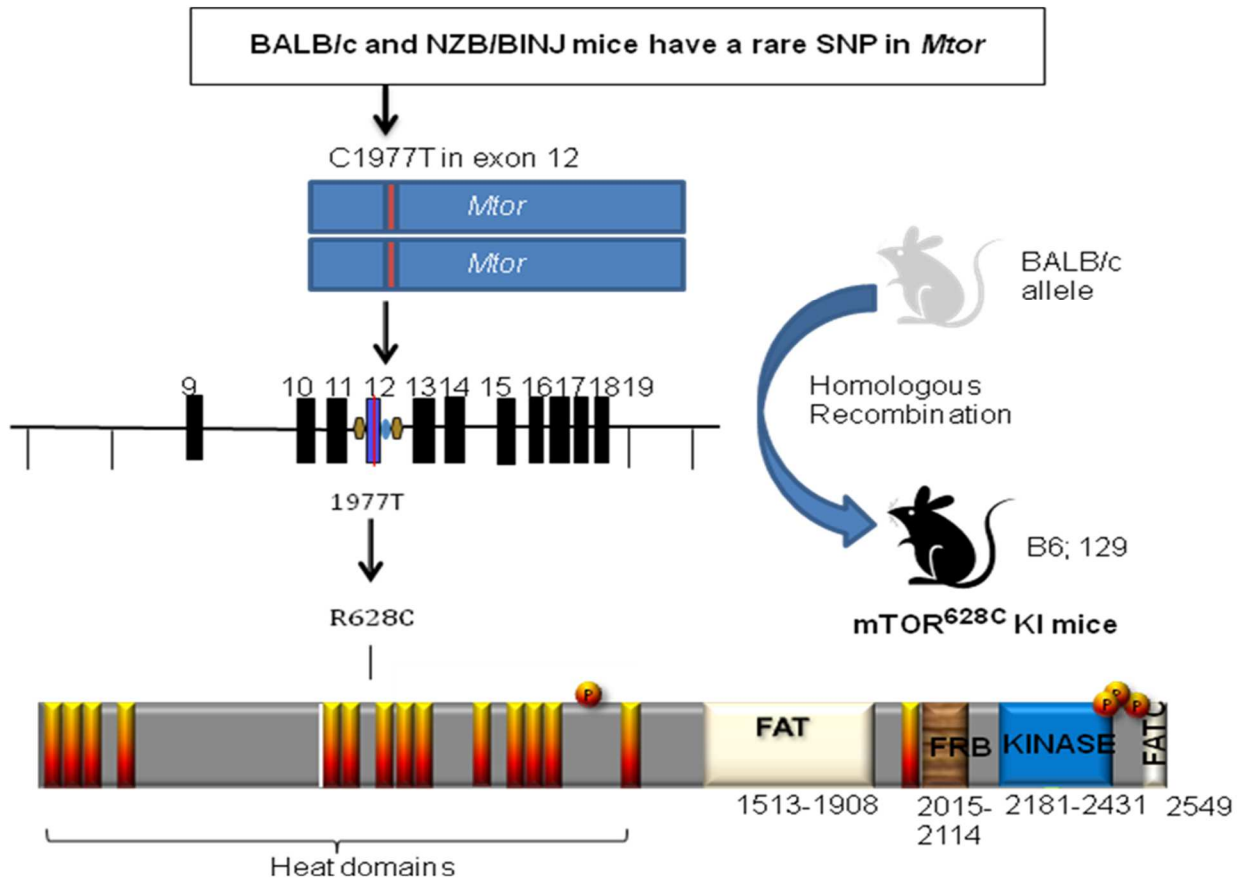


Figure 4: Diagram illustrating the introduction of the SNP at nucleotide 1977 in *Mtor*, originally found in the BALB/c and NZB mice, onto a B6;129 background through homologous recombination, and the resulting amino acid substitution at 628.

Unlike the mTOR KD mice, B6;129 mice harboring the introduced *Mtor* SNP (628C KI; crossed to cre mice to remove the disrupting neomycin cassette) are phenotypically normal, with normal levels of mTOR, RICTOR, RAPTOR, and DEPTOR (Zhang, Readinger et al. 2011). These mice have normal organ size, cell size, B-cell

development, splenic and thymic populations, and antibody formation (Zhang, Readinger et al. 2011).

Because of the role of the SNP in mTOR as a susceptibility allele for plasma cell tumor formation, we chose to evaluate the function of the altered protein in response to cell stressors, such as inflammatory, genotoxic, and oncogenic stress, all of which activate mTOR. Evaluating the function of the 628C variant of mTOR under stress conditions illustrated the oncogenic nature of the variant and shed light on mTOR's role in stress responses.

Project goals

In this project, we utilized two unique mouse models with altered mTOR to better understand the role of mTOR in cancer development, cancer cell signaling, and the response to cell stressors likely to be encountered by neoplastic cells. To evaluate the role of mTOR in cancer development and signaling, we studied the effects of mTOR knock-down (KD) on the development of AKT-driven thymic leukemias/lymphomas and on alterations of signaling pathways in these lymphomas. Using the mTOR KD mice as a model for pharmacologic inhibition of mTOR, we identified this altered signaling as a possible target for a combination therapy, and treated human T-cell lymphoblastic leukemia/lymphoma (T-ALL/LBL) cell lines with the combination therapy, revealing a cooperative combination therapy that may be efficacious in T-ALL/LBL treatment.

In a related project, we also studied the effects of the SNP (C1977T) in *Mtor* and the resulting single amino acid substitution (628C) found in BALB/c mice on the function of the mTOR protein using the 628C KI mice and cells derived from these mice. We looked at transcriptional changes in tissues from 628C KI mice under inflammatory

conditions, and found that multiple DNA damage response (DDR) genes were downregulated in KI cells. From this finding, we evaluated the response of mice and cells with mTOR 628C KI to DNA damage through irradiation, and to mTOR WT and 628C KI cells in the face of oncogenic stress. Overall, this unique mouse model allowed us to explore the effect of the SNP on the protein, and to explore mTOR's role in the stress response. Because of mTOR's role in promoting the growth and maintenance of cancer cells, a thorough understanding of mTOR signaling and the response of the cancer cell to pharmacologic mTOR inhibition are important components in the knowledge necessary to wisely approach targeted therapies.

Hypotheses

Chapter 3: *Genetic and pharmacologic inhibition of mTOR will delay tumor growth in mice with AKT-driven T-cell leukemia/lymphoma, and pathways concurrently inhibited by decreased mTOR can be utilized as targets for combined therapy.*

Chapter 4: *The BALB/c variant of mTOR, C1977T, has an altered function compared to the wild-type variant due to the single amino acid substitution at aa 628 (628C); this altered function leads to a difference in survival, the phosphoproteome, the transcriptome, and tumor formation in response to cell stressors.*

CHAPTER 2: General Methods

The methods described in this section are general methods used throughout both portions of the project (Chapters 3 and 4). For more detailed methods for each individual project, see the methods section of the appropriate chapter.

Mice

All animal studies were performed in compliance with the NIH Animal Care and Use Committee (Protocol LG009). The creation and preliminary characterization of the mTOR KD and 628C KI mice are described by Zhang, et al. (Zhang, Readinger et al. 2011).

Collection of cells and tissues

Tissues were collected from mice at a pre-defined study endpoint or humane endpoint and were either fixed in Telly's Fixative (4% formaldehyde and 2% glacial acetic acid in 70% EtOH) or 4% paraformaldehyde in PBS for 24 hours and transferred to 70% ethanol for long term storage. Tissue was also flash frozen in liquid nitrogen or was transported to the lab fresh on ice for downstream applications.

Fresh thymic tumors were crushed in a 40 μ m sterile filter in 1X PBS to create a single cell suspension. Depending on the downstream application, the single cell suspension was spun down and cell pellets were flash frozen for future use.

Spleens and femur bones were collected from WT and 628C KI mice. Spleens were crushed using the sterile end of a syringe plunger and cells were resuspended in 1X PBS and filtered through a 40 μ m sterile filter. ACK lysis buffer (Lonza, Walkersville, MD) was added to lyse remaining splenic red blood cells. B220+ splenocytes (splenic B-cells) were then isolated using MS MACS separation columns and B220+ beads

(Miltenyi Biotec, Auburn, CA) as recommended by the manufacturer. Bone marrow cells were collected by cutting the ends of fresh femur bones and using a 30 ½ G needle and 6 ml syringe to flush sterile, ice-cold PBS through the marrow cavity. The bone marrow contents were incubated briefly with ACK lysis buffer to lyse red blood cells. Cell pellets from B220+ splenocytes and bone marrow were flash frozen and stored at -80°C for use in downstream applications.

To create mouse embryonic fibroblasts (MEFs), uteri containing 13.5 dpc (days post conception) embryos were collected and individual embryos were separated. The heads and internal organs were removed, and the remaining tissues were macerated in 5 ml Trypsin-EDTA (Gibco, Life Technologies, Grand Island, NY). The tissue was incubated at 37°C in Trypsin-EDTA for 15 minutes, and remaining fragments were pipetted up and down to break up the debris. Cells were cultured overnight in 10cm dishes in Dubecco's modified eagle medium (DMEM, Gibco) supplemented with 10% fetal bovine serum (FBS) and 1% penicillin-streptomycin (Gibco). Media was changed the following day, and MEFs were expanded for two passages and frozen for future use.

Flow cytometry and protein analysis

Single cell suspensions from thymi or spleens, or of mouse embryonic fibroblasts (MEFs), were stained with the PE Annexin V Apoptosis Detection kit (Becton Dickson, San Jose, CA) for evaluation of apoptotic cells; the cell cycle was analyzed using propidium iodide (PI)/RNase Staining Buffer (Becton Dickson). Stained cells were analyzed using FACSCalibur (Becton Dickinson) and flow cytometry data was reviewed using FlowJo software (Ashland, OR).

Protein was isolated for immunoblotting from thymi, T-cell lymphoma cell lines, spleens, and bone marrow by lysing cell pellets in radioimmunoprecipitation assay buffer (RIPA) plus protease and phosphatase inhibitors (Santa Cruz Biotech, Dallas, TX). Lysates were passed through a 25 GA needle ten times and allowed to incubate on ice for 1 hour. MEF samples were lysed in a freshly-prepared buffer composed of 10% sodium dodecyl sulfate (SDS), protease and phosphatase inhibitors (Roche, Indianapolis, IN), and 1% tris and were sonicated at 4°C on high for 7.5 minutes, with 0.5 minute on, 1 minute off intervals. These samples were also then allowed to incubate on ice for 1 hour. Samples from both preparation methods were centrifuged at 12,000 rpm at 4°C for 20 minutes, and the supernatant, containing the proteins, was saved for future analysis. Protein concentrations were measured using the bicinchoninic acid (BCA) assay (Pierce™ BCA Protein Assay Kit, ThermoScientific; Rockford, IL). Lysates were prepared with 4% lithium dodecyl sulfate (LDS) loading buffer and approximately 12 µg of protein per sample was loaded onto 4-12% Bis-Tris or 4-20% tris-glycine gels (Novex, Life Technologies, Grand Island, New York) and separated by electrophoresis. Proteins were transferred to a nitrocellulose membrane via the iBLOT system (Life Technologies, Grand Island, NY).

Membranes were incubated with primary antibodies at 4°C overnight in 5% BSA/TBST (bovine serum albumin/tris buffered saline with 1% Tween-20), and the following day were rinsed in TBST and incubated in the appropriate secondary antibody at room temperature in 5% milk/TBST. Antibodies used throughout these projects are listed below (Table 1). Membranes were incubated for 1 minute with Super Signal West Dura or Femto Extended Duration Substrate (Life Technologies) and were imaged using

a Syngene Imager and the GeneSnap program from Syngene (Frederick, MD). Digital quantification of bands (densitometry) was performed using GeneTools (Syngene).

Table 1: Antibodies used in this project, including company and catalog number.

Target Antigen	Catalog #	Company
Phospho-4E-BP1 (T37/46)	2855	Cell Signaling
4E-BP1	9452	Cell Signaling
Phospho-AKT (S473)	9271	Cell Signaling
AKT	9272	Cell Signaling
ATM	2873	Cell Signaling
CDK4	2906	Cell Signaling
CDK6	3136	Cell Signaling
Cleaved Caspase 3	9661	Cell Signaling
Cyclin D1	2926	Cell Signaling
Cyclin D3	2636	Cell Signaling
FANCD2	ab108928	Abcam
Mtor	2972	Cell Signaling
c-MYC	ab32072	Abcam
P21	sc-397	Santa Cruz
P16	sc-1207	Santa Cruz
P27	2552	Cell Signaling
Phospho-PKCα (T638)	ab32502	Abcam
Phospho-PKCα (T497)	ab76016	Abcam
Phospho-PKCα (S657)	12356	Cell Signaling
PKCα	ab32376	Abcam
Phospho-P53 (Ser15)	9284	Cell Signaling
Phospho-RB (S780)	8180	Cell Signaling
RB	9313	Cell Signaling
Phospho-rpS6 (S240/244)	2215	Cell Signaling
RpS6	2217	Cell Signaling
Phospho-p70S6K (T389)	9205	Cell Signaling
P70-S6K (S6K)	9202	Cell Signaling

Protein expression for phospho and total S6, 4E-BP1, and AKT was also evaluated using a size-based, automated, capillary immunoassay system [Simple Western, Protein Simple, Santa Clara, CA; (Chen JQ 2013)]. This analysis was

performed by the Center for Cancer Research Collaborative Protein Technology Resource group.

Genotyping

DNA was prepared by the HotSHOT method [(hot sodium hydroxide and Tris; (Truett 2000)] from cell pellets, ear punches, or tail tips. PCR reactions were composed of buffer 2 and components from the Expand High Fidelity Kit (Roche) or of the GoTaQ Green master mix (Promega, Madison, WI) per the manufacturer's instructions, as well as 1 μ L each of the appropriate forward and reverse primers. Cycling conditions were optimized based on primer. Primers for determining the mTOR 628C KI or mTOR KD status (Zhang, Readinger et al. 2011) and for genotyping based on sex (McClive and Sinclair 2001) are previously described.

Microarray and RT-PCR

RNA was isolated using Trizol reagent (Invitrogen, Life Technologies), followed by purification using the Qiagen RNeasy MiniElute Cleanup kit (Qiagen, Venlo, Limburg). 1 μ g of RNA was labeled and amplified using the Message Amp-11-Biotin Enhanced Kit (Ambion, Life Technologies, Carlsbad, CA). RNA was hybridized to Affymetrix Mouse Genome 430 2.0 array cartridges while rotating at 45°C for 16 hours. Chips were washed in a GeneChip Fluidic wash station (Affymetrix, Santa Clara, CA) and scanned. Microarray analyses were performed using Affymetrix GCOS software (Santa Clara, CA), Partek software, and BRB-ArrayTools (developed by Dr. Richard Simon and BRB-ArrayTools Development Team). Data were normalized to internal controls. Significantly different genes were selected with p-values >0.05 and a fold change of >1.5 or <-1.5 .

cDNA for real time PCR (RT-PCR) was created from RNA samples using TaqMan® Reverse Transcription Reagents (Life Technologies, Grand Island, NY) and RT-PCR was performed using SYBR-Green PCR Master Mix (ABI, Foster, CA, USA) on a 7500 Fast Real-Time PCR System (Applied Biosystems, Foster City, CA, USA) with the following primers for CDK6: 3'-CCAAATCTGCTCAACCCATCG-5' and 3'-CAGGTTGTCCTTGTATCTCTCCAG-5', FANCD2 forward 3'- AGTATGGCCGTCGCTTGTGG-5', FANCD2 reverse 3'-GCAGCAAGCTCAGAACATCTTCC-5', FANCC forward 3'-CTGCTGTGGCTCTTGGTGTTTC-5', FANCC reverse 3'-AATACCTTCAGCTCCACCA TGC-5', FANCG forward 3'-CTCTTTCGGACCCTGCCTGAGG-5', FANCG reverse 3'-ACTCCAGTCCACGACTGATCAG-5'. Cycle threshold values (CT) were normalized to B-Actin or rRNA levels for each sample.

RNA including microRNAs (miRNA) was prepared from B220+ splenocytes from untreated and pristane-treated mice using the mRNeasy kit (Qiagen), per the manufacturer's instructions. RNA samples were shipped to Nanostring (Seattle, WA) for barcoded Nanostring array analysis of miRNA expression. Results were analyzed in nSolver (Nanostring) and in Microsoft Excel. MiRNAs with p-value >0.05, a fold change >1.5 and <-1.5, and FDR<5 were selected. RT-PCR for miRNA was performed on RNA samples containing miRNA using primers and a kit specific for detection of miRNA (Applied Biosystems). Samples were normalized to U6 expression levels.

Glycolysis analysis

Glycolysis in the WT, KI, and KD transformed and primary mouse embryonic fibroblasts was analyzed using the Seahorse XF Glycolysis Stress Test Kit (Seahorse, MA) and the XF analyzer per the manufacturer's instructions.

Statistical Analysis

Mouse survival was assessed using the Kaplan-Meier survival curve and the Log Rank Test (Graph Pad Prism, La Jolla, CA) analyses. RT-PCR results were analyzed using the $2^{-\Delta CT}$ method, and values were compared using a Student's T-test. Flow cytometry, RT-PCR, proliferation, IHC results were also compared using Student's T-test.

CHAPTER 3: Constitutive mTOR inhibition in mouse thymic pre-T LBL identifies *Cdk6* as a target for combination treatment of T-ALL/LBL

Abstract

The PI3K/AKT/mTOR pathway is frequently hyperactivated in T-cell acute lymphoblastic leukemia/lymphoma (T-ALL/LBL). To model inhibition of this pathway in lymphoma, mice with T-lymphocyte-specific, constitutively-active AKT (Lck-MyrAkt2) were crossed to mice with genetically reduced mTOR expression (mTOR knock down, KD). Mice with genetic reduction of mTOR had increased survival relative to wild-type mTOR mice (average survival of 24 versus 14 weeks, respectively), though both groups eventually developed thymic pre-T-cell lymphoblastic leukemia/lymphoma (pre-T LBL). A similar phenotype was observed when mTOR wild-type Lck-MyrAkt2 mice were treated for 8 weeks with the rapamycin analog, everolimus, an inhibitor of the mTORC1 complex. Transcriptional profiling of thymic lymphomas from the mice uncovered decreased expression of *Cdk6*, a critical proliferative control node in T-cell development and oncogenic transformation, in mTOR KD mice. Pharmacologic inhibition of mTOR in tumor cells also decreased CDK6 protein levels, suggesting the two proteins have a mechanistic relationship in the tumors. The combination of a mTOR inhibitor (rapamycin) and a CDK4/6 inhibitor (PD-0332991) cooperatively decreased the overall viability and signaling downstream of drug targets in mouse lymphoma cells and in human T-ALL/LBL cell lines. Our results suggest that this drug combination may be beneficial in the treatment of T-ALL/LBL.

Introduction

T-cell acute lymphoblastic leukemia/lymphoma (T-ALL/LBL) accounts for 15% of childhood and 25% of adult lymphoblastic leukemia and is often characterized by hyperactivation of the PI3K/AKT/mTOR pathway (Pui, Relling et al. 2004). In one study, deletion or mutational inactivation of *PTEN* or activating *PI3K* or *AKT* mutations were found in approximately half of primary T-ALL samples (Gutierrez, Sanda et al. 2009). *In vitro* pharmacologic inhibition of the PI3K/AKT/mTOR pathway decreased the viability of human T-ALL/LBL cell lines and caused G1 cell cycle arrest (Chan, Weng et al. 2007, Batista, Barata et al. 2011, Bressanin, Evangelisti et al. 2012). The frequent activation of this pathway and its role in cell growth has suggested mTOR as a target for pharmacologic inhibition, leading to clinical trials of mTOR inhibitors in ALL (<https://clinicaltrials.gov>). However, first-generation mTOR inhibitors, such as rapamycin, efficiently target only one of the two complexes formed by mTOR (TORC1) (Loewith, Jacinto et al. 2002), and can be associated with feed-back loops and eventual resistance (Carew, Kelly et al. 2011). While newer mTOR inhibitors target both complexes (TORC1/2), suppression of resistance mechanisms by combining them with additional drugs could further improve treatment efficacy.

To explore the effects of mTOR inhibition in a T-cell neoplasm with a hyperactivated PI3K/AKT pathway, we utilized the Lck-MyrAkt2 (Lck-Akt) mice, in which the T-lymphocyte-specific proximal *Lck* promoter drives a constitutively-active, myristoylated AKT2 protein (Ahmed, Franke et al. 1993, Malstrom, Tili et al. 2001). These mice spontaneously develop thymic pre-T cell lymphoblastic leukemia/lymphoma (pre-T LBL) between 75-200 days of age (Rathmell, Elstrom et al. 2003, Tan, Timakhov

et al. 2008, Timakhov, Tan et al. 2009). To diminish the hyperactive PI3K/AKT signaling, we inhibited mTOR both genetically and pharmacologically in these mice. This study highlights the modulation of CDK6 levels by mTOR and the use of mTOR inhibition in mouse models to explore molecular responses in T-ALL/LBL and to identify targets for combination therapy.

Methods

Mice. Animal studies were in compliance with NIH Animal Care and Use Committee Protocol LG009. Lck-Akt (Founder line 72; C57BL/6 background) transgenic mice were crossed with heterozygous *Mtor*^{tm1. Lgm} mice [mTOR KD mice, approximately 70% reduction in mTOR expression, B6;129 background; Figure 5 (Zhang, Readinger et al. 2011)] for two generations; offspring positive for Lck-Akt and homozygous for wild-type or knock down mTOR were selected. Mouse survival was assessed by a Kaplan-Meier survival curve and a Log Rank test (GraphPad Prism, San Diego, CA). In a separate experiment to control for the allelic variant (628C) of mTOR in the KD mice, *Mtor*^{tm1.1Lgm} mice with the allelic variant and normal mTOR levels [mTOR KI mice (Zhang, Readinger et al. 2011)] were crossed with Lck-Akt mice; no differences in survival were observed between Lck-Akt mice with or without the allelic variant (data not shown). Mice were genotyped for the Lck-Akt transgene (primers 5' AGG CAC TGC CCT CTT GAA GC-3' and 5' TTT GGG GTT CTG AAT GTG AG-3'), and for the disrupted mTOR gene as described (Zhang, Readinger et al. 2011). Tumors were collected at humane endpoint; a portion was fixed in Telly's fixative for 24 hours (h) and the remainder was frozen. Lck-Akt transgenic mice from founder line 55 (C57BL/6 background) (Timakhov, Tan et al. 2009) were given RAD001 (everolimus, 20mg/kg) or

vehicle (50µl) by gavage twice weekly, beginning at 8 weeks of age and continuing for 8 weeks. Mice from founder line 55 have a similar incidence of tumor formation as mice from founder line 72, though tumors arise more quickly in line 55 (~10wks compared to 16wks) (Timakhov, Tan et al. 2009).

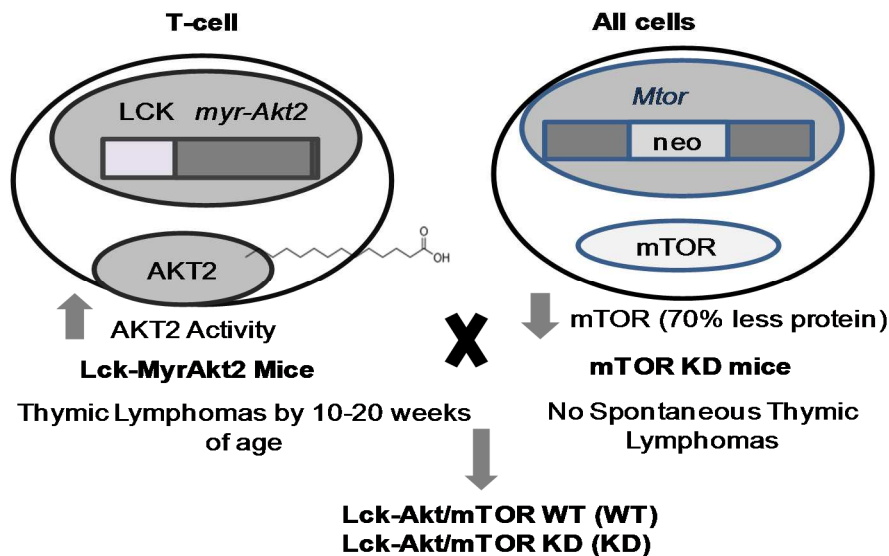


Figure 5: Schematic summarizing the characteristics of the strains bred to produce the Lck-Akt/mTOR WT (WT) and Lck-Akt/mTOR KD (KD) mice. Lck-MyrAkt2 mice have constitutively-active AKT due to myristoylation exclusively in T-lymphocytes, which is driven by a proximal LCK promoter; these mice spontaneously developed thymic lymphomas. mTOR knockdown mice have decreased mTOR expression due to a neomycin cassette inserted in the *Mtor* gene in cells throughout the body. The resulting offspring are referred to throughout as WT and KD based on mTOR status, but are positive for the Lck-Akt transgene.

Flow cytometry and protein analysis. Single cell suspensions from thymi of 4-week-old WT and KD mice and from murine thymic pre-T LBL were stained for CD4 and CD8 to determine double (CD4⁺,CD8⁺) and single (CD4⁺ or CD8⁺) positive T-cell populations by flow cytometry. Double negative (CD4⁻, CD8⁻) T-cells were identified as previously described (Hu, Deshpande et al. 2011). Viably frozen WT thymic pre-T LBL were transplanted into nude mice, then collected and cultured in vivo with either 1 nM of rapamycin or 625 nM of PD-0332991 (CDK4/6i, Pfizer) for 48 hours. Apoptosis of

treated cells was evaluated using the PE Annexin V Apoptosis Detection Kit 1 and cell cycle was analyzed using PI/RNase staining buffer (Becton Dickson, San Jose, CA). Cells were analyzed using FACSCalibur (Becton Dickinson) and FlowJo software (Ashland, OR).

Protein was isolated with RIPA lysis buffer plus protease inhibitors (Santa Cruz Biotech, Dallas, TX). Lysates were electrophoresed on 4-12% Bis-Tris gels (Novex, Life Technologies, Grand Island, NY) and were transferred to nitrocellulose membranes via the iBLOT system (Life Technologies). Antibodies were acquired from Abcam (c-MYC:ab32072, Cambridge, MA), Santa Cruz (p21:sc-397,p16:sc-1207; Dallas, TX), or Cell Signaling (mTOR:2972; CDK6:3136; CDK4:2906; Cyclin D3:2936; Cyclin D1:2926; p27:2552; and phospho-4E-BP1^{Thr37/46}:2855, 4E-BP1:9452; phospho-AKT^{S473}:9271, AKT:9272; phospho-RB^{S780}:8180, RB:9313;phopsho-S6^{S240/244}:2215, and S6:2217; Danvers, MA). A size-based, automated, capillary immunoassay system [Simple Western, Protein Simple, Santa Clara, CA (Chen, Heldman et al. 2013)] was utilized by the Center for Cancer Research Collaborative Protein Technology Resource group to measure phospho/total 4E-BP1 and AKT protein expression.

Pre-T LBL clonality. Analysis for T-cell clonality was performed on genomic DNA extracted from eight paraffin-embedded tumor tissue sections using the QIAamp DNA FFPE Tissue Kit (Qiagen, Valencia, CA). PCR amplification was performed using a two-step nested PCR that detects intralocus TCRG rearrangement (Knapp 2003) utilizing previously-described primers (Lista, Bertness et al. 1997). PCR reactions were prepared in 25µl total volume, with 3µl DNA, 5pmol of each primer, 0.5U of Taq polymerase (Invitrogen, Carlsbad, CA), and final concentrations of 80µM DNTP, 2mM

magnesium chloride, 20mM Tris-hydrogen chloride, and 50µl potassium chloride.

Cycling conditions were: 94°C for 4 minutes (m); 40 cycles at 94°C for 1m, 55°C for 1m, and 72°C for 1m; and 72°C for 5m. All PCR reactions were run in duplicate. Amplicons were visualized by high-resolution capillary electrophoresis using the QIAxcel Advanced Instrument (Qiagen) and QIAxcel ScreenGel Software. Two samples from mouse spleen and lymph node were amplified as polymorphic controls.

Pre-T LBL cell culture and fluorescence in situ hybridization (FISH). Thymic pre-T LBL single cell suspensions were cultured in Iscove's Modified Dulbecco Medium (IMDM; Life Technologies; plus 10% FBS, 1% penicillin-streptomycin, L-glutamine, non-essential amino acids, and sodium pyruvate, and 0.1% β-mercaptoethanol). A subset of cells were cultured with 0.2% colcemid for 2h, lysed with 0.075M KCL, and fixed with 3:1 methanol/glacial acetic acid. Probes for *TCRα* (BAC probe kindly provided by Thomas Reid, NCI) and *c-Myc* were labeled and hybridized overnight to metaphase spreads from fixed cells. Slides were incubated with FITC-labeled anti-DIG and avidin-Alexa 568 and stained with DAPI. Metaphase spreads were imaged on an inverted fluorescent microscope at 100X. At least 50 cells were assessed for the presence of t(14;15) translocations/sample (Timakhov, Tan et al. 2009).

Microarray and RT-PCR. RNA (1µg) was isolated from WT and KD thymic pre-T LBL using Trizol reagent (Invitrogen, Life Technologies), followed by purification with Qiagen RNeasy MiniElute Cleanup Kit (Qiagen). RNA was labeled and amplified with Message Amp-11-Biotin Enhanced Kit (Ambion, Life Technologies) and hybridized overnight to Affymetrix Mouse Genome 430 2.0 array cartridges (Santa Clara, CA). Chips were washed in a GeneChip Fluidic wash station (Affymetrix) and scanned. Microarray

analyses (ArrayExpress accession E-MTAB-3242, www.ebi.ac.uk/arrayexpress) were performed using Affymetrix GCOS, Partek, and BRB-ArrayTools (Richard Simon;BRB-ArrayTools Development Team). Data were normalized to internal controls. Genes expressed at significantly different levels between WT and KD mice had $p < 0.05$, FDR of < 0.1 , and 30% of expression data values had at least a 1.5-fold change in either direction from the gene's median value.

To assess levels of *Cdk6*, cDNA was prepared using TaqMan® RT Reagents (Life Technologies) and real-time PCR (RT-PCR) was performed using SYBR-Green master mix (ABI, Foster City, CA) on a 7500 Fast RT-PCR System (Applied Biosystems) with the following primers for *Cdk6*: 3'-CCAAATCTGCTCAACCCATCG-5' and 3'-CAGGTTGTCCTTGTATCTCTCCAG-5' and for *p16* as described (Zhang, Qian et al. 2003). Values were normalized to β -actin.

Drug treatment of murine pre-T LBL cells. Thymic pre-T LBL cells (100,000 cells/200 μ L, 96-well plates) were treated with 1nM rapamycin and/or 5nM-5 μ M PD-0332991 (SelleckChem, Houston, TX), each dissolved in DMSO. Cell viability was assessed after 24h (CDK4/6 inhibitors-Figure 4C) and 48h (mTOR inhibitor, CDK4/6 inhibitors, and combination) using CellTiter96® Aqueous One Solution (MTS Assay, Promega, Madison, WI). Experiments were performed in duplicate.

Matrix dose response screen in human T-ALL/LBL cell lines. Human T-ALL/LBL cell lines (CEM, CUTLL1, HALL, P12-ICHIKAWA, Jurkat, TIB-153, J.CaM1.6, and MOLT-3) were grown in RPMI (0.2% Normocin, 1% penicillin-streptomycin and L-glutamine, 10% FBS). To assess the activity of the drugs in combination, cell lines (25,000 cells/well in 96-well plates) were treated with a range of five doses of rapamycin

(0–100nM) and the CDK4/6 inhibitor, PD-0332991(0-1 μ M) individually and in combination [matrix dose response screen (Simmons, Patel et al. 2014)]. Viability at 48h post-treatment was assessed by MTS assay. Each screen was repeated twice, with duplicated plating/experiment. In addition, each cell line (6-well plates, 1.5x10⁶cells/well) was treated with 500nM PD-0332991, 1nM rapamycin, or the combination for 48h and collected for protein isolation. Drug activity of rapamycin and PD-0332991 was evaluated using Excess over Highest Single Agent (EOHSA) (Borisy, Elliott et al. 2003) and synergy scores were calculated using Combination Index (CI) methods [CompuSyn software <http://www.combosyn.com/>; CI<1 is synergistic (Chou 2005, Chou 2006, Chou 2010)]. Heat maps and CI plots for the dose matrices were generated with R v2.15.1 (Team 2011). Four T-ALL/LBL cell lines were treated with a range of PP242 (dual mTORC inhibitor; 0–2.5 μ M) and PD-0332991 doses (0–1000nM) in combination and assessed for viability.

Results

Pre-tumor thymocytes from mTOR KD mice have decreased mTOR activity. Lck-MyrAkt2 (Lck-Akt) mice spontaneously develop thymic pre-T LBL by 10-20 weeks of age (Tan, Timakhov et al. 2008, Timakhov, Tan et al. 2009), although their thymi are histologically normal at 4 weeks of age (Tan, Timakhov et al. 2008). mTOR signaling and T-cell development were evaluated in thymocytes from 4-week-old Lck-Akt/mTOR WT (WT) and Lck-Akt/mTOR KD (KD) mice prior to tumor formation. The downstream targets of mTOR, phospho-4E-BP1^{Thr37/46} and phospho-AKT^{S473}, were decreased in KD compared to WT thymocytes (Figure 6A and B). Total thymocyte number and size were similar in WT (n=3) and KD (n=3) pre-tumor thymi by flow cytometry. There was

no difference in the absolute number of double positive CD4+, CD8+ and single positive CD4+ or CD8+ thymocytes (Figure 7A, B, and C). Four stages of double negative (DN) thymocyte maturation are recognized, DN1-4. In thymi from 4-week-old mice there were fewer DN1 thymocytes in KD thymi ($p=0.031$), though all other double negative stages were similar between WT and KD thymi (Figure 8A, B, and C). Only a mild delay in development was observed in KD thymocytes at the DN1 stage, but this delay resolved and thymocyte populations were similar between KD and WT through remaining developmental stages, indicating the mTOR KD did not disrupt T-cell development in the thymi of these mice. A similar population of CD4 and CD8 single positive thymocytes has been reported in mTOR WT and KD mice that were not crossed to Lck-Akt mice (Zhang, Readinger et al. 2011).

A

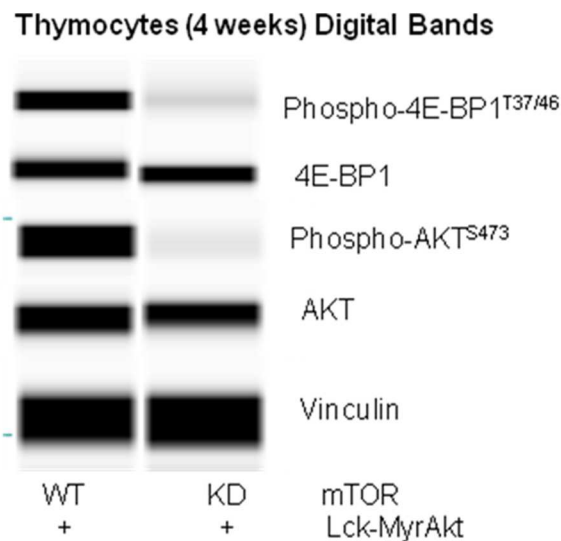


Figure 6A: Digital bands from a capillary-based immunoassay assessing levels of downstream targets of mTOR in pre-tumor thymocytes (4 weeks) in two representative mice. Phospho-4E-BP1^{T37/46} and phospho-AKT^{S473} were assessed **Figure 6 (cont'd)**. for WT and KD thymocytes from 4-week-old mice (before tumor formation). Vinculin served as the loading control.

B

Thymocytes (4 weeks) Chemiluminescence Peaks

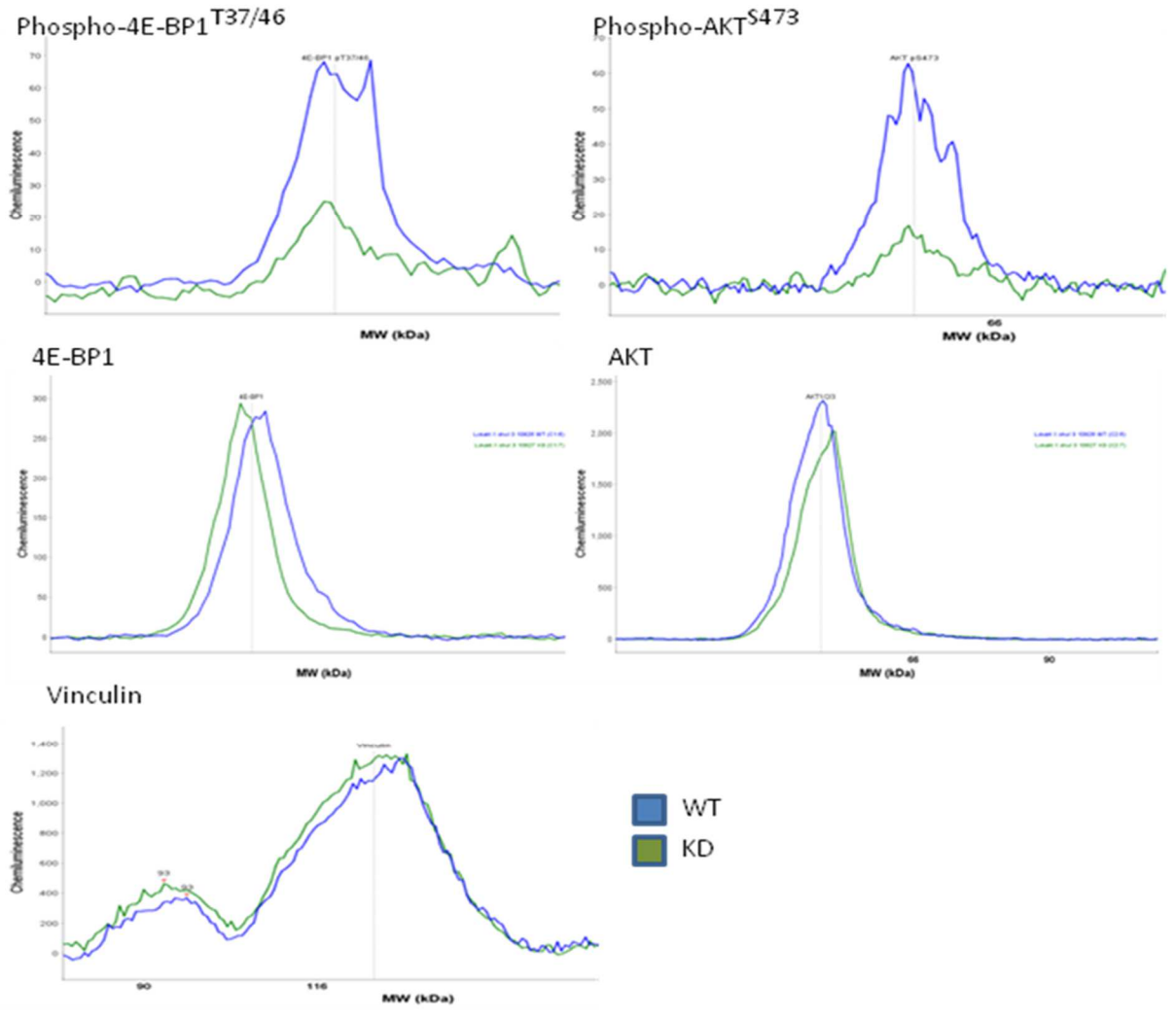


Figure 6B: Chemiluminescence peaks from a capillary-based immunoassay assessing levels of downstream targets of mTOR in pre-tumor thymocytes (4 weeks) in two representative mice. Phospho-4E-BP1^{T37/46} and phospho-AKT^{S473} were assessed for WT and KD thymocytes from 4-week-old mice (before tumor formation). Vinculin served as the loading control.

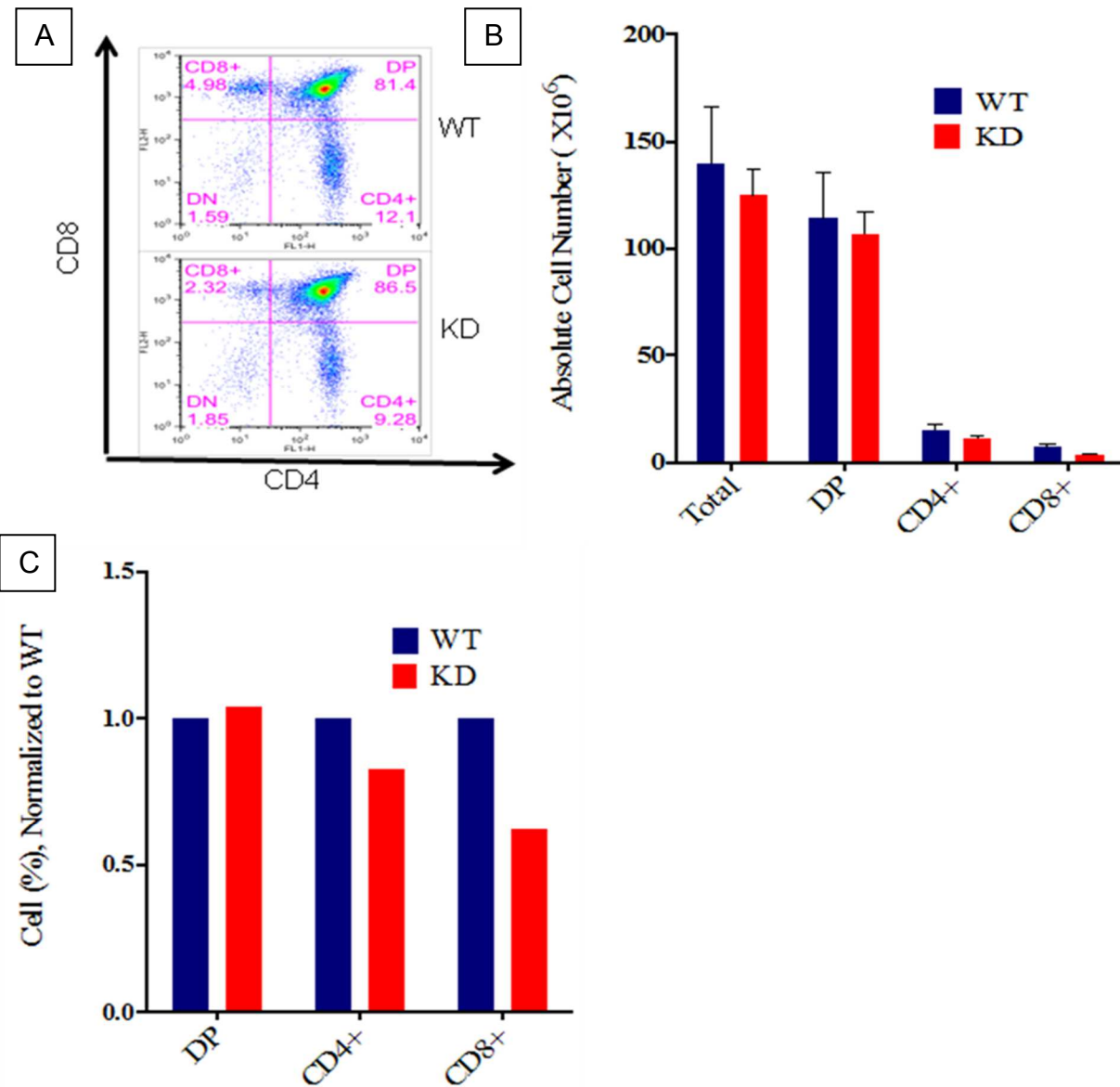


Figure 7: Flow cytometry scatter plots for thymic CD4 and CD8 labeling (A), with bar graphs of absolute numbers (B) and percents (C) of each cell type. 3 WT and 3 KD thymi were assessed, and error bars represent standard error of the mean. Absolute numbers of cells for each population were compared between WT and KD by Student's T Test.

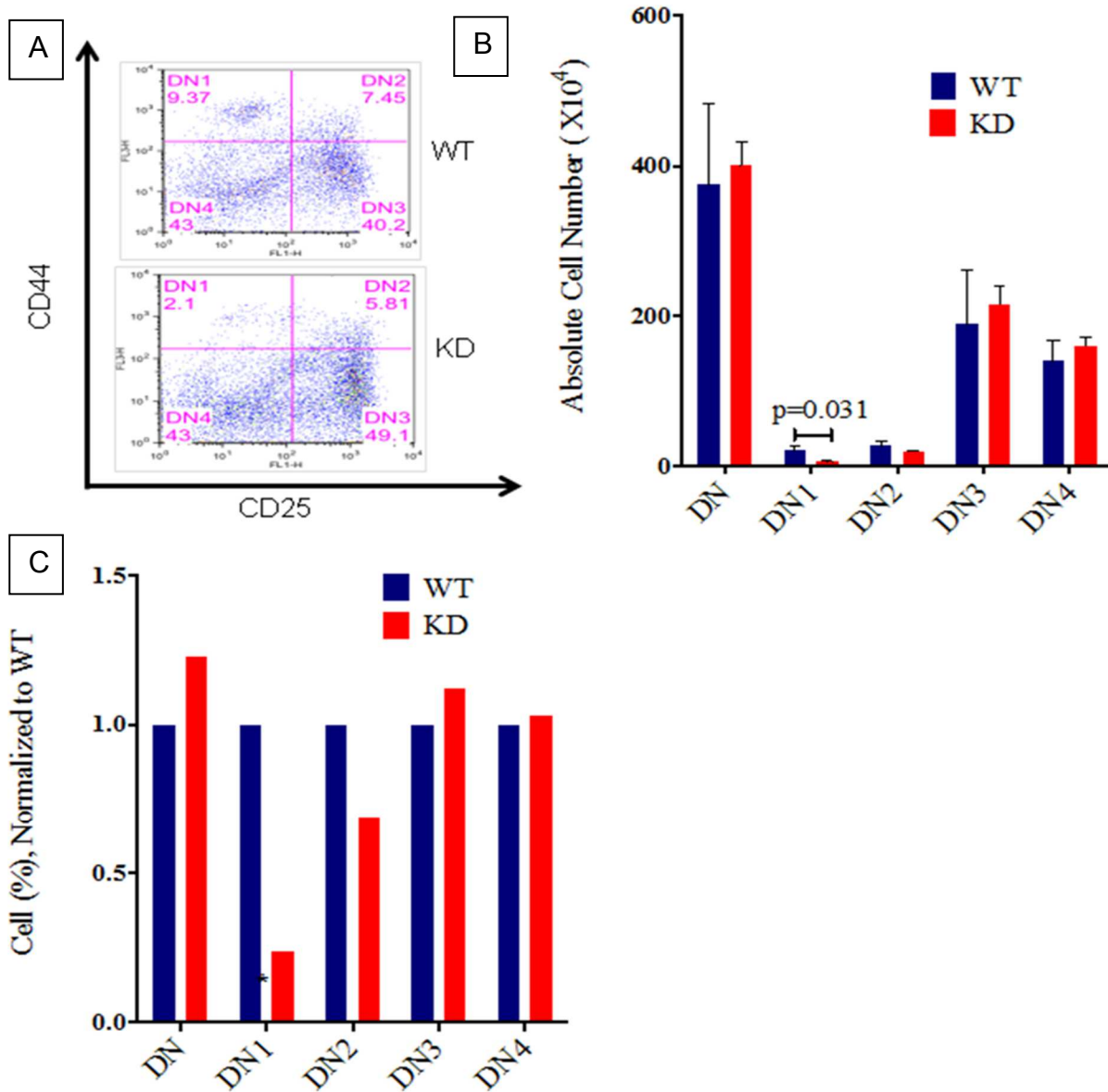


Figure 8: Flow cytometry scatter plots (A) and bar graphs of absolute numbers (B) and percentages of cells (C) for CD44 and CD25-labeled, lineage-depleted T-lymphocytes from pre-tumor thymi. Non-T-cells were depleted from thymi of 4-week-old mice, and remaining cells were labeled for CD25 and CD44. These markers define different populations of developing, double negative (DN), thymocytes. DN1 cells were significantly decreased in KD thymi ($p=0.031$). 3 WT and 3 KD thymi were assessed, and error bars represent standard error of the mean. Absolute numbers of cells for each population were compared between WT and KD by Students T Test.

Genetic and pharmacologic mTOR inhibition prolonged survival of Lck-Akt mice.

Over a period of >400 days, a similar proportion of 45 WT (75%) and 20 KD (71%) mice

developed pre-T LBL, which had a similar appearance in photomicrographs (Figure 9). However, the KD mice had a notably increased survival time compared to WT mice (Log Rank Test, $p=0.002$, Figure 10); KD mice survived an average of 168 days (median survival: 151d), while WT mice survived an average of 99 days (median: 92d). As in the pre-tumor thymocytes, phospho-4E-BP1^{Thr37/46} and phospho-AKT^{S473} levels were decreased in thymic pre-T LBL from KD mice (Figure 11). Pre-T LBL cells from WT mice ($n=2$) were a mixture of CD8+ and CD4+,CD8+ neoplastic T-cells, while cells from KD mice ($n=3$) were predominately CD8+ (representative tumors, Figure 12). PCR for T-cell antigen receptor rearrangement revealed that six of eight tumors were clonal (3/4 WT, 3/4 KD); pseudoclones were observed in the remaining two samples, likely a result of PCR failure in these samples (representative tumors, Figure 13).

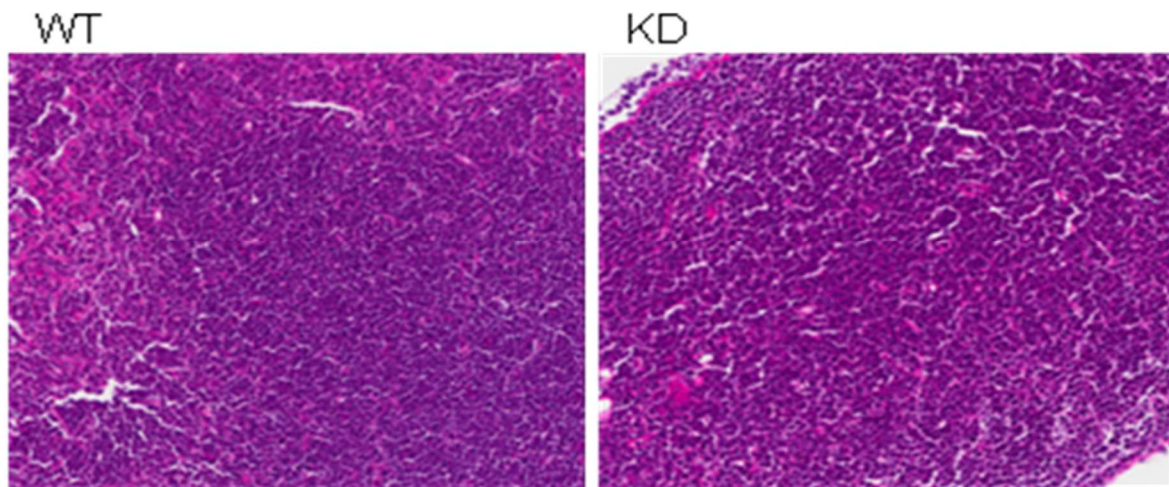


Figure 9: Photomicrographs of thymic lymphomas from WT and KD mice. Hematoxylin and Eosin, Imaged at 20X magnification.

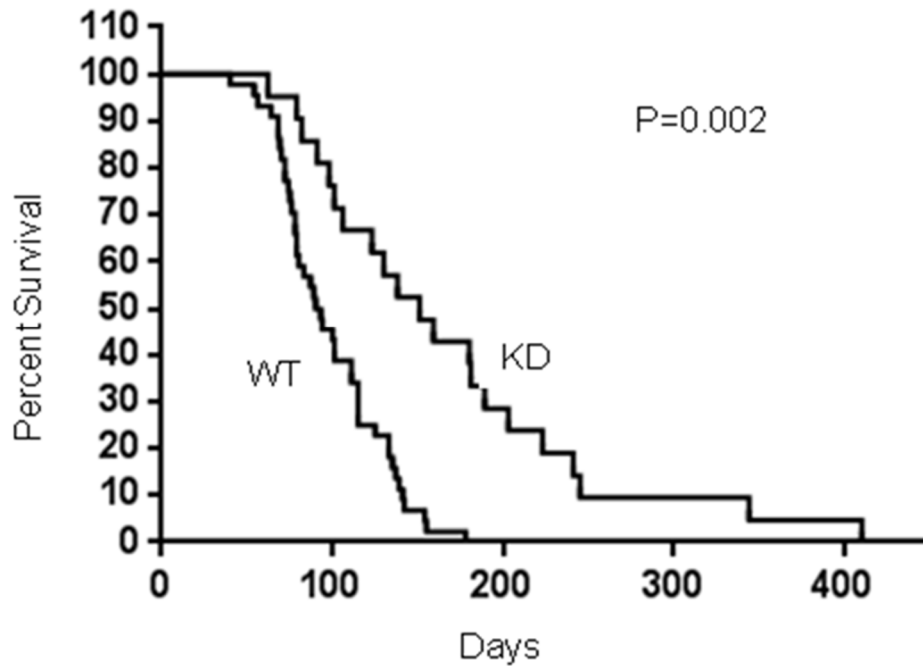


Figure 10: Survival curve for Lck-Akt/mTOR WT and Lck-Akt/mTOR KD mice. Survival associated with thymic pre-T cell lymphoblastic leukemia/lymphoma (pre-T LBL) was evaluated in KD (n=20) and WT mice (n=45) by Kaplan Meier survival analysis and a Log Rank test.

A

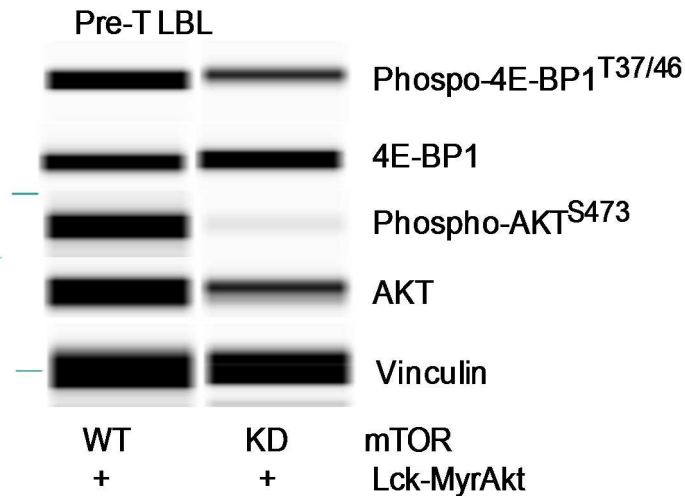


Figure 11A: Digital bands from a capillary-based immunoassay assessing levels of downstream targets of mTOR in pre-T LBL from two representative mice.

Phospho-4E-BP1^{T37/46} and phospho-AKT^{S473} were assessed for WT and KD pre-T LBL cells. Vinculin served as the loading control.

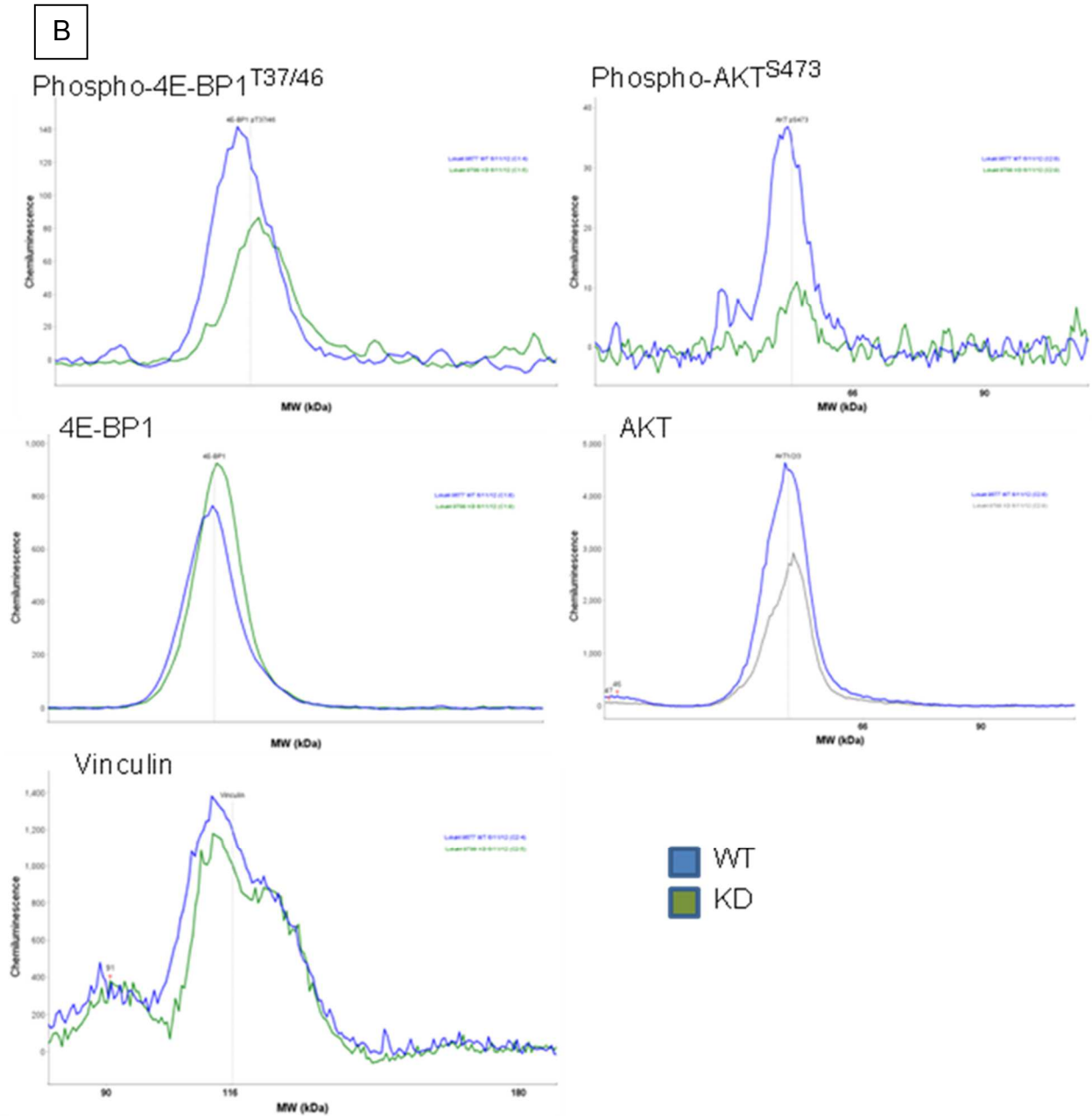


Figure 11B: Chemiluminescence peaks from a capillary-based immunoassay assessing levels of downstream targets of mTOR in pre-T LBL from two representative mice. Phospho-4E-BP1^{T37/46} and phospho-AKT^{S473} were assessed for WT and KD pre-T LBL cells. Vinculin served as the loading control.

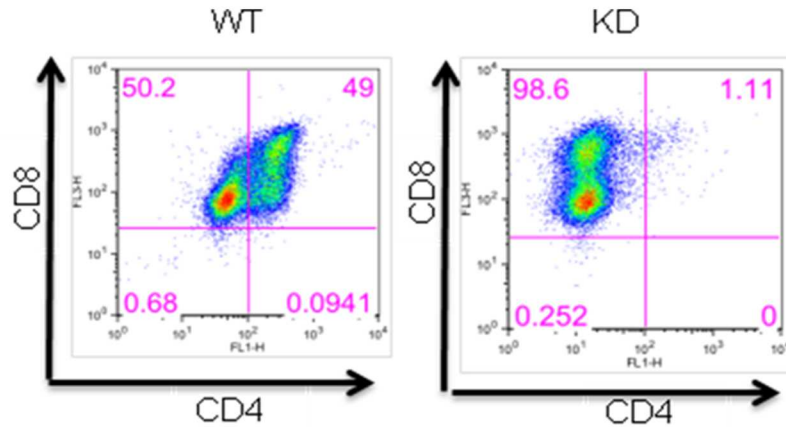


Figure 12: Flow cytometry scatter plots of CD4 and CD8-labeled populations in thymic pre-T LBL from WT and KD mice. The CD4, CD8 status of WT (n=2) and KD (n=3) thymic pre-T LBL was assessed by flow cytometry (representative scatterplots shown for WT and KD).

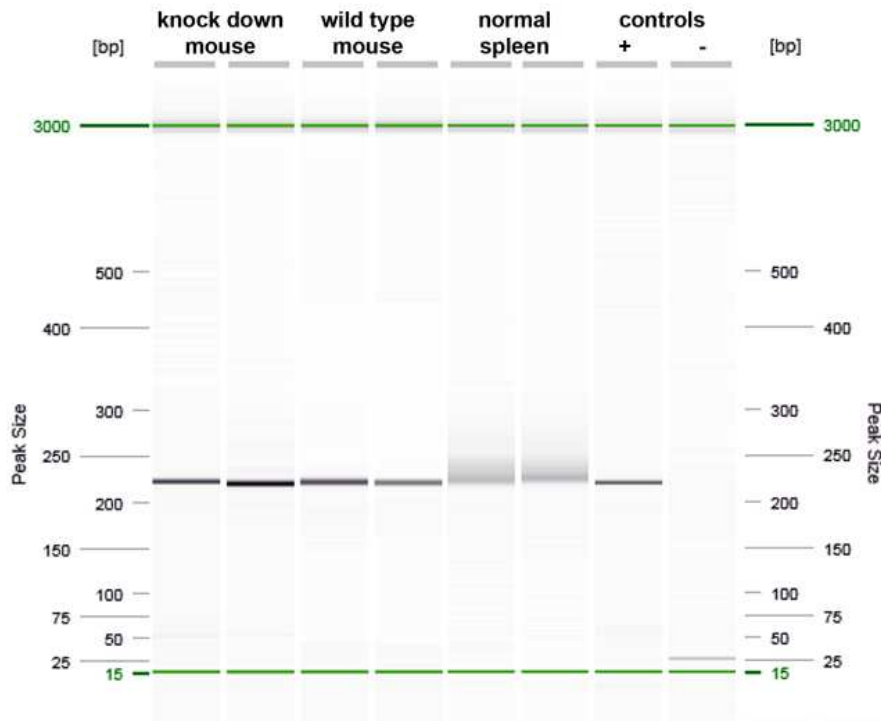


Figure 13: Clonality of pre-T LBL assessed by nested PCR for T-cell receptor rearrangement. WT (n=3) and KD (n=3) pre-T LBL thymic tumors were assessed by nested PCR for T-cell antigen receptor rearrangement (PARR: PCR reactions were run in duplicate). The normal spleen samples have the expected polymorphic (non-clonal) pattern. Negative control = water and positive control = known clonal T-cell lymphoma. Two representative tumors are shown.

As Lck-Akt mice frequently develop a t(14;15) translocation involving *T-cell receptor α /Myc* (Timakhov, Tan et al. 2009), we hypothesized that the increased survival in KD mice could be associated with a decrease in translocation frequency. FISH screening for t(14;15) in thymic pre-T LBL cells from 11 WT and 8 KD mice (Figure 14) revealed a slight increase in translocations in KD cells (50% versus 45% in WT; Figure 15). Four (36%) WT pre-T LBL and 4(50%) KD pre-T LBL did not have the translocation and two WT tumors (18%) had three *Myc* signals (trisomy 15). MYC expression levels were similar in WT and KD tumor cells without the translocation, and were lower in pre-tumor thymocytes (Figure 15). The similar proportion of t(14;15) observed in the WT and KD tumors suggests that the increased survival in the KD mice is not associated with a decrease in *Myc* translocation.

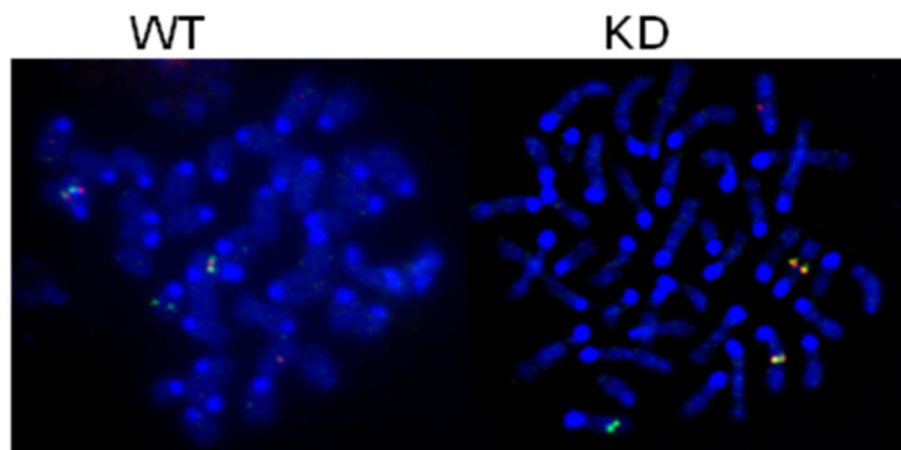


Figure 14: *TCR α /Myc* translocations in WT and KD mice. Representative metaphase spreads from WT and KD tumor cells with the t(14;15) at 100X magnification. *Myc* signals are green and *Tcra* signals are red. Juxtaposed green and red signals (yellow) were indicative of the t(14;15) recombinant chromosomes.

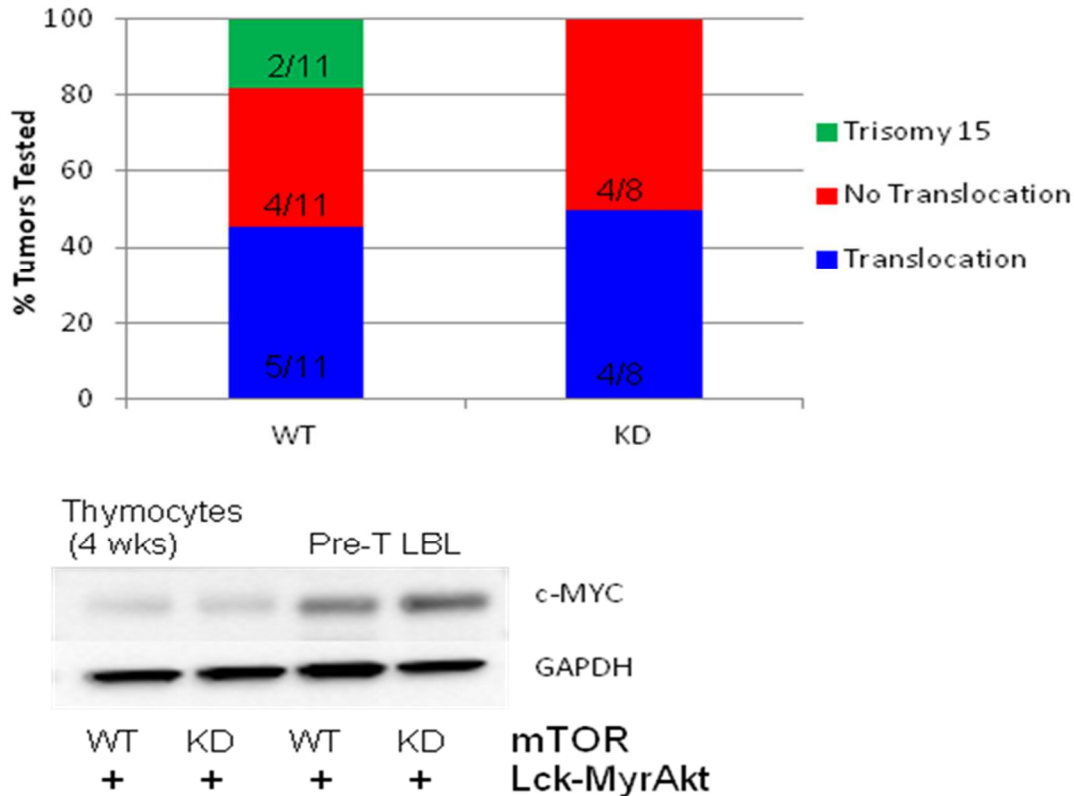


Figure 15: Proportions of *TCR α /Myc* translocations and MYC protein levels in WT and KD pre-T LBL. Percentages of WT (n=11) and KD (n=8) tumors with or without *Tcra/Myc* translocation by FISH. MYC protein levels in representative WT and KD pre-tumor thymi (from 4-week-old mice) and pre-T LBL are shown.

In parallel, Lck-Akt mice with WT mTOR were treated biweekly with 20mg/kg everolimus (RAD001, n=12) or vehicle (n=10), beginning at 8 weeks of age and continuing for 8 weeks or until signs of tumor progression. Mice treated with everolimus had significantly improved survival ($p < 0.001$, Log Rank Test, median survival: 155d versus 73.5d in vehicle-treated, Figure 16), echoing results seen in the genetic mTOR KD mice. As the everolimus treatment was begun after neoplastic transformation occurred in these mice, this result suggests that mTOR inhibition delayed tumor progression, but did not alter the populations from which the tumor arose (as supported by the thymic flow cytometry results in the genetic mTOR KD mice).

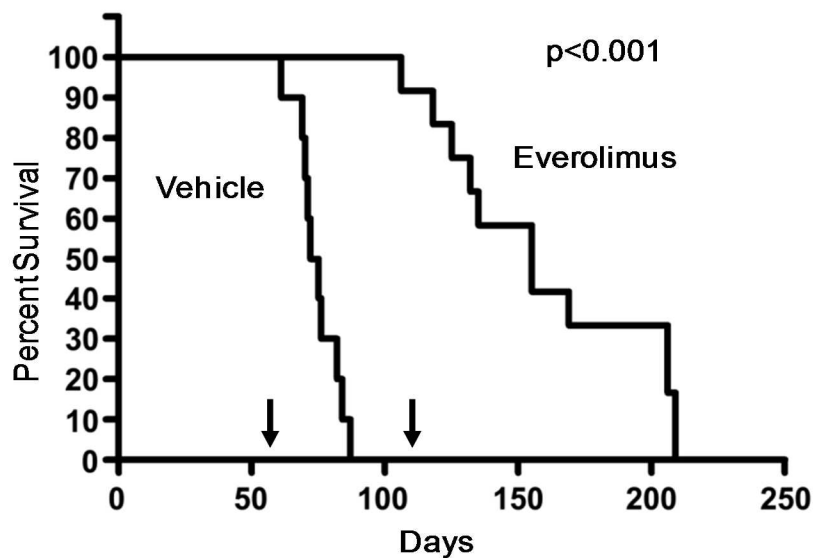


Figure 16: Survival curve from Lck-Akt mice treated with a mTOR inhibitor (everolimus). Lck-Akt transgenic mice were treated by gavage with everolimus (20 mg/kg twice weekly; n = 12) or vehicle (50 μ l PBS; n = 10) starting at 8 weeks of age. Treatment of both groups continued for 8 weeks or until mice showed signs of illness. Arrows indicate start and completion dates of the drug treatment. Survival was evaluated by Kaplan-Meier survival analysis and a Log Rank test ($p < 0.001$).

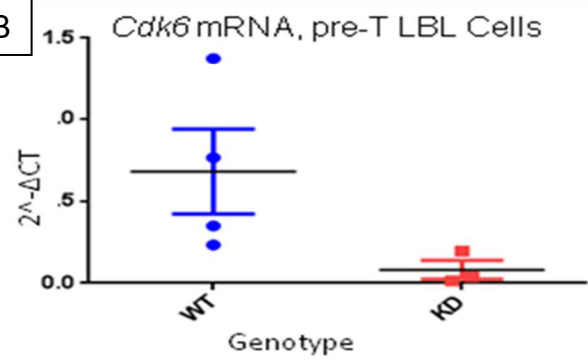
CDK6 is decreased in KD thymic pre-T LBL. To elucidate possible mechanisms explaining the increased survival in KD mice, we performed gene expression profiling on thymic pre-T LBL tumors from both WT and KD mice. Transcriptional profiling revealed 98 differentially-expressed genes; 49 up-regulated and 49 down-regulated ($p < 0.05$, fold change > 1.5 or < -1.5 , and $FDR < 0.1$; Figure 17A). *Cdk6* was one of the most down-regulated genes in lymphomas from KD mice ($p = 0.001$, fold change = -7.7, $FDR = 0.06$); both *Cdk6* transcripts (Figure 17B) and CDK6 protein levels (Figure 17C,D) were decreased in lymphomas from KD mice. By contrast, WT tumors had increased levels of CDK6, and pre-tumor thymi from WT and KD mice had similar, low levels of CDK6 protein (Figure 17D), suggesting that the decrease in CDK6 occurred during tumor development in KD mice. The reduced CDK6 expression in KD pre-T LBL was

not attributable to differential expression of the *Cdk6* regulator p16Ink4a (*Cdkn2a*), as its expression was similar at the RNA and protein level in WT and KD tumors (Figure 18). In contrast, expression of cyclin D1 and cyclin D3 (the main activator of CDK6) proteins were higher in KD compared to WT lymphomas, and like CDK6, CDK4 and cyclinD3 were not differentially expressed in the WT and KD pre-tumor thymocytes (Figure 19). Levels of the cell cycle inhibitors, p21 and p27 (CDKN1A and B) were also increased in the KD pre-T LBL cells (p27 increased in 2 out of 3 KD tumors, Figure 17C, Figure 19); increased levels of p21 have previously been reported with pharmacologic CDK4/6 inhibition (Paternot, Colleoni et al. 2014), and p27 phosphorylation and localization are reported to be regulated by mTOR (Hong, Larrea et al. 2008). The results suggest a possible mechanistic relationship between chronically low levels of mTOR and subsequently low levels of CDK6 during tumor development/maintenance.

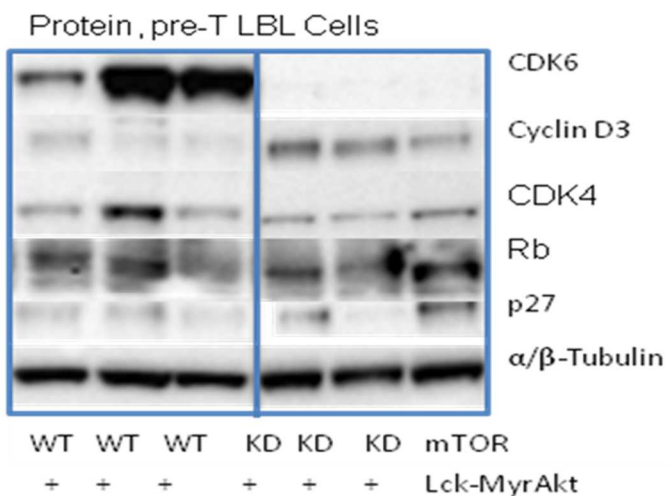
A



B



C



D

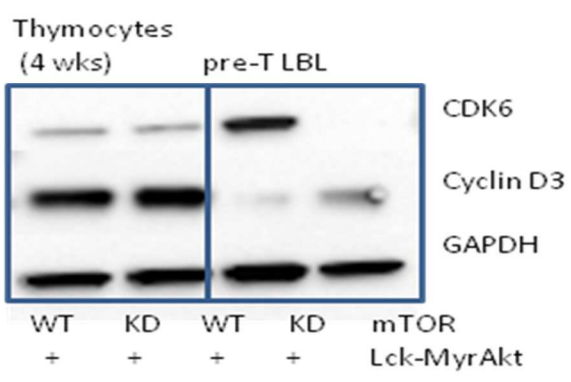


Figure 17: Transcript and protein levels of CDK6 and protein expression of other cell cycle regulators in WT and KD thymic pre-T LBL.

Figure 17 (cont'd): **A.** 98 genes were differentially expressed between WT (n=4) and KD (n=3) thymic lymphomas, as shown in a heat map from microarray results (green=down regulated, red=up regulated). One gene, *Cdk6*, is highlighted. **B.** Levels of *Cdk6* transcripts were evaluated in WT (n=4) and KD (n=3) pre-T LBL cells by RT-PCR. **C.** Also shown are CDK6, CDK4, cyclin D3, RB, and p27 protein levels in 3 WT and 3 KD pre-T LBL cells. **D.** CDK6 and cyclin D3 protein expression levels were compared between pre-tumor thymi and pre-T LBL in representative WT and KD mice.

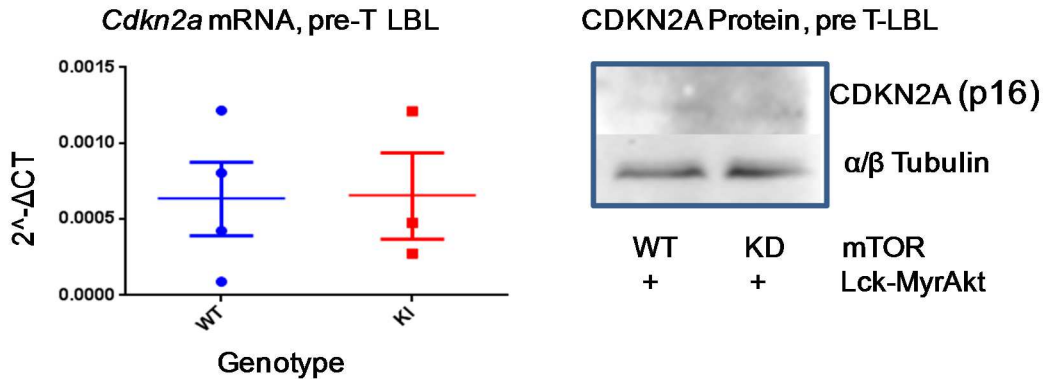


Figure 18: Protein and transcript levels of *Cdkn2a* (p16) in WT (n=4) and KD (n=3) tumors. Levels of *Cdkn2a* (p16) mRNA by RT-PCR, as well as CDKN2A (p16) protein levels in representative WT and KD pre-T LBL tumors by immunoblot.

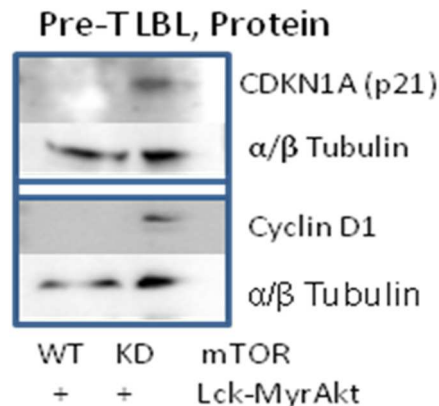


Figure 19: Levels of CDKN1A (p21) and cyclin D1 protein in a representative KD tumor compared to a WT tumor.

Murine pre-T LBL is sensitive to inhibition of mTOR and/or CDK4/6. To test whether pharmacologic reductions in mTOR in pre-T LBL tumor cells mimicked the effects of reduced CDK6 expression seen in KD tumors, we treated pre-T LBL cell lines derived from WT and KD mice with the mTOR inhibitor, rapamycin (1nM, 48h). Both

WT and KD cells were sensitive to rapamycin (post-treatment viability: WT=20%, KD=30%; Figure 20A), suggesting that chronically low mTOR levels did not lead to rapamycin resistance in the KD tumors. Notably, CDK6 levels were decreased in rapamycin-treated WT cells, showing that acute inhibition of mTOR signaling decreases CDK6 levels in neoplastic T-cells (Figure 20B), providing further support for a mechanistic relationship between low mTOR and low CDK6 levels. Because the pre-T LBL tumors in the WT and KD mice differentially expressed CDK6 (Figure 17), we explored the consequences of inhibiting both CDK6 and CDK4 in cell lines from these tumors (no specific CDK6 inhibitor is available). We treated WT and KD pre-T LBL cells with increasing doses of the CDK4/6 inhibitor PD-0332991 (palbociclib, Pfizer) for 24 hours. Both WT and KD tumor cells showed similar decreases in viability with increased doses of the CDK4/6 inhibitor (Figure 21). Treatment of WT pre-T LBL cells with both rapamycin and PD-0332991 led to a G1 arrest (approximately 80% of cells in G1, compared to approximately 65% in G1 in untreated cells, Figure 23), while rapamycin treatment induced a higher rate of apoptosis than PD-0332991 treatment (approximately 50% compared to 20% in untreated cells and 30% in cells treated with PD-0332991, Figure 22).

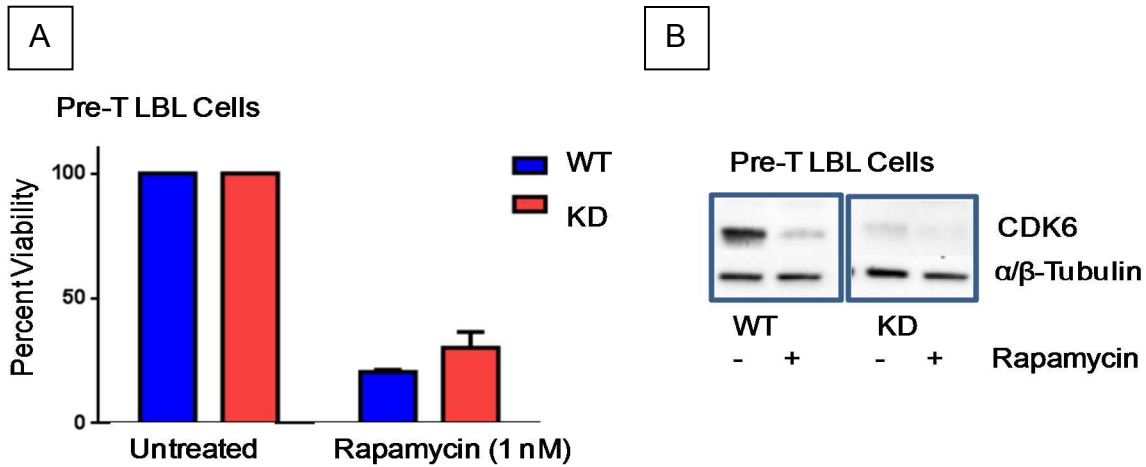


Figure 20: Viability and CDK6 protein levels from WT and KD thymic pre-T LBL cells treated with rapamycin. **A.** WT and KD thymic pre-T LBL cells (n=3/group) were treated in culture with 1 nM rapamycin, and percent cell viability in relation to untreated cells was assessed at 48 hours. The experiment was repeated twice, with four technical replicates per experiment. Representative data from one experiment is shown, with error bars indicating the standard error of technical replicates. **B.** Levels of CDK6 protein were evaluated after 48 hours of treatment with 1nM rapamycin in cell lines established from WT and KD pre-T LBL tumors. Representative WT and KD cells lines are shown.

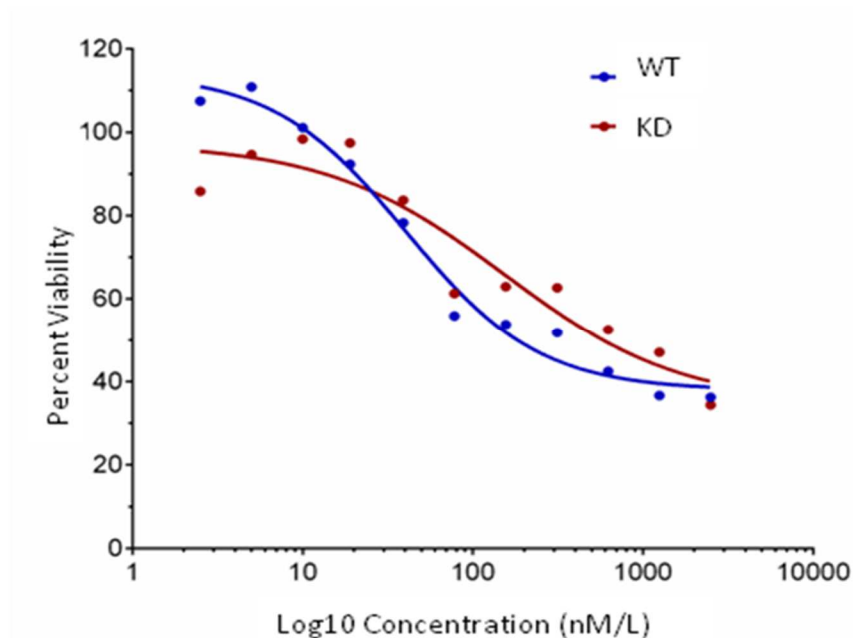


Figure 21: Viability of WT and KD pre-T LBL cells with increasing doses of a CDK4/6 inhibitor (PD-0332991). WT and KD pre-T LBL cells were treated for 24 hours with a CDK4/6 inhibitor (Pfizer PD-0332991) over a range of doses. The experiment was performed twice, and a representative experiment is shown.

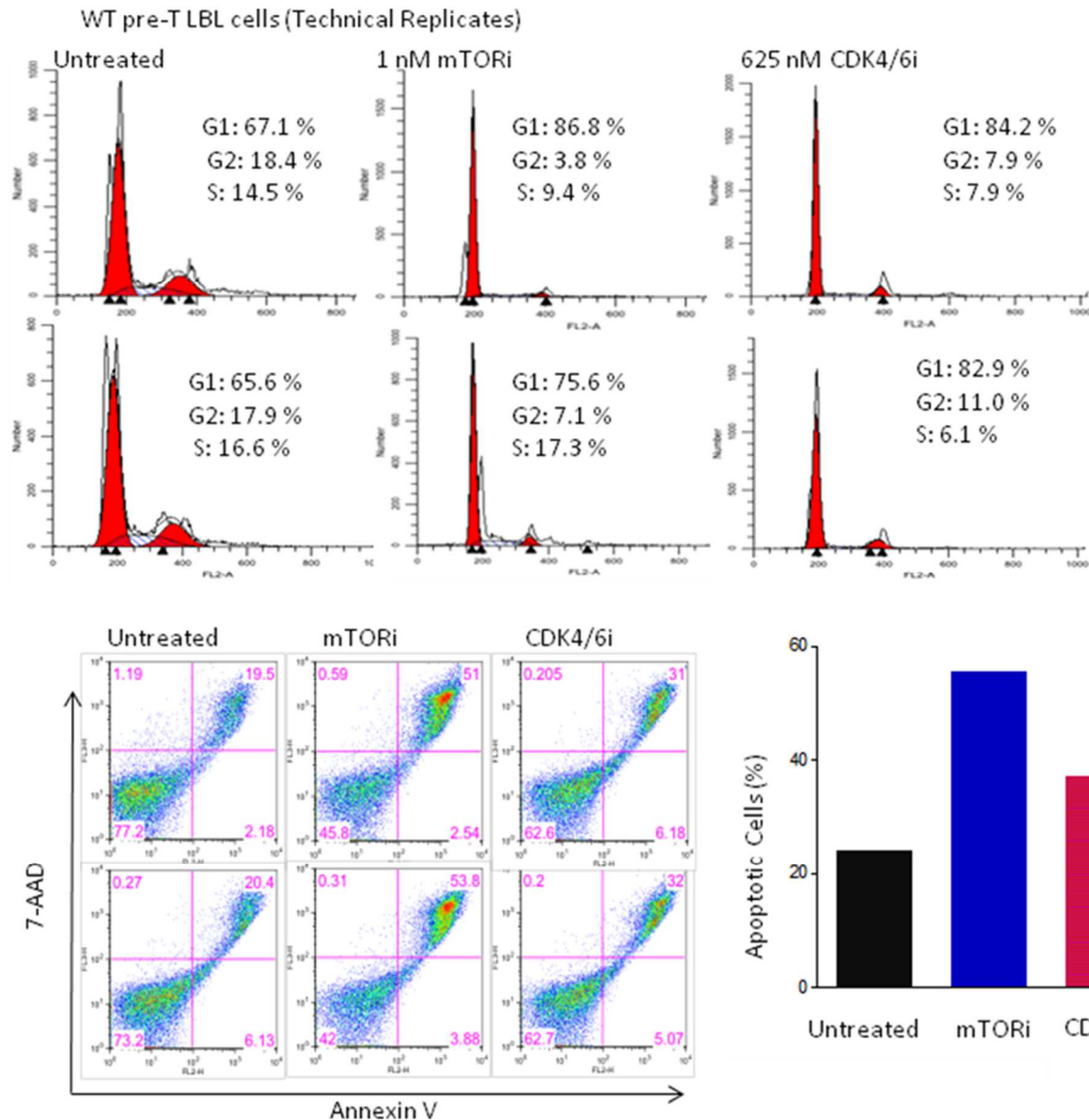


Figure 22: Cell cycle and apoptosis were analyzed post treatment with a mTORi and a CDK4/6i in mTOR WT pre-T LBL cells. WT thymic pre-T LBL cells were treated with 1 nM rapamycin (mTORi) and 625 nM PD-0332991 (CDK4/6i) for 48 hours, and cell cycle and apoptosis were evaluated by flow cytometry. Technical replicates are shown in this figure.

Given that decreased mTOR and CDK6 levels in KD pre-T LBL were associated with prolonged survival in the KD mice, we treated WT pre-T LBL cells with a combination of rapamycin (1nM) and PD-0332991(500nM), as well as each individual

drug. WT tumor cell viability was decreased to a greater extent by the combination than by each single agent (Figure 23).

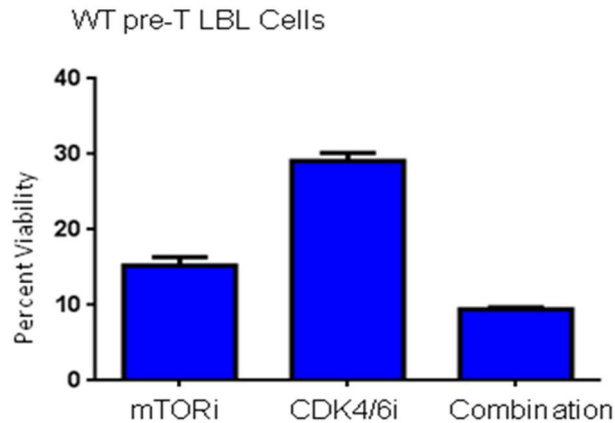


Figure 23: Percent viability of WT thymic pre-T LBL cells treated with a mTORi, a CDK4/6i, and a combination of the two inhibitors. WT thymic pre-T LBL cells were treated for 48 hours with 1 nM rapamycin (mTORi), 500 nM PD-0332991 (CDK4/6i), and the combination of the two compounds. Percent viability shown is in comparison to untreated cells. The experiment was repeated twice, with four technical replicates per compound (Error bars=SEM for technical replicates in the representative experiment).

The combination of CDK4/6 and mTOR inhibition is cooperative in human T-

ALL/LBL cell lines. Genetic and pharmacologic inhibition of mTOR in murine pre-T

LBL had an associated decrease in CDK6 and delayed tumor progression; the

combination of a mTOR inhibitor and a CDK4/6 inhibitor also decreased viability in

murine pre-T LBL cells. As a result, we examined the combined effect of these two

inhibitors in a series of human T-ALL/LBL cell lines. Human T-ALL and T-LBL fall under

the same WHO classification, and have minor variations based on bone marrow

involvement and differential gene expression; these tumors share morphological,

immunophenotypic and genetic similarities (Hoelzer and Gökbuget 2009). We treated T-

ALL/LBL cell lines with PD-0332991 and rapamycin in a combination dose matrix. Dose

responsive combination activity on cell viability was evident in all of the cell lines (Figure 24A) and was reinforced by positive excess of inhibition as shown by Excess over Highest Single Agent graphs (EOHSA; Figure 24B). Synergy Combination Index scores were calculated and are available in Figure 25 (CI<1 is synergistic). Phospho-RB^{S780}, the downstream target of CDK6, was reduced to a greater extent in the presence of the combination compared with its reduction when the lines were treated with PD-0332991 alone (Figure 26A). This result suggests that the concentration of PD-0332991 used did not fully inhibit CDK4/6 activity and that rapamycin cooperated with PD-0332991 in reducing the level of phospho-RB. Rapamycin has also been reported to decrease phospho-RB in breast cancer cell lines that express HER-2 (García-Morales, Hernando et al. 2006). Total RB levels were also decreased by PD-0332991 and the combination in all of the cell lines (except for Jurkat), as previously reported [Figure 26B, (Fry, Harvey et al. 2004, Dean, Thangavel et al. 2010)]. Levels of CDKN1B (p27) protein were similar across treatments for all cell lines, except for an increase in p27 in P12 cell line with combination treatment (Figure 26B).

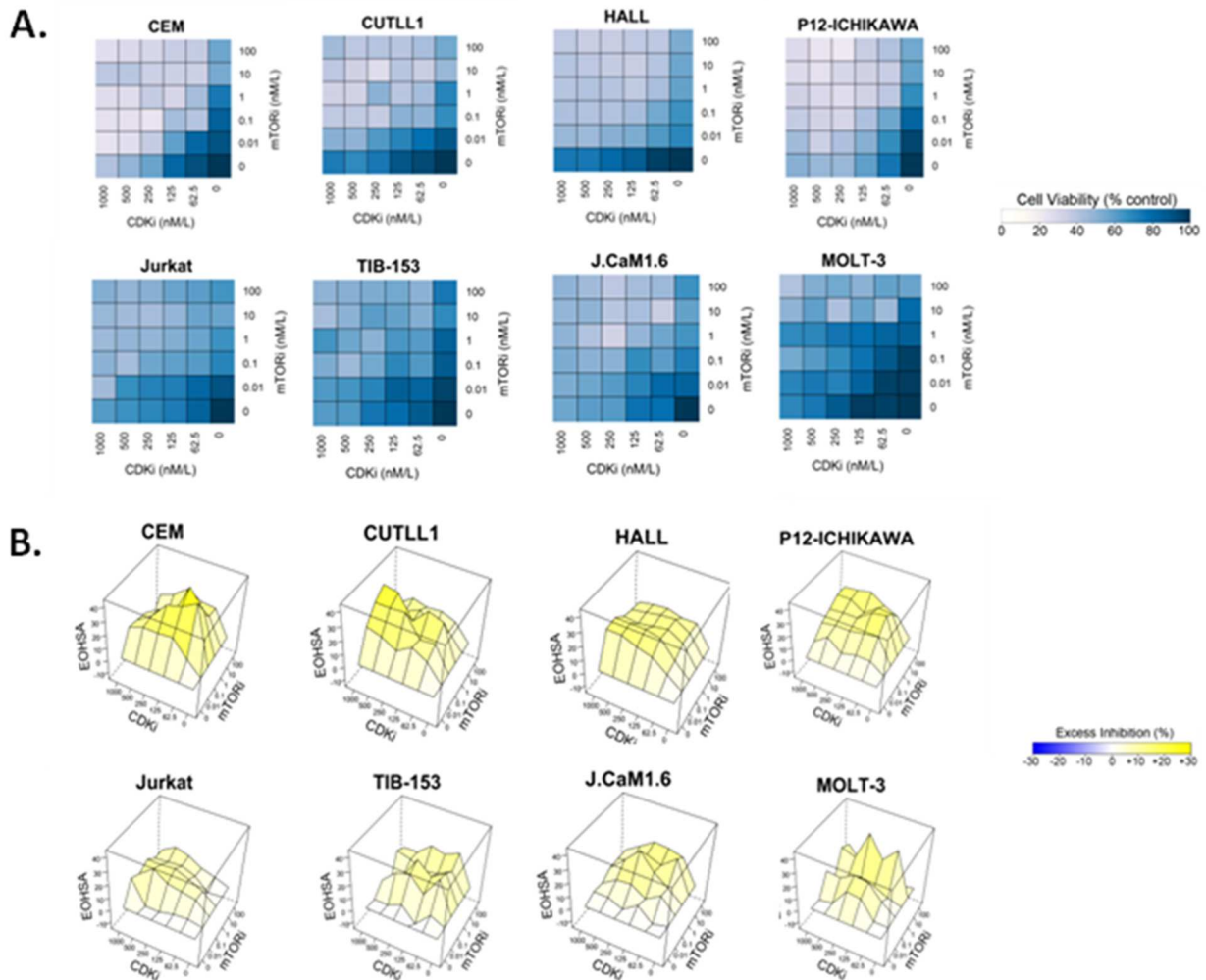


Figure 24: Activity of the combination of a CDK4/6 inhibitor (PD-0332991) and a mTOR inhibitor (rapamycin) evaluated in human T-ALL/LBL cell lines. A. Heat maps of 48-hour viability relative to control in 8 T-ALL/LBL cell lines (CUTLL1, CEM, Jurkat, J.CaM1.6, TIB153, HALL, MOLT3, and P12 Ichikawa) treated in matrix format with a range of five doses of rapamycin (mTORi, 0nM to 100nM, increasing 10-fold for each dose) and five doses of PD-0332991 (CDK6i, 0nm-1 μ M, starting at 62.5nM and increasing 2 fold for each dose) individually and in combination (matrix dose response screen). Lighter blue squares represent lower viability, while darker blue is high percent viability. Values are averaged results from 4 replicate experiments. **B.** Graphs showing the Excess over Highest Single Agent (EOHSA) for T-ALL/LBL cell lines treated with increasing doses of PD-0332991 and rapamycin, representing the difference in viability between cells treated by the single agent and the combination at each dose.

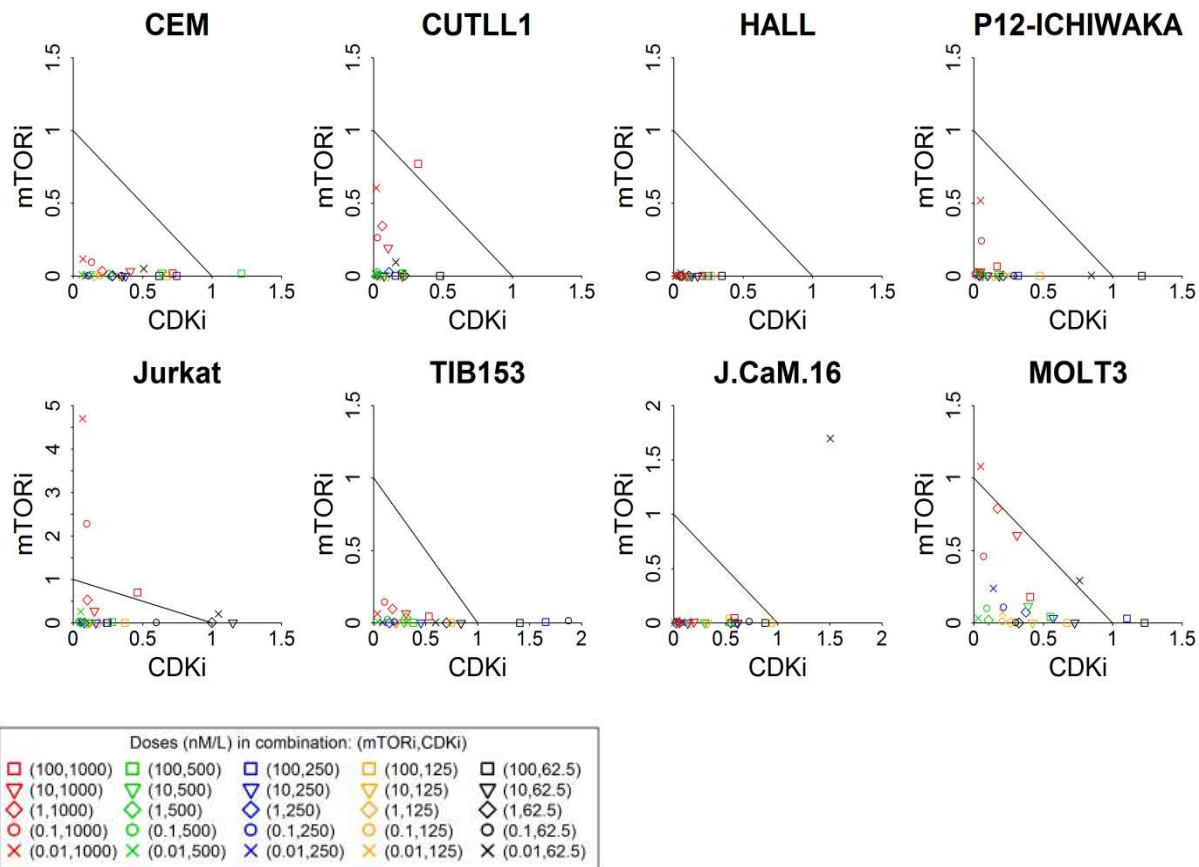


Figure 25: Combination index of T-ALL/LBL cell lines treated with a mTORi (rapamycin), a CDK4/6i (PD-0332991), and a combination of the two agents. The IC₅₀ normalized isobolograms generated with CompuSyn (Chou 2005) based on the median-effect and Combination Index (CI) equations for the nonconstant ratio combination design (Chou 2006). The diagonal line represents the additive effects of drugs (CI=1); data points below and above the additivity line correspond to synergistic (CI<1) and antagonistic (CI>1) effects of specific dose combinations, respectively.

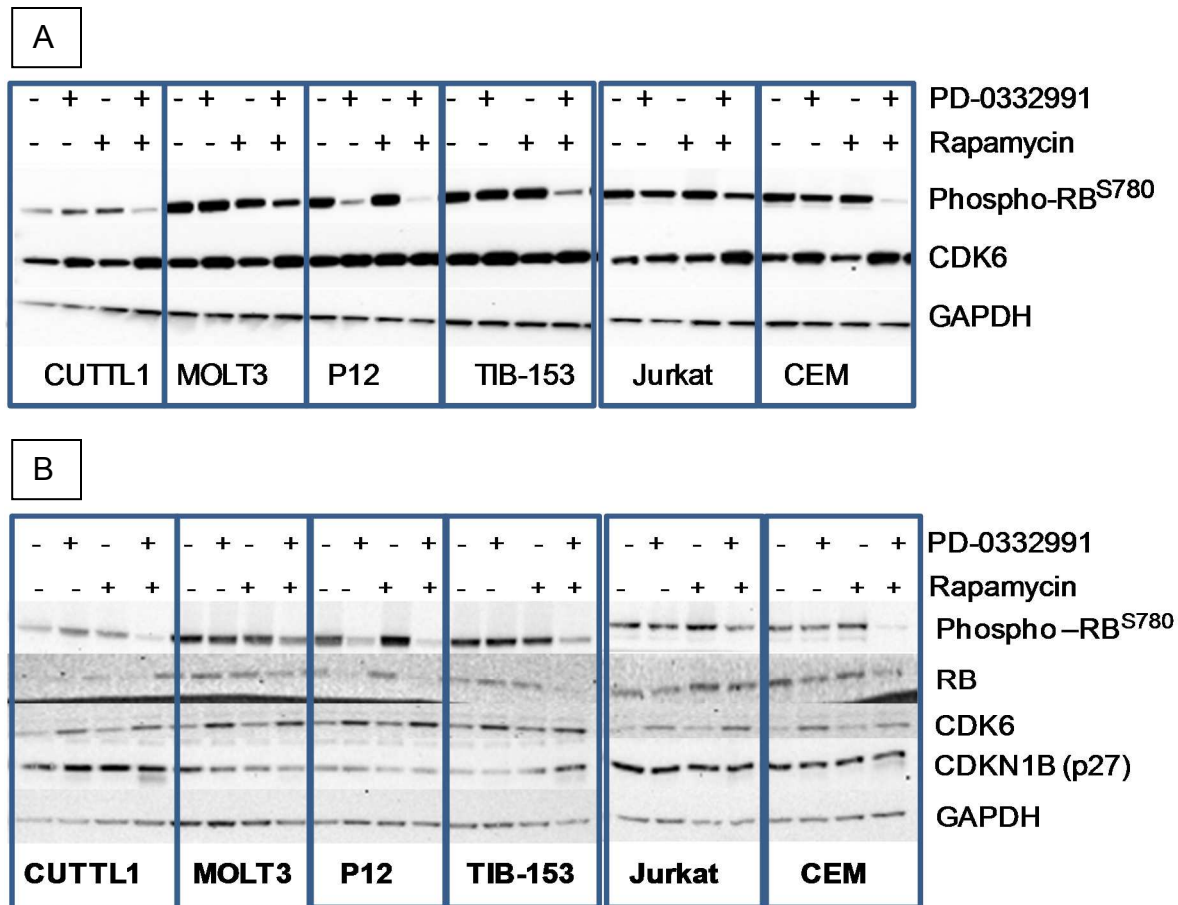


Figure 26: Cell cycle proteins from six T-ALL/LBL cell lines treated with PD-0332991, rapamycin, and the combination of the two agents. Western blots from six T-ALL/LBL cell lines treated with 500nM PD-0332991 and 1 nM rapamycin, or the combination of the two agents for 48 hours. Samples were run on two different gels due to space restrictions on the gel. Figures A and B represent duplicate experiments.

Although rapamycin induced lower levels of CDK6 in the mouse lymphoma cells (Figure 20), it did not do so consistently in the human T-ALL/LBL lines (Figure 26A and B). PD-0332991 alone and in combination led to increased CDK6 levels in the human lines. As expected, treatment of the T-ALL/LBL lines with 1nM rapamycin or the combination decreased the phosphorylation of mTOR target, ribosomal protein S6^{S240/244} (Figure 27). Phospho-AKT^{S473}, however, was also increased in some of the T-ALL/LBL lines treated with PD-0332991 or combination treatment (Figure 27).

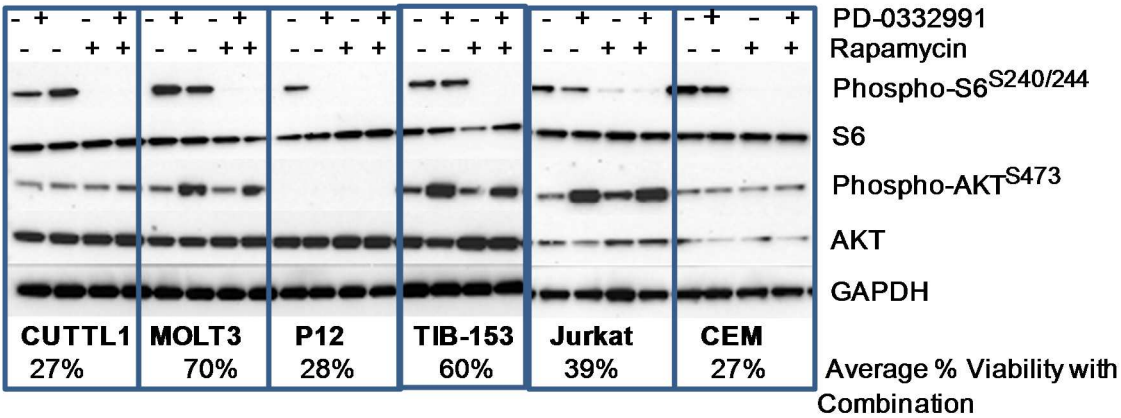


Figure 27: Downstream targets of mTOR, phospho-ribosomal S6^{S240/244} and phospho-AKT^{S473} were evaluated in T-ALL/LBL cell lines treated with 1 nM rapamycin, 500 nM PD-0332991, and the combination of the two agents. Average percent cell viability over 4 replicates when treated with the combination of 1nM rapamycin and 500nM PD-0332991 is listed below the immunoblot images for each cell line.

To determine whether pharmacologic inhibition of both mTORC1/2 might abrogate the effects seen on phospho-AKT, the dual TORC1/2 kinase inhibitor PP242 was evaluated in combination with PD-0332991 in a subset of the T-ALL/LBL cell lines (CEM, TIB-153, Jurkat, and MOLT-3; Figure 28). Treatment with 1nM rapamycin alone or in combination with 500nM PD-0332991 served for comparison. With increasing doses of PP242 (0-2.5 μ M), viability was decreased in all cell lines compared to treatment with PD-0332991 alone (Figure 28). However, compared with the combination of rapamycin plus PD-0332991, the dual inhibitor was only mildly more potent in two (CEM and TIB-153) of the four lines tested. When signaling was examined in TIB-153, the most notable difference was the absence of phospho-AKT^{S473} in cells treated with the PP242/PD-0332991 combination, and its presence in cells treated with the rapamycin/PD-0332991 combination (Figure 29). In addition, phospho-RB was also

decreased to a greater extent by this combination. This difference is likely attributable to the suppression of mTORC2 by PP242.

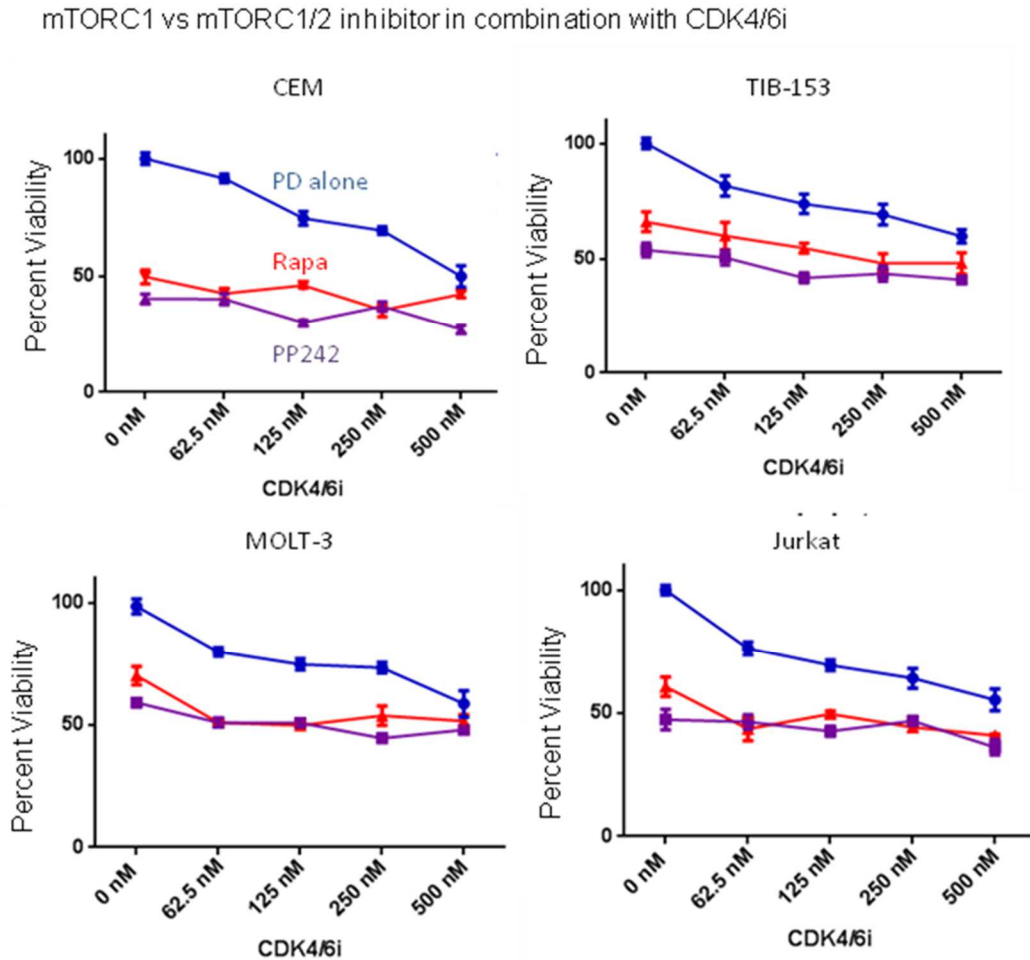


Figure 28: Four representative T-ALL/LBL cells lines treated with increasing doses of a dual mTOR inhibitor, PP242, or a mTORC1 inhibitor, rapamycin, in combination with increasing doses of a CDK4/6 inhibitor (PD-0332991) for 48 hours. Percent viability is in comparison to untreated cells. These results are the average of two replicate experiments.

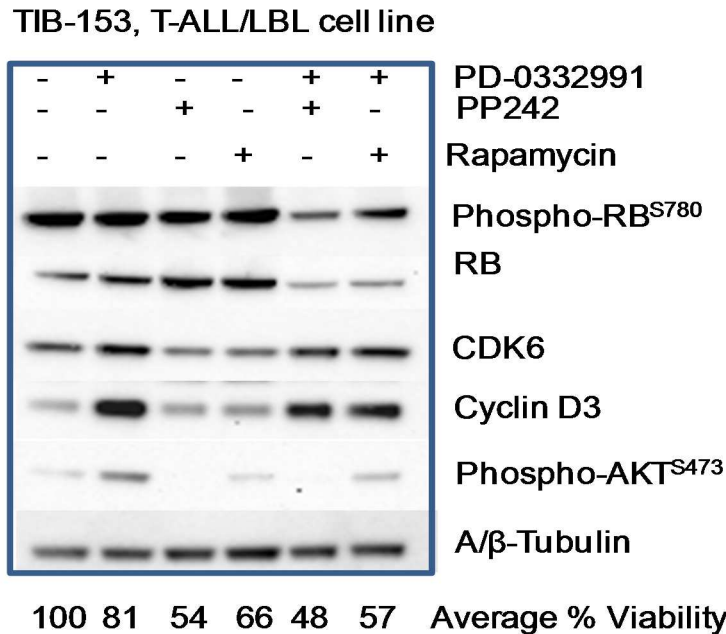


Figure 29: Immunoblot analysis of one T-ALL/LBL cell line (TIB-153), evaluating phospho-RB, RB, CDK6, cyclin D3, and phospho-AKT^{S473} after treatment with the combination of PP242 (1.25 μ M) and the CDK4/6 inhibitor (500 nM), as well as the combination of rapamycin (1 nM) and the CDK4/6i (500nM). Average percent cell viability from duplicate experiments for each treatment condition are listed below the immunoblot images.

Discussion

As the constitutive ablation of mTOR in mice leads to embryonic lethality, development of a viable mTOR knock-down mouse has made it possible to study the genetic effects of mTOR knock-down in vivo. Previously described phenotypes of this mouse include an increased lifespan, provided the animals are protected from infectious stressors, as their B-cell development is impaired (Zhang, Readinger et al. 2011, Wu, Liu et al. 2013, Zhang, Pruitt et al. 2013). Here, we used a constitutively-active *Akt2* allele under control of a T-cell-specific promoter (*Lck*) to examine susceptibility of the mTOR knock-down mouse to development of pre-T LBL. *Lck-Akt/mTOR* KD mice lived substantially longer (2mo.) than their *Lck-Akt/mTOR* WT littermates. As a similar proportion of the WT and KD mice died with thymic lymphoma (75% vs. 71%,

respectively), it may be inferred that, compared with the WT mice, lymphoma development in the KD mice may have been delayed and/or that the lymphomas were less aggressive.

Although mTORC1 and mTORC2 are both continuously inhibited in the mTOR KD mouse, pharmacologic treatment of the Lck-Akt/mTOR WT mice with the mTORC1 inhibitor, everolimus, before and during lymphoma development was able to phenocopy the increased lifespan of the Lck-Akt/mTOR KD mouse, although the KD mice lived longer than the everolimus treated mice. The importance of mTORC1 activity was also recognized in a different mouse model with inactivated mTORC1 and mTORC2 (Hoshii, Kasada et al. 2014). In that report, a mutant K-ras gene that induced both T-cell leukemia and a myeloproliferative neoplasm (MPN) was evaluated in mice whose mTORC1 component Raptor or mTORC2 component Rictor was genetically disrupted. Raptor disruption prevented the T-cell leukemia, but not MPN, while Rictor disruption did not prevent either disease (Hoshii, Kasada et al. 2014). mTORC1 inactivation through deletion of Raptor also suppressed death in a Notch-driven mouse model of T-ALL/LBL (Hoshii, Kasada et al. 2014). Our findings here, which evaluate AKT-driven pre-T LBL, strengthen the inference that development of thymic pre-T LBL may depend on mTOR.

CDK6 protein was reduced in the mTOR KD lymphomas and treatment of WT pre-T LBL with rapamycin also led to reduced CDK6, highlighting the mechanistic role of mTOR in affecting CDK6 levels in the tumors. In contrast to CDK6, expression cyclin D3 was lower in WT tumors compared with KD tumors. These differences were limited to lymphomas, as the two proteins had similar expression in the WT and KD pre-tumor

thymi. It is tempting to speculate that the differences in CDK6 and cyclin D3 expression were selected during lymphomagenesis. Since pre-T LBL from the WT and KD mice were susceptible to pharmacologic inhibition of mTOR and CDK4/6 and they share similarities with human T-ALL/LBL, including upregulation of the PI3K/AKT pathway, we tested the sensitivity of human T-ALL/LBL lines to combined inhibition of mTOR and CDK4/6 pathways. CDK4/6 inhibitors, including PD-0332991, are in clinical trial for a variety of cancers, including acute leukemias (Choi and Anders 2014). CDK4/6 inhibition is particularly relevant because primary human T-ALL/LBL samples have high levels of CDK6 protein by immunohistochemistry (Chilosi, Doglioni et al. 1998), and cyclin dependent kinase inhibitors such as Cdkn1a (p21), 1b (p27) and Cdkn2a (p16) are often deleted or absent by immunohistochemistry in T-ALL/LBL (Yamada, Hatta et al. 1997). In addition, Notch activating mutations, which occur commonly in T-ALL/LBL, can induce the expression of cyclin D3, which, when it interacts with CDK6, leads to aberrant cell cycle progression (Hu, Deshpande et al. 2011, Sawai, Freund et al. 2012). In this study, the human T-ALL/LBL cell lines evaluated had relatively high baseline levels of CDK6 and phospho-RB proteins. Furthermore, we found that the combination of the mTOR inhibitor, rapamycin, and the CDK4/6 inhibitor, PD-0332991, was active and cooperative in all eight T-ALL/LBL cell lines examined. In breast cancer, combined treatment with PI3K and CDK4/6 inhibitors has been found to be synergistic, especially in tumors that harbor *PIK3CA* mutations (Vora, Juric et al. 2014), underlining the potential relevance of combination treatment of neoplasms with hyperactive PI3K/ATK/mTOR and CDK4/6 signaling. One potentially important signaling effect of the combination of mTOR and CDK4/6 inhibitors in the T-ALL/LBL lines was the decreased

levels of phospho-RB. In addition, our data suggest that, when used in combination with the CDK4/6 inhibitor, PD-0332991, a dual mTORC1/mTORC2 inhibitor, PP242, may reduce the levels of phospho-RB and phospho-AKT as well as the viability of some, but not all, T-ALL/LBL lines to an even greater degree than the combination of PD-0332991 and the mTORC1 inhibitor, rapamycin. The potential therapeutic advantage of adding an mTORC1/TORC2 inhibitor in combination with CDK4/6 inhibition should be considered in the treatment for T-ALL/LBL.

CHAPTER 4- A rare, naturally occurring SNP in *Mtor* (C1977T) is associated with increased sensitivity to stress at the cellular and organismal level

Introduction

mTOR, the mechanistic target of rapamycin, is a serine/threonine kinase at the center of numerous cell signaling pathways involved in cell growth, energy metabolism, protein and lipid synthesis, and autophagy. mTOR belongs to a family of serine/threonine kinases (Phosphatidylinositol 3-kinase-related kinases (PIKKs)) that includes ataxia-telangiectasia mutated (ATM), ataxia- and Rad3 related (ATR), and DNA-dependent protein kinase catalytic subunit (DNA-PKcs) [(Lempiainen and Halazonetis 2009), (Hardt, Chantaravisoot et al. 2011)], which are integral members of the stress and DNA damage repair (DDR) signaling pathways. The role of mTOR in DDR, however, has not been clearly elucidated. In yeast, TORC1 signaling is needed for cells to progress through S-phase and for cell viability after genotoxic stress (Shen, Lancaster et al. 2007). In mammals, mTOR has been shown to incorporate stress signals, including low energy, hypoxia, and DNA damage, often through TSC1/2 [reviewed in (Laplane and Sabatini 2012)]. DNA damage, in particular, has been shown to signal mTORC1 through p53-dependent transcription, including induction of TSC2 and PTEN expression [(Feng, Zhang et al. 2005), (Stambolic, MacPherson et al.)], though the interactions between mTOR and p53 have proven to be complex and redundant. Evidence of mTOR's role in DDR is also found in neoplasia, where mTOR inhibitors have been reported to have a radiosensitizing effect, allowing the tumors to

respond more completely to radiation treatment, including soft tissue sarcomas (Murphy, Spalding et al. 2009), breast cancer (Albert, Kim et al. 2006), and pituitary adenomas (Vender, Dhandapani et al. 2011). The association between mTOR inhibition and increased sensitivity to irradiation supports the role of mTOR in DNA damage and cell stress responses.

Increased sensitivity to DNA damage can be an inherited phenotype. Many tumor syndromes are associated with mutations or alterations in genes involved in DDR, including Fanconi Anemia, Bloom's syndrome, and breast cancer families with BRCA1 mutations (Ford, Easton et al. 1994, Jackson and Bartek 2009). In mice, BALB/c mice, in particular, are hypersensitive to irradiation, with decreased survival post-irradiation (Roderick 1963, Okayasu, Suetomi et al. 2000), and a higher rate of radiation-induced mammary tumors (Yu, Okayasu et al. 2001). Mammary cells from BALB/c mice exposed to 3 Gy irradiation exhibited higher rates of chromosomal aberrations than cells from C57Bl/6 mice, especially in later passages (Ponnaiya, Cornforth et al. 1997). Similarly, skin fibroblast lines from a variety of mouse strains were evaluated for radiation-induced chromatin damage; fibroblasts from BALB/cAN had the highest number of chromatid breaks, and continued to have the most breaks 4-hours post irradiation (Potter, Sanford et al. 1988). Differences in chromatid breaks seen in skin fibroblasts from BALB/c mice versus DBA mice were linked to genes on chromosomes 1 and 4. Lower levels and activity of DNA-PKs associated with a polymorphism in the gene *Prkdc* (DNA-dependent protein kinase catalytic subunit) have also been proposed as a cause for decreased DDRs in BALB/c mice (Okayasu, Suetomi et al. 2000, Yu, Okayasu et al. 2001). In this study, we propose that a rare SNP

in the Chr 4 gene, *Mtor*, found in BALB/c and NZB mice is another possible cause for decreased DDRs in BALB/c mice.

Using our mouse model containing the BALB/c allele of *Mtor* (C1977T; R628C), we evaluated the effect of the altered variant of mTOR, which has an amino acid substitution at aa628 (628C). Specifically, we compared the role of the allelic variants R628 and 628C in response to three different types of stress (capable of putting selection pressure on neoplastic cells): inflammatory, genotoxic and oncogenic.

Materials and Methods

Mice. All animal studies were in compliance with NIH Animal Care and Use Committee Animal Study Protocol LG009. To explore the consequences of the single nucleotide polymorphism in mTOR naturally found in BALB/c mice, transgenic mice were created with a SNP (C1977T) in the *Mtor* gene through homologous recombination on a B6;129 background [knock in (Zhang, Readinger et al. 2011)]. These knock in mice were genotyped as previously described (Zhang, Readinger et al. 2011).

3 WT mice and 3 628C KI mice were injected intraperitoneally with 0.4 ml pristane and were euthanized after 7 days. Untreated WT and KI mice (3/group) served as controls and were collected at the same time. Spleens and bone marrow were collected fresh from these mice and processed for transcriptional analyses.

Six WT, 7 heterozygous (HET), and 7 628C KI male mice were irradiated at 8 Gy at approximately 60 to 75 days of age in a Gammacell 40 irradiator (Best Theratronics, Ottawa, ON, Canada). Mice were observed over time, and were collected at a humane endpoint. Survival was analyzed by a Kaplan-Meier survival curve and a Log Rank Test.

Another cohort of male WT (n= 57) and 628C KI (n= 39) mice were irradiated starting at 5 weeks of age with 1.75 Gy gamma irradiation, once weekly for 4 weeks. These mice were also observed over time for survival and for the formation of thymic lymphomas. Because the mice began to develop rectal prolapses, the feed was supplemented with metronidazole (138 mg/kg of chow, fed ad libitum) to eliminate causative infections.

Isolation of keratinocytes from newborn WT and 628C KI pups, expansion and Ras transformation of these keratinocytes, and grafting of the keratinocytes onto nude mice was performed by Christophe Cataisson of Stuart Yuspa's Laboratory (Laboratory of Cancer Biology and Genetics, NCI), as previously described (Lichti, Anders et al. 2008).

Microarray and RT-PCR. B220+ splenocytes and bone marrow cells were collected from WT and 628C KI mice. Three WT mice (2 females and 1 male) were untreated, three (2 females and one male) were treated with 0.4 ml pristane intraperitoneally and were harvested 7 days later. Spleens were crushed using the sterile end of a syringe plunger and dissociated cells were resuspended in cold 1X PBS and filtered through a 0.40 μ m sterile filter. ACK lysis buffer (Lonza, Walkersville, MD) was added to lyse red blood cells. B220+ splenocytes were then isolated using MS MACS separation columns and B220+ beads (Miltenyi Biotec, Auburn, CA) as recommended by the manufacturer. Bone marrow cells were collected by cutting off the ends of the femur bones and using a 30 $\frac{1}{2}$ G needle and 6 ml syringe to flush sterile, ice-cold PBS through the marrow cavity. ACK lysis buffer was used to remove red blood cells from the collected marrow contents. Cell pellets from B220+ splenocytes and bone marrow were flash frozen and stored at -80°C until RNA isolation.

RNA was isolated using Trizol reagent and the Qiagen RNeasy MiniElute Cleanup kit (Qiagen). 1 µg of RNA was labeled and amplified using the Message Amp-11-Biotin Enhanced Kit (Ambion, Life Technologies, Carlsbad, CA) per the manufacturer's instructions. RNA was hybridized to Affymetrix Mouse Genome 430 2.0 array cartridges at 45°C for 16 hours. Chips were washed in a GeneChip Fluidic wash station (Affymetrix, Santa Clara, CA) and scanned.

Partek software was used to analyze the .Cel files obtained when the arrays were scanned. Data were normalized to internal controls and an ANOVA comparing WT and 628C KI was performed. Significantly different genes between WT and 628C KI mice were selected with values for WT + KI signals > 100 (higher than background), p-values <0.05, and a fold change >1.5 or <-1.5. Principal component analyses were also performed in Partek.

Cell culture. Mouse embryonic fibroblasts (MEFs) were created from 13.5 day post conception WT and 628C KI embryos. The embryos were separated, the heads and internal organs removed, and the remaining tissues were macerated in 5 ml Trypsin-EDTA (Gibco, Life Technologies, Grand Island, NY). The dissociated tissue was incubated at 37°C in the Trypsin-EDTA for 15 minutes, and then the remaining fragments were pipetted up and down to break up the cell debris. Cells were cultured overnight in 10cm dishes in DMEM (Gibco) supplemented with 10% fetal bovine serum (FBS) and 1% penicillin-streptomycin (Gibco). Media was changed the following day, and MEFs were expanded for two passages and frozen for future use.

A subset of MEFs were transformed using the SV40 Large T Antigen. The pBAB2 -SV40 plasmid (shared by Dr. Andre Nussenzweig) was amplified in OneShot

TOP10 Chemically Competent *E. Coli* (Invitrogen, Life Technologies, Grand Island, NY) and isolated using the HiSpeed Plasmid Purification Midi and Maxi Kit (Qiagen, Venlo, Netherlands). The plasmid was first passaged through BOSC packaging cells co-transfected with the PCL2-eco- retrovirus packaging vector (shared by Dr. Andre Nussenzweig) with the addition of Fugene6 (Promega, Madison, WI). The BOSC cells produced virus for 48 hours, at which point viral supernatant was collected and mixed with 10 µg/ml polybrene (EMD Millipore, Billerica, MA). The polybrene-spiked viral supernatant was placed over plated MEFs, which were spun at 2500 rpm for 90 minutes. Selection was performed by the inclusion of 1 mg/ml G418 sulfate (Corning; Cellgro, Manassas, VA) in the media over several days. Transformed MEFs were expanded under antibiotic selection and viably frozen for downstream applications.

Transformed MEFs were used in colony formation assays, in which cells were plated in a 10cm dish, allowed to grow to confluency, and were irradiated at 2, 4, 6, or 8 Gy in a cesium sealed source irradiator (Shepherd model 68, dose rate approx 3 Gy/min). Irradiated cells were trypsinized and 1000 cells of each genotype treated with each dose were plated in 10cm dishes in triplicate. Colonies allowed to form over 10 days were fixed in ice cold methanol and stained with a 0.5% crystal violet solution in 25% methanol. Colonies of greater than 50 cells were counted. Colony counts for untreated and treated cells were used to calculate the plating efficiency [average # of colonies for the three untreated dishes per sample/1000 (the number of cells plated)] and the surviving fraction [average # of colonies for three dishes per sample/(1000*plating efficiency for sample)].

Comet Assay. Fresh bone marrow cells from WT and 628C KI mice were collected and samples were split in half. One half of the sample was irradiated at 6 Gy, and the other served as a control. Cells were spun down and resuspended in 37 degree low melting agarose (CometAssay LMAgarose, Trevigen, Gaithersburg, MD) following the manufacturer's instructions and were replated onto CometSlides (Trevigen). After lysis (in Lysis Solution, Trevigen) and unwinding (in an alkaline unwinding solution, 0.4g NaOH and 250 μ l of 200 mM EDTA), slides were placed into an alkaline electrophoresis solution (pH>13) in the CometAssay Electrophoresis II unit (Trevigen) and were electrophoresed for 30 minutes at 21 V, per the manufacturer's instructions. Slides were rinsed in 70% EtOH and deionized water and dried overnight. The following day, slides were stained with 1X Sybr Gold (Life Technologies) and imaged at 10X on a fluorescent scope. In captured images, at least 50 comets were scored using CometScore (TriTek Corporation). Comet analysis results are here reported as Tail moment, which is a measurement of tail migration distance as well as the percent DNA in the tail.

Immunoblotting, immunohistochemistry, and immunofluorescence. Primary MEFs were plated into 10cm dishes and allowed to expand for 1 passage. Cells were then plated in T25 flasks, which were irradiated once confluent. Media was removed and flasks were frozen at the appropriate time points. Lysis buffer, composed of 10% SDS, 1% tris, phosphatase inhibitor (PhosStop, Roche), and cOmplete protease inhibitor (Roche), was pipetted directly onto frozen cells, and a rubber scrapper was used to remove cells. The samples were then sonicated on high for 7.5 minutes, with 0.5 minutes on, 1 minute off intervals and were allowed to incubate on ice for 1 hour. Samples from both preparation methods were centrifuged at 12,000 rpm at 4°C for 20

minutes, and the supernatant, containing the proteins, was saved. Protein concentration was measured by BCA assay and 12 µg protein for each sample was electrophoresed on 4-12% Bis-Tris gels (Novex). Proteins were transferred to nitrocellulose membranes using the iBLOT (Invitrogen), and membranes were blocked in 10% milk/TBST (TBS plus .1% Tween-20) for 30 minutes at room temperature, incubated with primary antibody overnight in 5% BSA/TBST at 4°C, and incubated with secondary antibody in 5% milk/TBST for 1 hour. Rinsed membranes were incubated for 1 minute with Super Signal West Dura or Femto Extended Duration Substrate and were imaged using a Syngene Imager and the GeneSnap program from Syngene (Frederick, MD).

Immunohistochemical staining for cleaved caspase 3 was performed on 4% paraformaldehyde-fixed, paraffin embedded sections of small intestine and bone marrow from 3 irradiated WT and 3 irradiated 628C KI mice (irradiated at 8 Gy starting at 8 weeks of age). Slides were deparaffinized in xylene and rehydrated through graded alcohols. The slides were blocked in 3% hydrogen peroxide in methanol, and antigen retrieval was performed in a bath of pH 9.0 Target Retrieval solution (Dako, Atlanta, GA) incubated in a hot vegetable steamer (steam retrieval) for 15 minutes. Slides were allowed to cool, and then incubated with Background Buster (Innovex Biosciences, Richmond, CA). The primary antibody was used at a concentration of 1:300 in antibody diluent (Dako) overnight at 4°C. After rinsing in 1X PBS with .02% Tween-20 (Sigma-Aldrich), slides were incubated with goat-anti rabbit secondary antibody (Dako) conjugated with biotin. The slides were incubated with ABC reagents (Vector Laboratories, Burlingame, CA), rinsed, and then incubated with DAB for 7 minutes

(diaminobenzidine, Dako). Slides were counterstained with hematoxylin. The stained slides were dehydrated through graded alcohols and xylene, cover slipped, and imaged with the AT2 slide scanner (Aperio, Leica Biosystems, Buffalo Grove, IL). The ImageScope color deconvolution algorithm (Aperio, Leica Biosystems) was used to analyze the amount of positive pixels from DAB labeling (categorized as strong, moderate, and weak labeling) in the bone marrow and in the crypts of the small intestine.

Primary WT and KI MEFs were plated onto chamber slides pre-treated with L-lysine and allowed to adhere overnight. Slides were irradiated and media was removed at the appropriate time point. Cells were fixed in 4% paraformaldehyde, rinsed, and blocked with 1X PBS containing 1% BSA. MEFs being stained for F-actin were incubated with Texas red-conjugated phalloidin (Life Technologies) and mounted with Vectashield mounting media containing DAPI (Vector Laboratories). MEFs to be labeled for PKC α were permeabilized with 0.01% TritonX-100, blocked with 10% goat serum in 1X PBS, and labeled with the PKC α antibody (1 to 400 dilution) overnight at 4°C. The slides were rinsed and incubated with the secondary antibody, conjugated to FITC, and coverslips were mounted with Vectashield mounting media + DAPI. Slides were imaged with an Olympus Fluorescent scope at 40X.

Flow cytometry and proliferation. Apoptosis of irradiated MEFs was evaluated at 3 hours and 18 hours post 4 Gy irradiation using the PE Annexin V Apoptosis Detection Kit 1 and cell cycle was analyzed using PI/RNase staining buffer (Becton Dickson, San Jose, CA). Cells were analyzed using FACSCalibur (Becton Dickinson), and FlowJo (Ashland, OR).

Irradiated embryonic fibroblasts were plated at 10,000 cells/well in a 96 well plate and imaged every 6 hours starting 4 hours after 4 Gy irradiation in the intra-incubator imaging system, Incucyte (Essen Biosciences, Ann Arbor, MI).

Results

Characterization of 628C KI mice. To predict the effect of the rare single nucleotide polymorphism (SNP, C1977T) in *Mtor* found in BALB/c mice, which leads to an amino acid substitution (R628C), the SNP was introduced onto a B6;129 background through homologous recombination and the effects of injection with pristane were evaluated. CBC/chemistry panels and histology of multiple tissues before and after pristane treatment were within normal limits (Figure 47, Appendix A). Evaluation of downstream targets phospho-4E-BP1, phospho-S6, and phospho-AKT revealed inconsistent differences in the ability of mTOR to phosphorylate downstream targets in the spleen of both untreated and pristane-treated WT and 628C KI mice (Figure 48, Appendix A). As such, the consequences of the 628C amino acid substitution on the function of protein remained unclear.

The expression levels of microRNAs in the B220+ splenocytes of untreated and pristane-treated WT and 628C KI mice were also evaluated. Nanostring microRNA analysis (which uses molecular barcodes for individual miRNAs similar to a microarray) was performed on RNA isolated from B220+ splenocytes of both 628C KI and WT mice. Three microRNAs, miR-30a, miR-101, and miR-423-5p, were significantly increased in splenocytes of untreated KI versus WT mice by Nanostring (Figure 49, Appendix B). No differences were found in these miRNAs in the pristane-treated animals. All three miRNAs were predicted to regulate members of the mTOR pathway by Ingenuity

Pathway Analysis (IPA, Qiagen). The trend of up regulation of these miRNAs in KI mice, as seen by Nanostring, was similar in RT-PCR evaluation in multiple animals, but was not statistically significant, bringing into question the role of miRNAs for this model (Figure 49, Appendix B).

Finally, because mTOR is involved in cellular metabolism, we assessed the levels of glycolysis in mouse embryonic fibroblasts (MEFs) using Seahorse XF Glycolysis Stress Test, both primary and immortalized by SV40 (transformed) in WT, mTOR KD, and 628C mTOR KI fibroblasts. In transformed fibroblasts, glycolysis (as measured by the glycolytic capacity) was significantly decreased in mTOR KD cells compared to mTOR WT cells (Figure 50, Appendix C), though there was no difference in glycolysis in untransformed MEFs. Further experiments were not pursued since differences were not noted between untransformed WT and KI MEFs.

Predicted effects of 628C allele. To predict the effect of the 628C aa substitution on the function of the protein mTOR, two computer algorithms were used. The algorithms used by the site Polyphen [<http://genetics.bwh.harvard.edu/pph/> (Adzhubei, Schmidt et al. 2010)] reported a 99% probability that the mutation is damaging to the protein. Similarly, the algorithm used at the Panther database [<http://www.pantherdb.org>; (Huaiyu Mi 2012)] describes a probability of 93% that the mutation is deleterious. Based on modeling performed by Aron Marchler-Bauer and Gabi Marchler, in the Conserved Domain Database group (NCBI, NIH), the amino acid substitution is predicted to fall within a HEAT domain of the protein. HEAT domains are sites in proteins that tend to form curves; they are also often sites of protein-protein interaction (Perry and Kleckner 2003), suggesting that this amino acid substitution may affect

protein-protein binding. A SNP leading to an amino acid substitution at the same location in the protein mTOR (amino acid 628) has been reported in human colon cancer [COSMIC, Catalog of the Somatic Mutations In Cancer, <http://cancer.sanger.ac.uk/cancergenome/projects/cosmic/> (Forbes, Bindal et al. 2011)]; the arginine was replaced by a histidine, and was again predicted to be deleterious to protein function (Polyphen, Panther).

Transcriptional differences in cells exposed to inflammatory stress. Because mTOR has been associated with plasma cell tumor formation in BALB/c mice after intraperitoneal (IP) pristane injection, we examined the transcriptional profile of bone marrow and B220+ splenocytes (splenic B-cells) 7 days after IP pristane injection. Microarray analysis revealed 268 differentially expressed genes between pristane-treated wild-type mTOR mice (WT), and knock in 628C mTOR mice (KI) in B220+ splenocytes (141 upregulated and 127 downregulated in KI), and 2511 differentially expressed genes between WT and KI whole bone marrow (902 upregulated and 1609 downregulated in KI). Principal component analysis of differentially expressed genes indicated the largest difference between WT and KI cells in the bone marrow from pristane-treated mice (Figure 30), so we chose to focus on the bone marrow. Ingenuity Pathway Analyses (IPA, Qiagen), a knowledge-based network analysis tool, identified enriched networks in differentially expressed genes from the bone marrow of pristane-treated mice (Table 2 and Appendix D). DNA replication, recombination, and repair was a top enriched pathway (number of molecules = 182, p-value range = 1.87 E -02 to 2.31E-06; subnetworks and individual p-values displayed in Appendix D). We chose to focus on DNA replication, recombination, and repair because of mTOR's association

with the DNA damage response (DDR), the sensitivity of BALB/c mice to DNA damage, and the relevance of DNA damage to cancer.

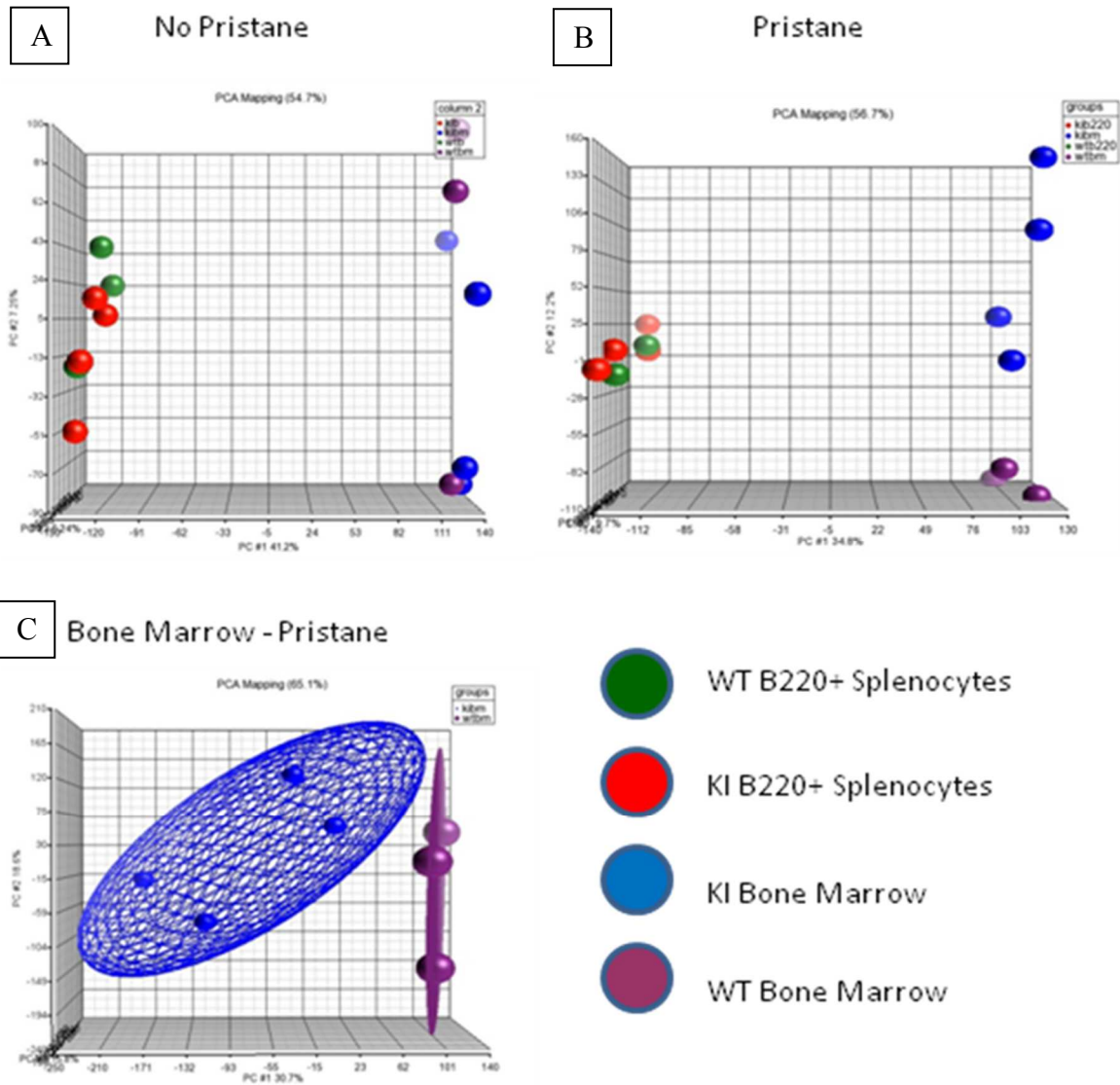


Figure 30: Principal components analyses of genes from tissues of the non-pristane-treated animals (A), pristane-treated animals (B), and bone marrow of pristane-treated animals (C); the genes are most different in the pristane-treated bone marrow. KI is short for 628C knock in mice, and WT is short for wild-type animals.

Table 2: Top enriched molecular and cellular function networks in bone marrow from pristane-treated animals identified by Ingenuity Pathway Analysis. P-values are listed as a range because each network includes subnetworks, which have individual p-values. Subnetworks and individual p-values displayed in Appendix D.

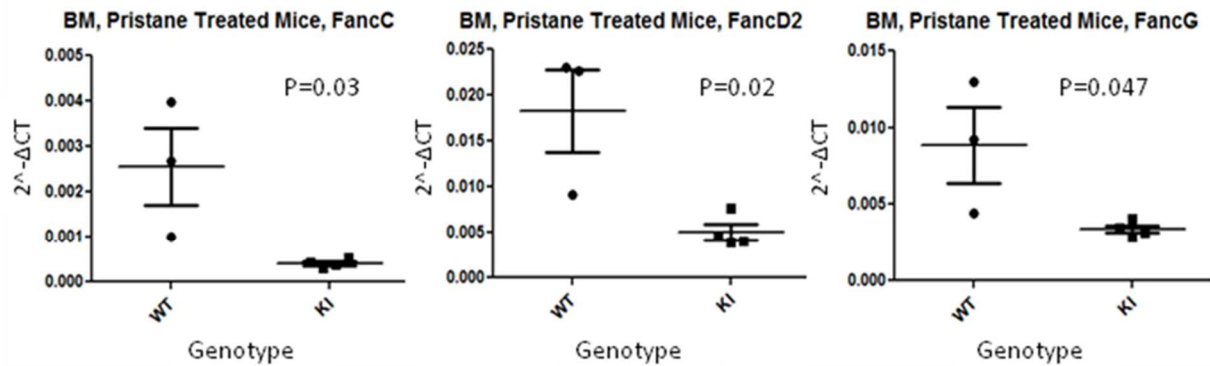
	Top Enriched Networks in BM	P-Values	# of Molecules
1	Cell Morphology	1.91E-02 to 2.09 E-08	184
2	Small Molecule Biochemistry	1.78E-02 to 5.35E-06	108
3	DNA Replication, Recombination, and Repair	1.87E-02 to 2.31 E-06	182
4	Molecular Transport	1.38E-02 to 8.39E-06	59
5	Gene Expression	1.15E-02 to 1.02E-05	49

Of the differentially expressed genes identified by IPA in the DNA replication, recombination, and repair network, several genes fell under the category of DDR (Table 3, Appendix D, Table 6). Many of these genes were downregulated in the 628C KI mice. Of these genes, loss of *Fancd2*, *Fancg*, *Wrm*, and *Brca1* are associated with decreased DDR and increased tumor formation in human patients (Ford, Easton et al. 1994, Niedernhofer, Lalai et al. 2005, Jackson and Bartek 2009). FANCD2 in particular, is a hub in the network of Fanconi Anemia proteins, which are involved in interstrand crosslinking DDR (Niedernhofer, Lalai et al. 2005). A decrease in expression of Fanconi anemia genes *Fancd2*, *Fancc*, and *Fancg* was confirmed by real time PCR (RT-PCR) in samples from the bone marrow of pristane-treated mice used in the microarray, but was not consistently different in bone marrow from additional pristane-treated animals (Figure 31).

Table 3: Differentially expressed genes associated with DNA damage response (z score = 0.864, p-value of overlap = 0.002) identified by Ingenuity Pathway Analysis in bone marrow from pristane-treated mice. Fold change is for KI gene expression in relation to WT expression.

Gene	Fold Change	Gene	Fold Change	Gene	Fold Change
ALKBH8	-1.5	FANCD2	-1.892	RAD23A	-2.804
ATF2	-2.5	FANCC	-2.0	RBM38	-1.762
ATRX	-2.4	FANCG	-1.894	SIRT2	2.602
BRCA1	-1.941	HIPK1	-2.437	SOX10	-2.100
BTG2	-2.672	IKBKG	-1.926	STRA13	1.9
CASP9	-1.808	IRF3	1.823	STXBP4	-1.8
CHCHD6	1.8	MAPKAPK2	-1.6	TAOK1	-2.158
CHEK1	-1.878	MBD4	1.661	TLK2	-2.040
CIB1	1.741	MIF	1.874	TOP1	-3.933
CUL4A	-1.882	NEK1	-1.794	TRIP12	-1.6
DCK	-2.1	Paxip1	-1.652	UBE2T	1.531
DDIAS	-1.9	POLH	-4.417	WRN	-2.398
DTL	-2.4	PSME4	-2.2	YY1	-1.669

FANC genes in WT and KI Bone Marrow, confirmation in microarray samples



FANC genes in WT and KI Bone Marrow, additional animals

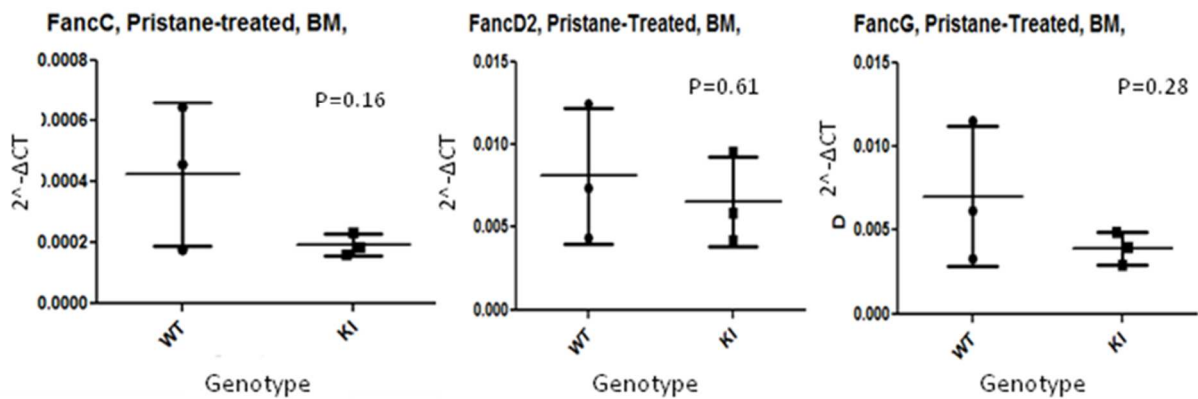


Figure 31: *Fancd2*, *Fancc*, and *Fancg* transcripts are lower in bone marrow from pristane-treated KI mice by RT-PCR in samples from microarray analysis, but not in additional animals. $2^{-\Delta\Delta CT}$ values for 3 individual WT and 4 KI samples are shown for each gene from the microarray, and 3 WT and 3 KI samples are shown for additional bone marrow samples. P-values are based on Student T-test.

Phenotypic changes associated with DNA damage. Because of the differential expression of DNA replication, repair, and response genes identified by transcriptional profiling in mTOR 628C KI mice, and because BALB/c mice, which carry the SNP in *Mtor*, are hypersensitive to DNA damage, we evaluated the response of the mTOR WT and 628C KI mice to DNA damage through a lethal total body irradiation (TBI) dose of 8 Gy. WT, heterozygous (HET), and KI mice were irradiated in 3 separate studies and were evaluated for survival. The KI mice had significantly decreased survival, with 20%

of KI mice surviving compared to approximately 80% of WT mice (Figure 32, representative experiment). Tissues collected at 18 days post irradiation revealed hemorrhage and severe pancytopenia in the bone marrow in both WT and KI mice (Figure 33). CBC revealed severe anemia (15 to 20%, normal range = 33-52%) and pancytopenia. Additional findings included testicular degeneration, lympholysis in lymph nodes, marked extramedullary hematopoiesis in the spleen with a large population of atypical, highly-proliferative round cells, likely erythroid or myeloid precursor repopulating the spleen and compensating for loss of bone marrow precursors.

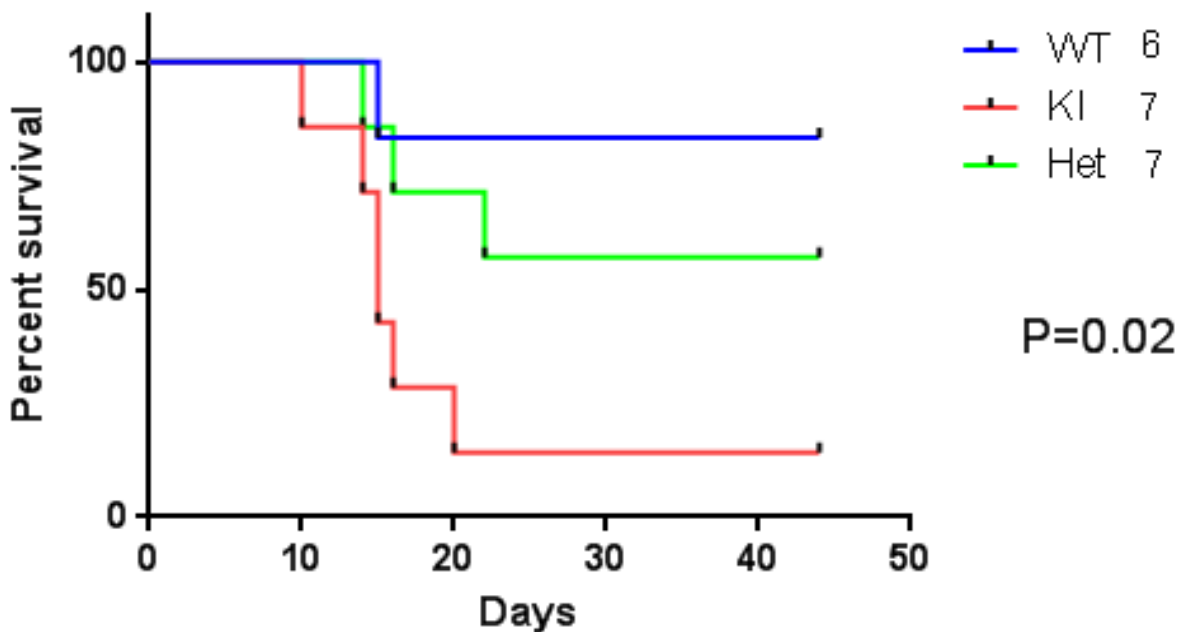


Figure 32: Kaplan-Meier survival curve for mTOR WT, heterozygous (Het), and 628C KI mice treated with 8 Gy gamma irradiation. P-value is from the Log-Rank test. A representative experiment is shown.

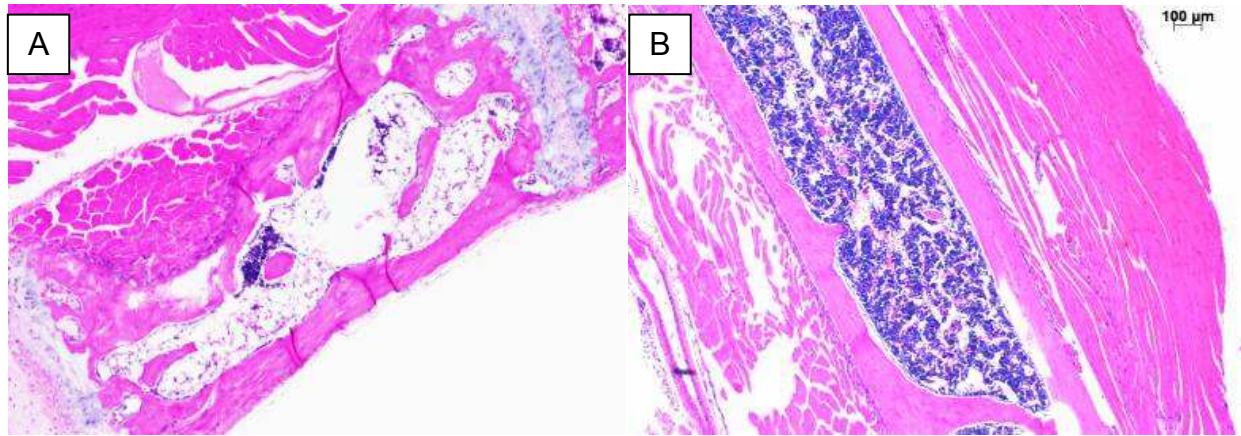


Figure 33: Severe bone marrow depletion (pancytopenia) in irradiated mice collected 18 days post 8 Gy total body irradiation (A), in comparison to untreated, aged-matched mice (B). Images taken at 10 X. Representative mice shown (findings are similar for WT and KI mice).

Apoptotic cells, characterized by pyknosis and karyorrhexis, were apparent in bone marrow and crypts of the small intestine, 3 hours post 8 Gy TBI, from both WT and 628C KI mice (n = 3 each). Immunohistochemical staining for cleaved caspase 3, a marker of apoptosis, and analysis by color deconvolution in Aperio ImageScope, showed no difference in levels of cleaved caspase 3 labeling between WT and KI mice in the bone marrow, and slightly less labeling in small intestinal crypts of KI mice, indicating a similar level of apoptosis in WT and KI mice at this time point post-irradiation (Figure 34).

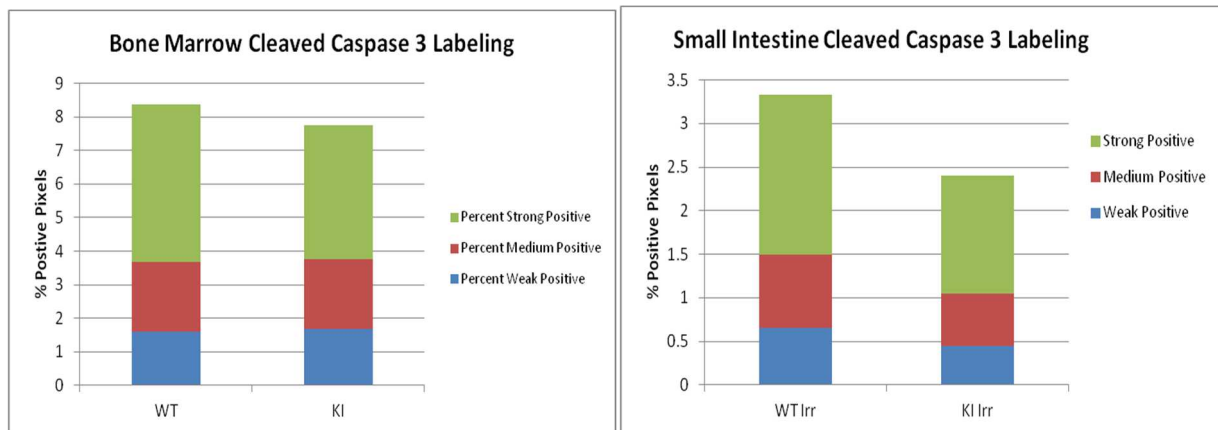
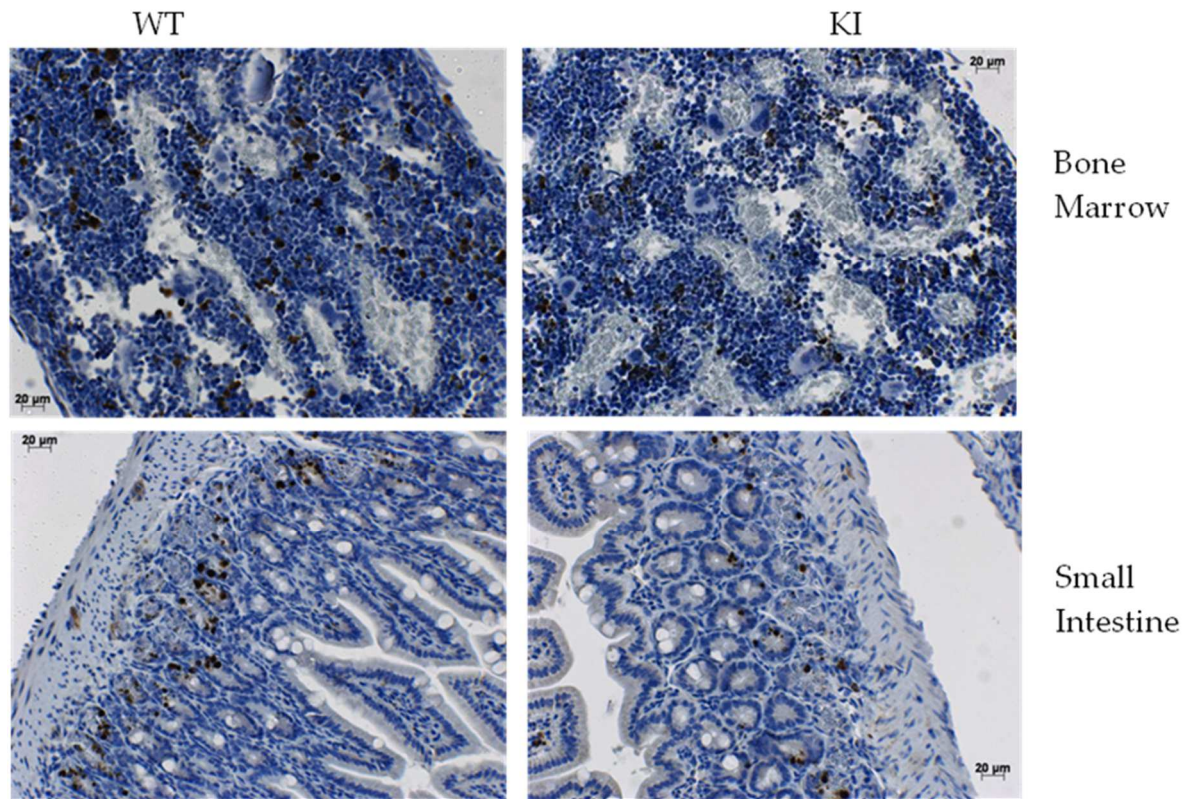


Figure 34: Cleaved caspase 3 labeling in WT and KI bone marrow and small intestines, with quantification of labeling by color deconvolution (% positive pixels). Sections of bone marrow and small intestine counterstained with hematoxylin and labeled with DAB. Labeling was characterized as strong positive, medium, and weak positive. Images captured at 20X on Aperio ImageScope.

Assessing DNA damage by Comet Assay in bone marrow treated ex vivo. Bone marrow cells from WT and 628C KI mice were collected. Each sample was divided in

two, and one half was irradiated ex vivo at 6 Gy and collected at 2.5 hours post-irradiation for analysis by Comet Assay (the untreated cells served as individual controls for each sample). The Comet Assay assesses the amount of DNA damage present in individual cells by suspending the cells in agarose and subjecting them to an electrical current. In cells with greater damage, fragmented DNA migrates farther through the agarose, creating a longer comet tail. In this assay, KI bone marrow cells had a greater average tail moment ($p = 0.1$) than WT cells, indicating greater DNA damage than WT bone marrow cells (Figure 35A,B).

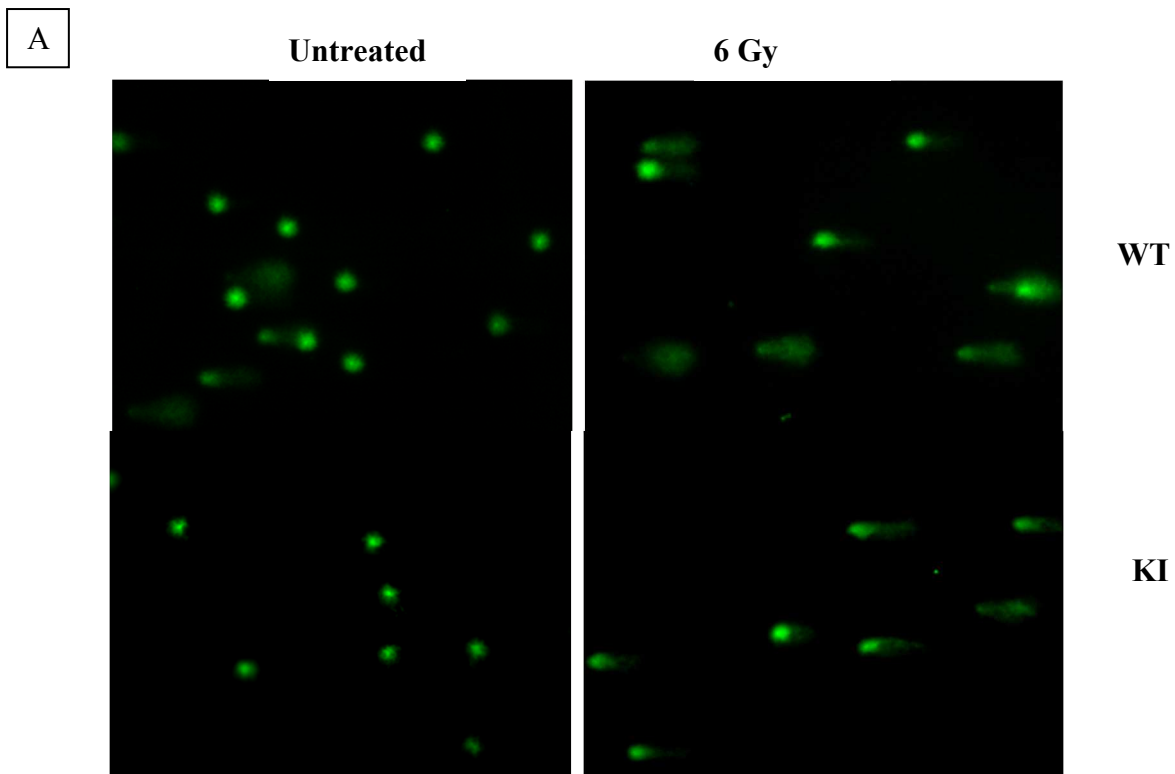


Figure 35A: Representative comets from untreated and irradiated (6 Gy) WT and 628C KI bone marrow cells 2.5 hours post irradiation.

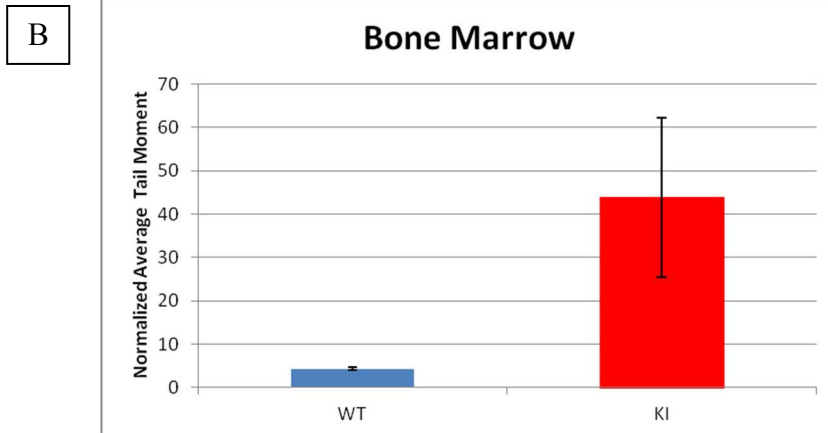


Figure 35B: Comparison of the average tail moment from WT and KI irradiated bone marrow cells. Error bars represent standard error and the average is for >50 comets/sample. Tail moments were normalized to untreated controls for each sample.

Assessing DNA damage by Comet Assay and micronuclei in mouse embryonic fibroblasts. Mouse embryonic fibroblasts (MEFs) were created from mTOR WT and 628C KI mice. MEFs were irradiated at 4 Gy and collected for Comet Assay directly after irradiation (5 minutes) and one hour post irradiation. Like the KI bone marrow, KI MEFs had a significantly greater average tail moment at 5 minutes ($p=0.001$, Student's T-test) and one hour ($p<0.001$) after irradiation, indicating increased damage and suggesting decreased repair of the damage (Figure 36).

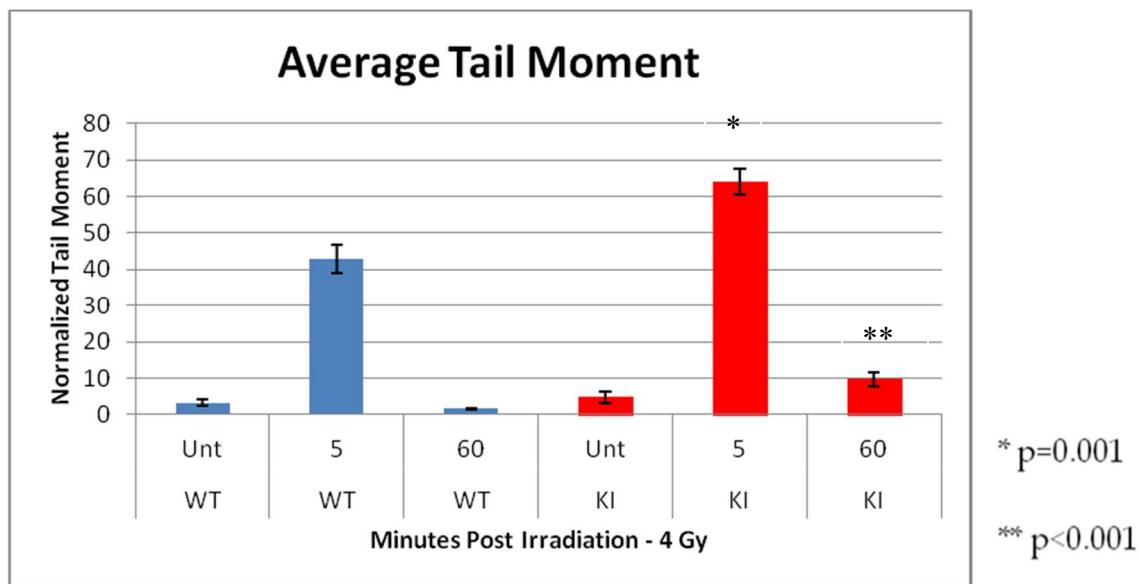
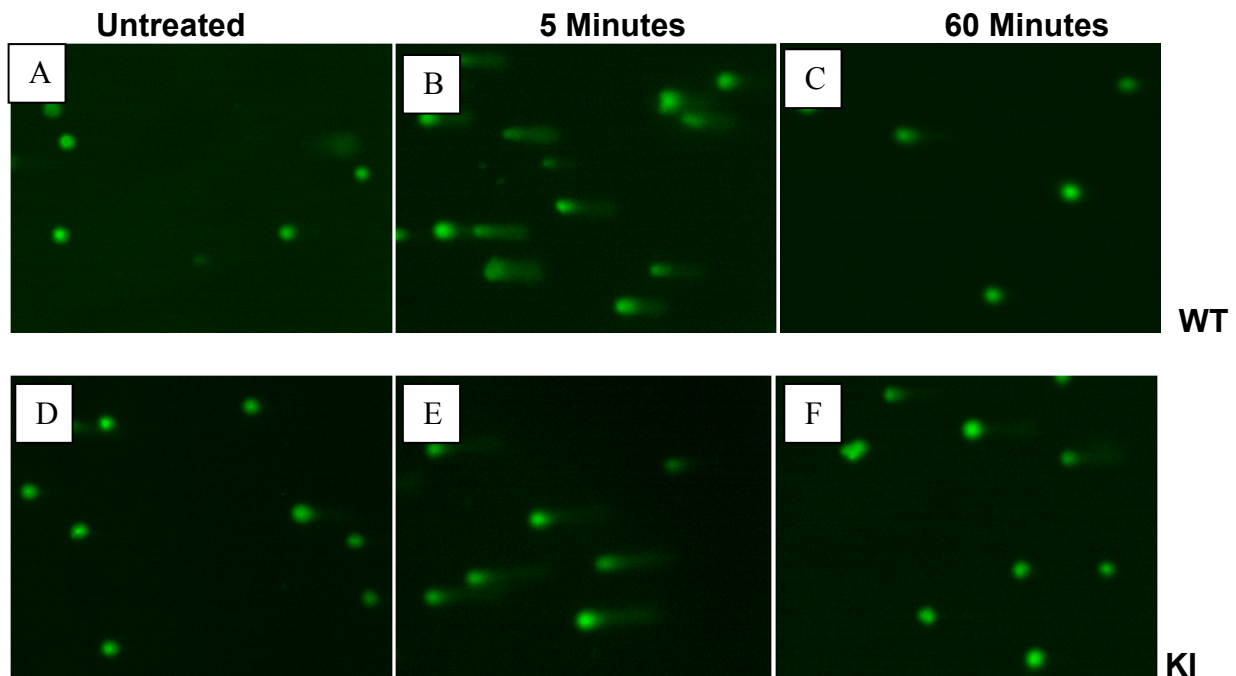


Figure 36: Representative comets from untreated and treated WT and KI MEFs at 5 minutes and one hour after 4 Gy gamma irradiation, and comparison of average tail moment from WT and KI MEFs at these time points. Time points with significantly different tail moments are marked with stars. Error bars represent the standard error of the mean from 50 assessed comets for each time point.

Finally, micronuclei are fragments of DNA that break off from the chromosomes during cell division when there is DNA damage in a cell (Fenech, Kirsch-Volders et al.

2011). Percent cells with multinuclei can be used as a measurement of DNA damage, and thus genotoxicity. Micronuclei were counted in 500 DAPI-stained nuclei from WT and 628C KI MEFs at each time point post 4 Gy gamma irradiation. At all time points post irradiation, KI MEFs had a greater percentage of cells with micronuclei, with the greatest difference between WT and KI occurring at later time points (12 and 24 hours, Figure 37), again suggesting greater DNA damage and less repair in 628C KI cells.

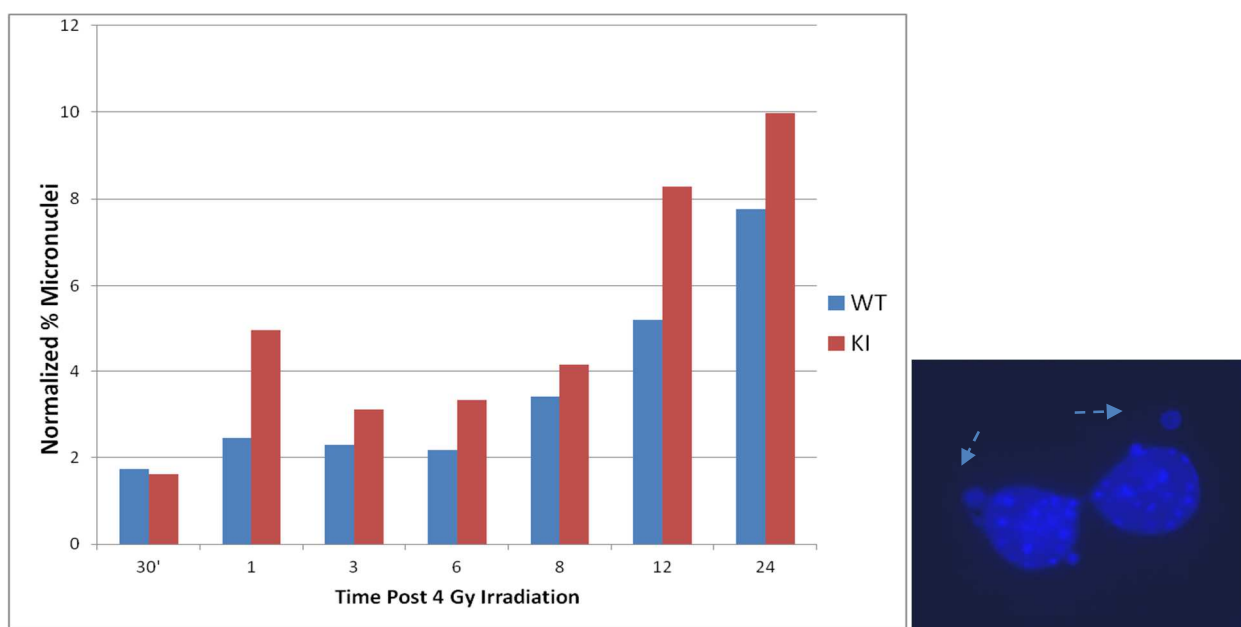


Figure 37: Percent cells with micronuclei for WT and KI MEFs irradiated at 4 Gy and collected at time points post irradiation. Percent cells with micronuclei out of 500 observed cells, normalized to untreated controls. Also pictured are representative DAPI stained nuclei with micronuclei (40X magnification). Blue arrows point to example micronuclei.

Assessing DNA damage by colony formation in transformed MEFs. Mouse embryonic fibroblasts (MEFs) from both WT and KI mice were immortalized with SV40 large T antigen and were exposed to a range of doses (0-8 Gy) of gamma irradiation. A low number of cells irradiated at each dose were plated and colonies were allowed to

form over 10 days. Stained colonies were counted and the surviving fraction was calculated for WT and KI MEFs. Fewer colonies developed in KI plates at each dose of irradiation (2 Gy, 4 Gy, and 6 Gy; Figure 38A). As such, KI MEFs had significantly lower surviving fractions at each dose of irradiation (2 Gy, $p = 0.007$; 4 Gy, $p = 0.001$; 6 Gy, $p = 0.006$; Student's T-test, Figure 38B).

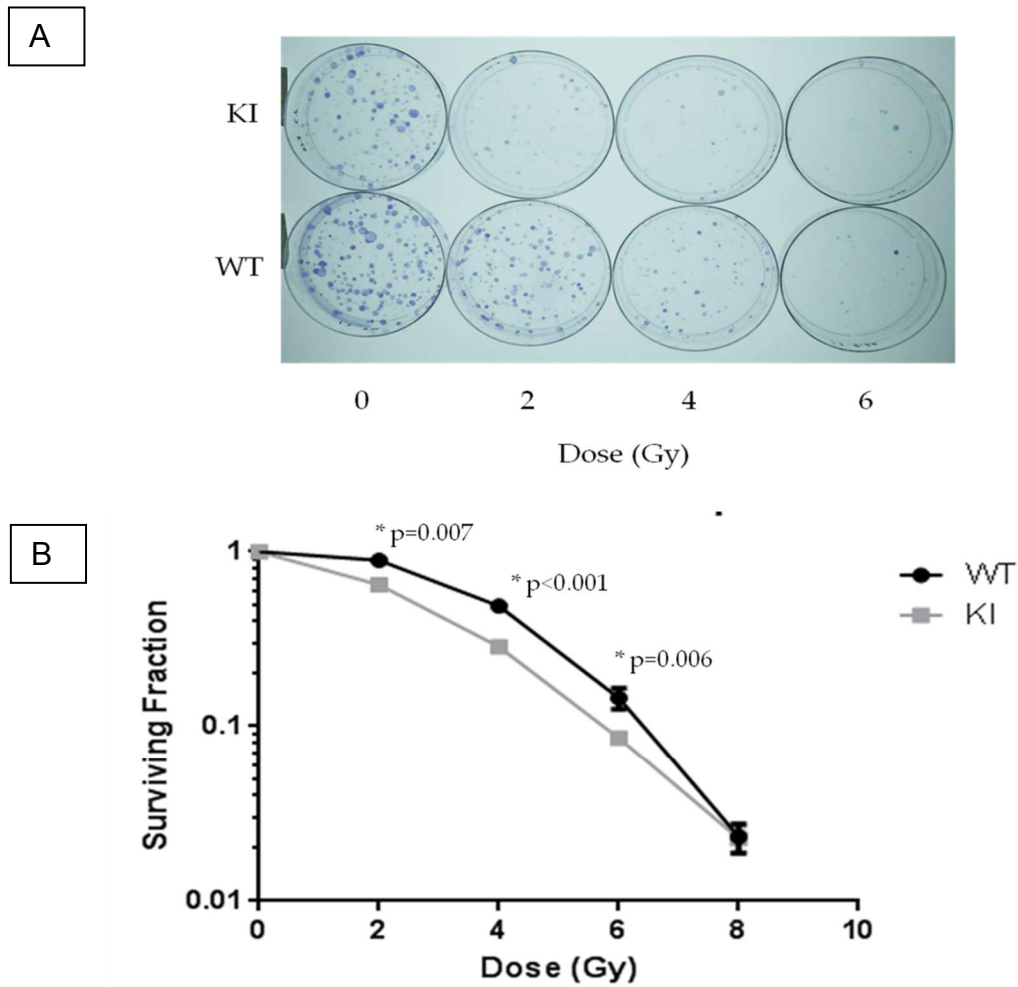


Figure 38: Colony formation and surviving fraction of transformed WT and KI MEFs 10 days after 2, 4, 6, and 8 Gy gamma irradiation. A. Colonies of transformed MEFs, stained with crystal violet, grown from 1000 cells/dish in the 10 days post irradiation at 2, 4, and 6 Gy. Also shown is the untreated control (0). **B.** Surviving fraction of transformed MEFs, calculated from colony formation at 10 days post irradiation. Significant difference between WT and KI was determined by Student T-test and is indicated by a star and p-value. Error bars represent standard error of the mean.

DNA damage response proteins following irradiation in MEFs. DNA damage response proteins and downstream signaling of mTORC1 and mTORC2 were evaluated by immunoblotting at different time points up to 6 hours post 4 Gy irradiation in primary MEFs. ATM, which is in the same protein family as mTOR and is one of the first proteins activated in DDR was decreased at all time points in KI MEFs. Levels of FANCD2 were increased by 30 minutes until 3 hours post-irradiation in WT MEFs; FANCD2 levels in the KI MEFs were not detectable until 1 hour post irradiation and remained low (Figure 39). These results were consistent with the low levels of *Fancd2* transcripts in bone marrow from pristane-treated KI mice. Phospho-p53 levels at Serine 15 and total p53 levels (data not shown) were similar both before and after treatment.

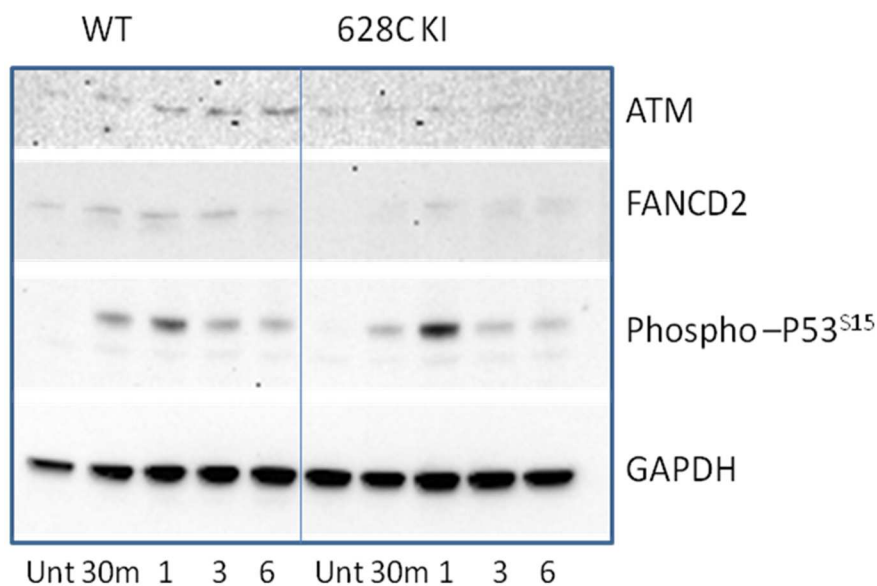


Figure 39: Immunoblot of DDR proteins at 30 minutes, 1 hour, 3 hours, and 6 hours post 4 Gy gamma irradiation in mTOR WT and 628C KI primary MEFs. Untreated samples are included as controls.

Downstream targets of mTOR following irradiation in MEFs. Interestingly, while phospho-p70-S6K was increased in WT MEFs with time post irradiation, indicating

increased mTOR activity in irradiated cells, it was in low abundance in both untreated and irradiated KI MEFs, showing no change following irradiation. A similar, more dramatic pattern was apparent for all three phosphorylation sites in PKC α (PRKC α), which increased in WT MEFs with time post irradiation, but were low and did not change in KI MEFs (Figure 40). The main role of PKC α is in maintaining cytoskeletal structure (Sarbasov, Ali et al. 2004), though PKC α is also involved in apoptosis (Lista, Bertness et al. 1997). As such, PKC α localization and cytoskeletal structure (F-actin) were assessed in WT and KI MEFs by immunofluorescence post irradiation. PKC α remained localized within the cytoplasm of MEFs after irradiation (Figure 41) and F-actin patterns were unaltered by irradiation in WT and KI MEFs at all time points (Figure 42, untreated and 6 hours post irradiation, representative images). Apoptosis and cell cycle were assessed by flow cytometry at 3 and 18 hours post 4 Gy irradiation, and no differences were noted in post-irradiation apoptosis or cell cycle at either time point (See Appendix E, Figure 51, 52)

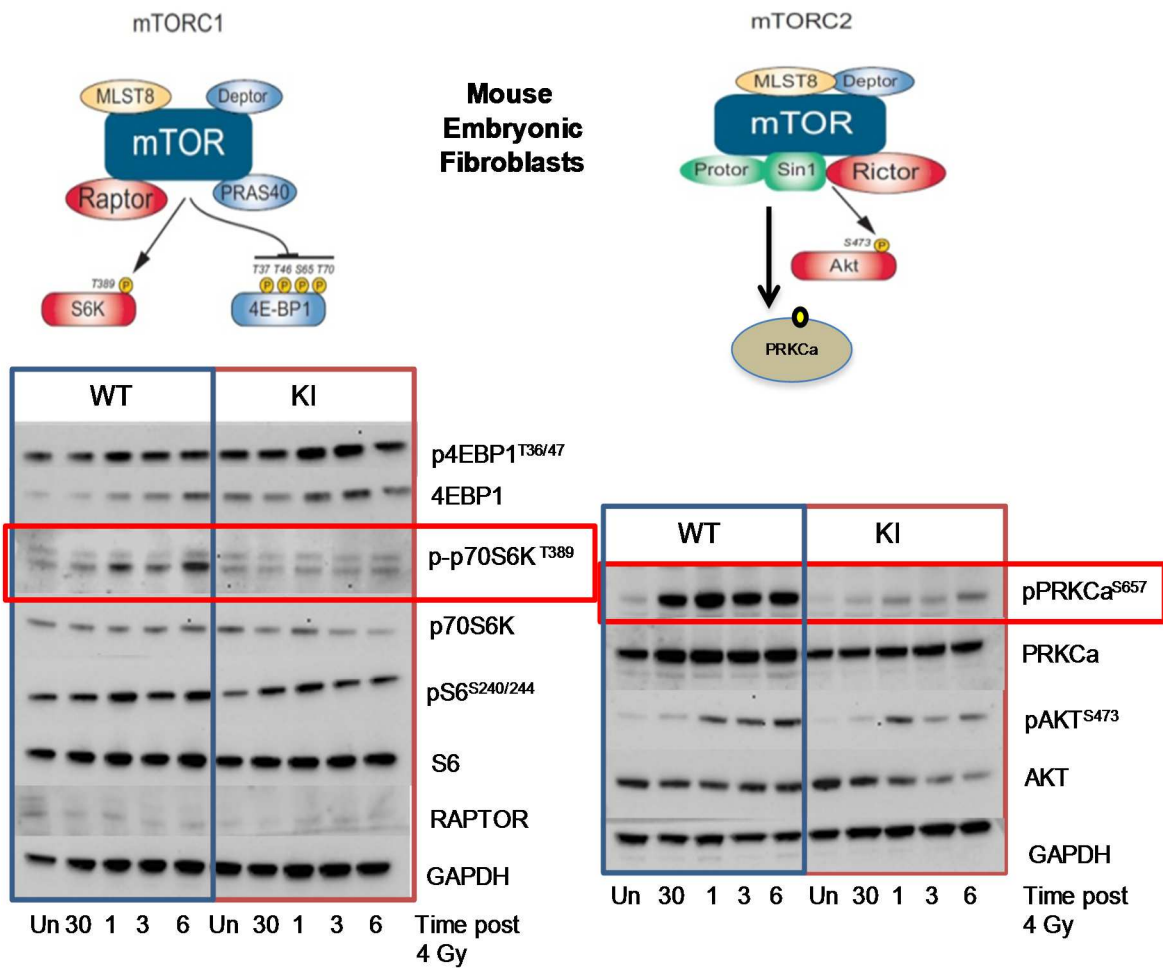


Figure 40: Downstream targets of mTORC1 and mTORC2 at time points post 4 Gy irradiation in WT and 628C KI MEFs. Representative diagrams of the main targets of mTORC1 and 2 are also included for reference.

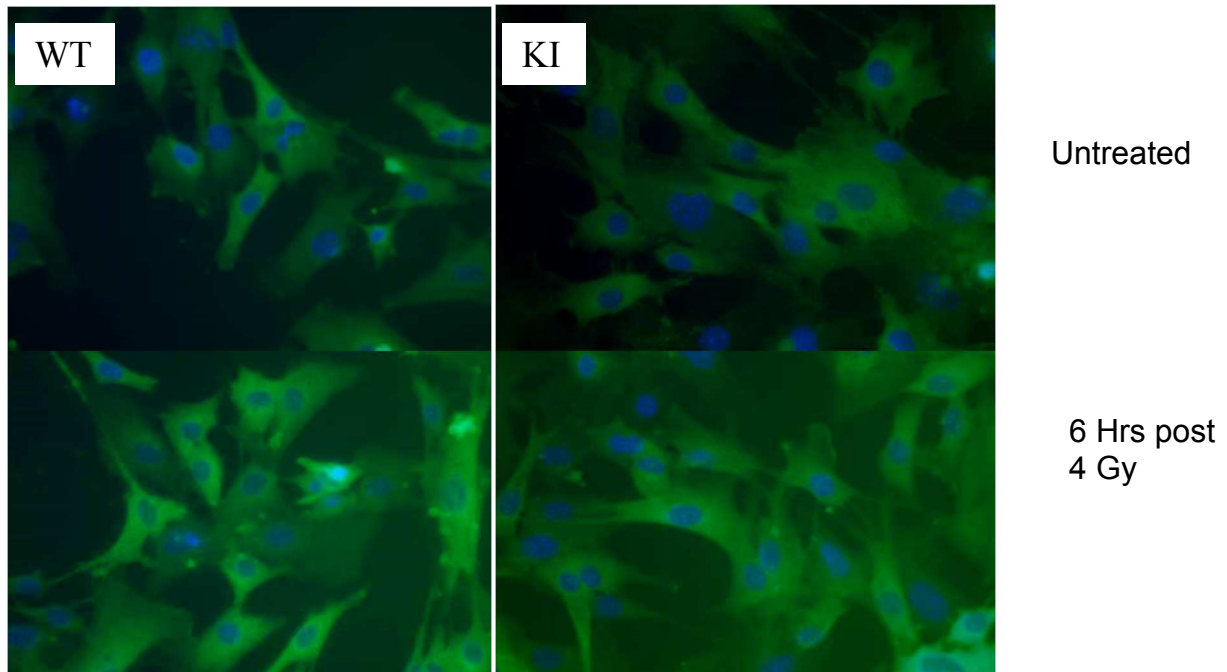


Figure 41: PKC α labeling in untreated and 4 Gy-irradiated WT and 628C KI MEFs 6 hours post irradiation. Green fluorescent signal is PKC α , while the blue signal is DAPI. Images are taken at 40X magnification.

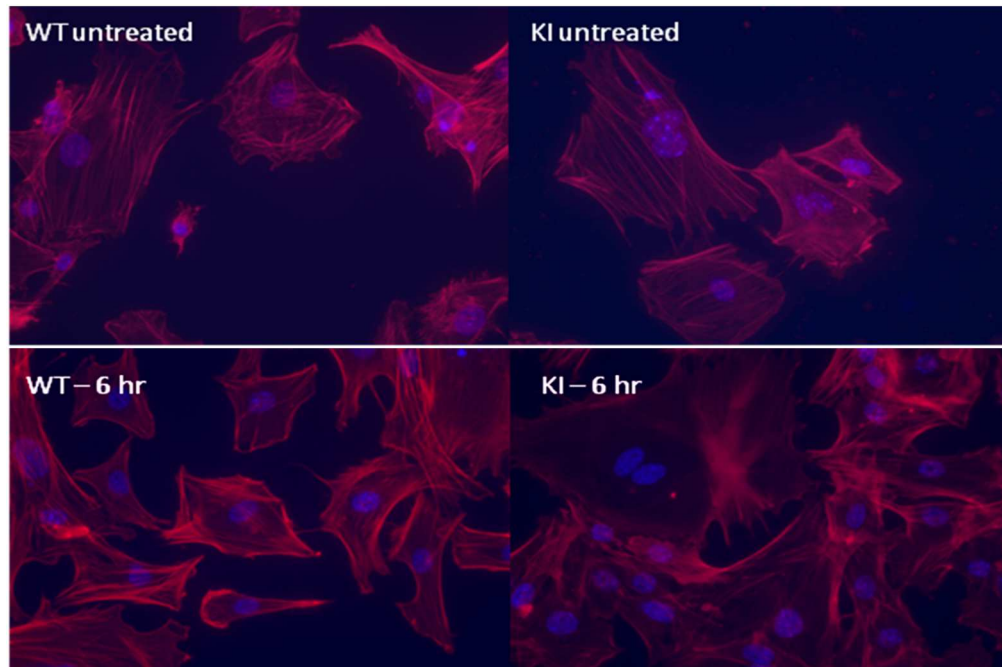


Figure 42: Labeling for F-actin in untreated WT and 628C KI MEFs, and in WT and KI MEFs 6 hours post 4 Gy irradiation. F-actin is in red, while nuclei are blue (DAPI). Images were taken at 40X magnification.

Proliferation. PKC α has also been shown to play a role in cell proliferation in endometrial cancer (Haughian and Bradford 2009), colon cancer cells (Scaglione-Sewell, Abraham et al. 1998) and human osteoblasts (Lampasso, Marzec et al. 2002). Proliferation was assessed in primary WT and KI MEFs by observing cell growth and confluency every 6 hours in the Incucyte (Essen Bioscience) post irradiation at 2 Gy and at 4 Gy. At 2 Gy, proliferation was suppressed post irradiation in comparison to untreated cells in the WT MEFs (Figure 43), but not in the KI MEFs ($p < 0.001$, Student T-Test). Proliferation was mildly suppressed at 4 Gy in WT MEFs compared to KI MEFs ($p = 0.003$).

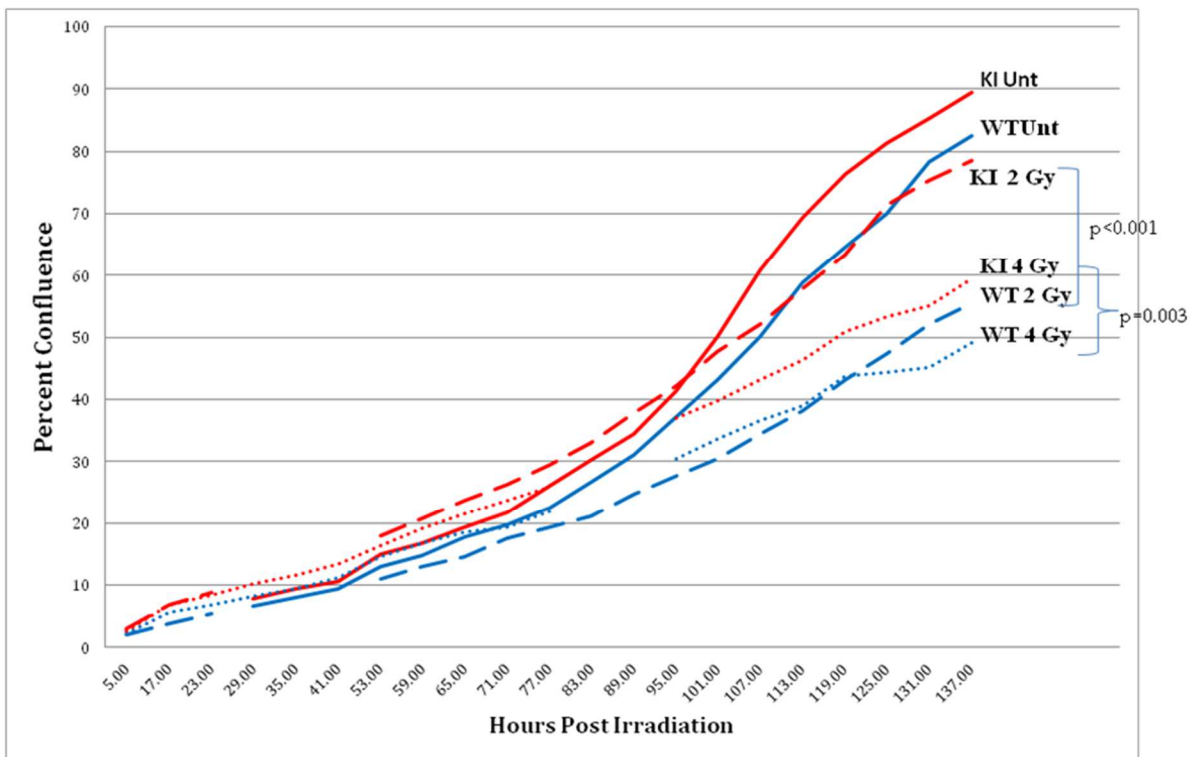


Figure 43: Proliferation based on percent confluence in untreated and irradiated WT and 628C KI MEFs. Red lines are for KI MEFs, while blue lines are for WT MEFs. Percent confluence values are the average of 45 wells/sample and error bars represent standard error of the mean. P-values are by Student's T-test.

Irradiation-induced thymic lymphoma. To further evaluate the role of the altered 628C mTOR protein in the DDR and in neoplasia, we used a well-known model of tumor formation in mice, in which mice are exposed to fractionated doses of irradiation starting at 5 weeks of age and continuing to receive small doses once weekly for four weeks. This schedule of fractionated irradiation induces the formation of thymic lymphomas in many strains of mice (Kominami and Niwa 2006, Zhao, Zhou et al. 2011). We irradiated our mTOR WT (n=51) and 628C KI (n=37) mice following this dosing scheme. Both WT and KI mice developed thymic lymphomas that spread to multiple tissues throughout the body including liver, spleen, kidneys, lymph nodes, and occasionally heart. However, KI mice developed thymic lymphomas at a higher rate and more rapidly than WT mice (70% survival in KI versus 90% survival in WT mice, $p=0.05$, Log rank test, Figure 44). These findings, in conjunction with the proliferation data and the susceptibility of BALB/c mice with this allele to plasma cell tumor formation, suggested that the 628C allele of mTOR can function as an oncogene in an environment of inflammatory or genotoxic stress, perhaps by allowing the accumulation of DNA damage.

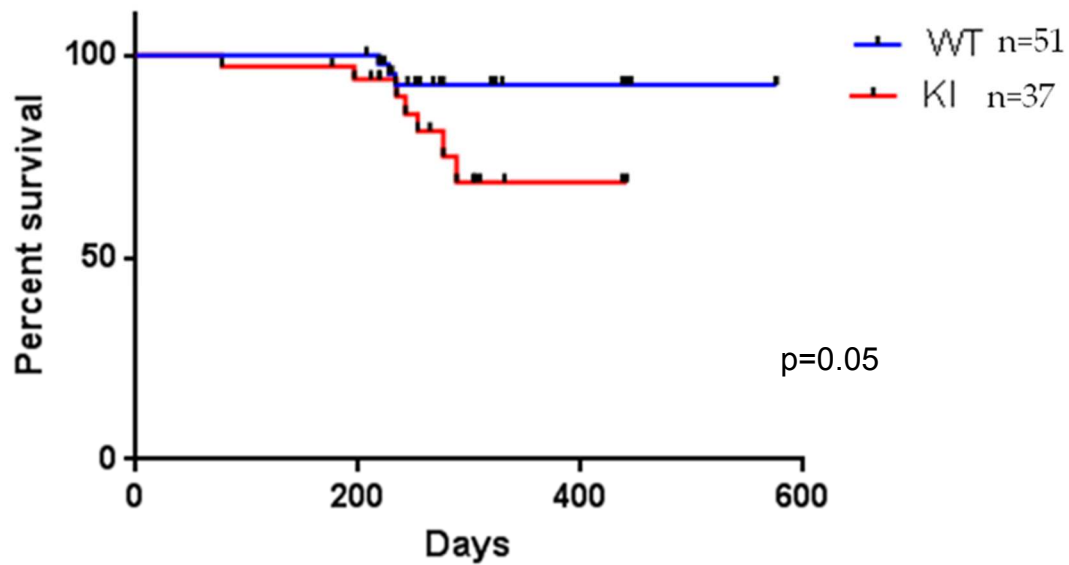


Figure 44: Survival curve of WT and 628C KI mice exposed to fractionated doses of 1.75 Gy, once weekly for 4 weeks, that developed thymic lymphomas. Survival was assessed by Kaplan-Meier survival analysis and Log Rank Test.

Ras-transformed 628C KI keratinocytes form larger papillomas more rapidly than WT keratinocytes. To test the response of the 628C variant of mTOR to oncogenic stress in a tumor model, we isolated keratinocytes from newborn WT and KI mice. The keratinocytes were transformed with a mutant RAS and grafted onto the backs of nude mice. Nude mice with KI cells developed significantly more papillomas and developed them at a quicker rate (Figure 45) than nude mice with grafts of transformed WT cells. In addition, papillomas were larger on the KI mice than the WT mice (Figure 45). As in irradiated MEFs, protein levels of FANCD2 and all three phosphorylation sites for PKC α were decreased in KI keratinocytes, including those that were RAS transformed (Figure 46); phospho-PKC α ^{T638} had the greatest decrease in KI keratinocytes. As with the MEFs, this indicated that mTOR signaling downstream of mTORC2 is decreased under stress conditions, in this case, oncogenic stress.

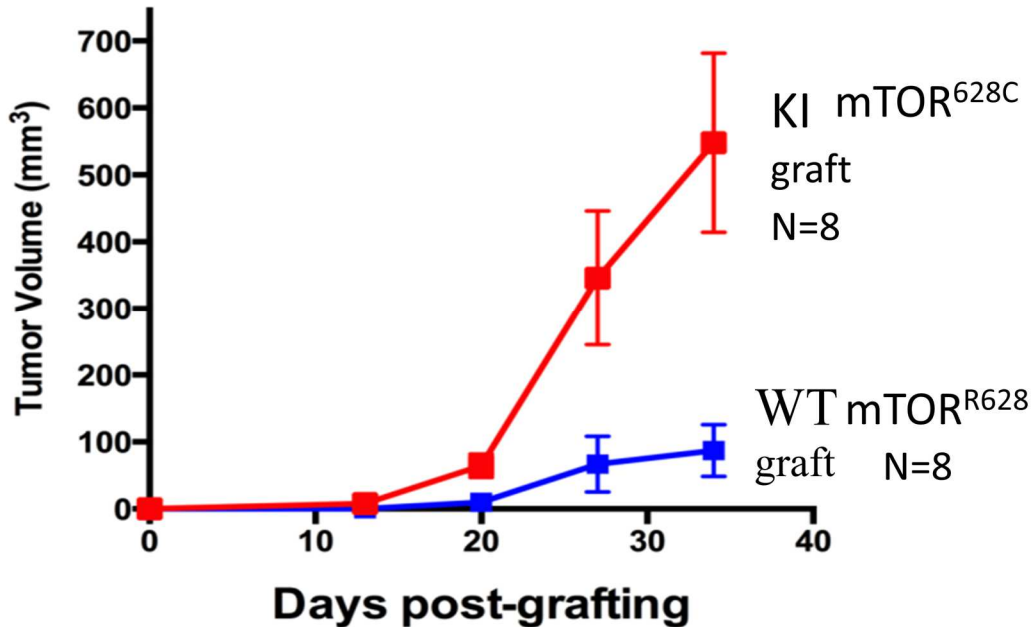


Figure 45: Papilloma volume from WT and 628C KI Ras-transformed keratinocytes grafted onto nude mice.

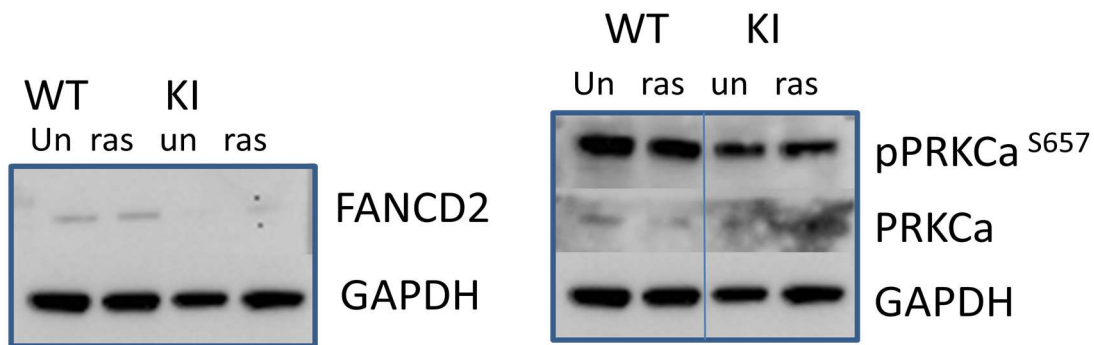


Figure 46: Immunoblots of FANCD2 and phospho-PKCα (PRKCa) in WT and 628C KI keratinocytes, both untreated (Un) and Ras-transformed (ras).

Under different types of cellular stress, including inflammatory, genotoxic, and oncogenic stress, DDR genes and proteins were down-regulated in 628C KI mice and cells, and 628C KI mice were more sensitive to DNA damage. In addition, downstream targets of mTOR, specifically phospho-PKCα, were decreased in KI cells exposed to irradiation. KI cells proliferated at a greater rate post irradiation and formed larger

papillomas, and KI mice developed post-irradiation thymic lymphomas, suggesting that the 628C allelic variant of mTOR is oncogenic under conditions of genotoxic and oncogenic stress, perhaps due to accumulation of DNA damage.

Discussion

mTOR is a crucial hub at the core of numerous signaling pathways in cells. We studied the role of an altered form of mTOR in response to stress. To better understand this role, we used a mouse model with a naturally-occurring single nucleotide polymorphism in *Mtor* (C1977T) that leads to a single amino acid substitution (R628C) in the HEAT domain of the protein, a region which is not well studied. Though mice with this SNP, such as BALB/c mice, appear to have normal survival under baseline conditions, these mice have decreased survival and a higher incidence of tumor formation under conditions of cell stress [(Okayasu, Suetomi et al. 2000) (Yu, Okayasu et al. 2001) (Ponnaiya, Cornforth et al. 1997)]. In conjunction, several prediction methods, including online algorithms and protein modeling programs suggest the 1977T SNP is likely to be damaging to the function of the protein.

Using transcriptional profiling under pristane-induced inflammatory conditions, we identified DNA replication, recombination, and repair as major enriched pathways in differentially expressed, often downregulated, genes in mTOR 628C KI mice. The association of inflammation induced by the oil pristane and DNA damage has been previously shown, as co-culturing neutrophils with B-cells exposed to pristane induces DNA strand breaks in the B-cells (Shacter, Lopez et al. 1991). In addition, the mTOR inhibitor, rapamycin, has been shown to reduce papilloma formation in inflammatory

skin cancer models by decreasing DNA damage (Dao, Pandeswara et al. 2015) and subsequently reducing the rate of *Ras* mutations.

Mice and cells with the 628C allelic variant of mTOR were more sensitive to irradiation, with decreased survival. Greater damage in KI cells at later time points suggests a potential decrease in DDR, as well. mTOR has been associated with DDR, most commonly through interactions with p53 [(Feng, Zhang et al. 2005), (Feng 2010), (Akeno, Miller et al. 2015), (Cam, Bid et al. 2014)]. However, phospho-p53 was similar between WT and KI irradiated MEFs, suggesting that in this system, signaling through mTOR onto DNA damage pathways may be mediated by other genes.

Of the down-regulated genes in the 628C KI bone marrow, a cluster of genes were associated with the Fanconi anemia pathway, which is involved in interstrand crosslink repair (Niedernhofer, Lalai et al. 2005), including FANCD2, FANCC, FANCG, and BRCA1. In both the irradiated KI MEFs and the untreated and Ras-transformed KI keratinocytes, FANCD2 was decreased compared to WT cells. FANCD2 has been reported to be regulated by mTOR through a variety of mechanisms, including the NF- κ B pathway (Guo, Li et al. 2014) and transcriptional regulation (Guo, Li et al. 2014), and thus is a possible link between the altered mTOR and decreased DDR.

While mTOR inhibition through rapamycin has been shown to decrease the incidence of tumor formation in inflammatory skin tumor models (Dao, Pandeswara et al. 2015), and aging mTOR knock down mice (KD) have a lower incidence of tumor formation (Wu, Liu et al. 2013), mice with the 628C allelic variant in mTOR express normal levels of mTOR but are more sensitive to tumor formation with perturbation. Specifically, BALB/c mice develop pristane-induced plasma cell tumors (Potter and

Wiener 1992) and irradiation-induced mammary tumors (Yu, Okayasu et al. 2001). In this study, genetically engineered mice with the allelic variant of mTOR were more susceptible to developing irradiation-induced thymic lymphomas and cells from these mice lead to larger papillomas when grafted onto nude mice. These findings, in addition to the sustained proliferation seen in irradiated KI MEFs (compared to suppressed proliferation in irradiated WT MEFs), suggests that the 628C allelic variant may be oncogenic under genotoxic stress conditions. Several activating mutations in mTOR have been described, suggesting that mTOR is a proto-oncogene [(Hardt, Chantaravisoot et al. 2011) (Grabiner, Nardi et al. 2014)]; typically these mutations are in the C-terminal region of the protein.

In yeast, TORC2 signaling has been associated with maintaining genomic stability (Shimada, Filipuzzi et al. 2013), perhaps pointing to a mechanism of decreased DDR in our model, which had significantly decreased phospho-PKC α downstream of mTORC2. However, a cursory examination of cytoskeleton structure by ICC and apoptosis by flow cytometry, which are two cell processes regulated by PKC α , did not reveal differences in irradiated KI MEFs. Another potential mechanism for decreased DDR in our model is decreased DNA damage sensing as well as repair mechanisms, as suggested by the decrease in FANCD2 and other DDR signaling proteins. Given that studies have found that FANCD2 is controlled by mTOR (Shen, Oswald et al. 2013), this is a likely connection to pursue. Interestingly, proliferation in the KI MEFs was only minimally inhibited by irradiation and associated DNA damage, allowing the cells to continue to grow despite unrepaired mutations. Studies in yeast (Searle, Schollaert et al. 2004) and cancer suggest that inactivation of *Pkca* may contribute to this phenotype.

These accumulated mutations could lead to further signaling disruption within the cell and eventually tumorigenesis. Clearly, additional experiments are needed to determine the mechanism by which the allelic variant is oncogenic.

mTOR signaling is complex and has many different roles in the cell depending on environmental signals and the input from other signaling pathways. It is likely that the effect of the 628C allelic variant of mTOR on downstream signaling is multifaceted, and can have a variety of affects depending on the cellular environment. However, we have shown that the allelic variant is associated with increased sensitivity to irradiation, increased DNA damage, a decrease in certain DDR proteins, and that this allelic variant may serve as an oncogene in situations of genotoxic or oncogenic stress. These findings support the need for further research into mTOR inhibitors as cancer therapy, and into mTOR's role in the DNA damage response.

CHAPTER 5: Synthesis and Conclusions

mTOR is a crucial cellular switch at the hub of numerous pathways. A variety of upstream signals such as energy, metabolites, and cell stress can moderate mTOR signaling, which the cell uses to maintain a delicate balance between catabolic and anabolic processes, such as growth and autophagy, and proliferation and apoptosis. To further complicate mTOR signaling, other cell signaling pathways feed into the PI3K/AKT/mTOR signaling at multiple levels, and a variety of feedback loops fine tune this signaling. Thus, in evaluating the mTOR pathway, we are gaining insight into a complicated, multifactorial system that responds dynamically to various cellular inputs; responses may vary temporally and spatially and among cell types. Mouse models of decreased and/or altered mTOR protein provide valuable tools to assist in understanding the consequences of this complicated pathway in vivo.

In these studies, novel mouse models of decreased mTOR (KD) and an allelic variant of mTOR (KI) were used to explore the role of mTOR in neoplasia and under stress conditions. The mTOR KD mouse has 70% less functional mTOR protein (Zhang, Readinger et al. 2011) and can be used as a model of pharmacologic inhibition of mTOR signaling. Because complete inhibition of mTOR in mice is embryonic lethal, most genetic models of mTOR inhibition use genetic knock outs of different components of mTORC1 or 2, such as Rictor or Raptor (Hoshii, Kasada et al. 2014). These models, however, are only specific to complex 1 or 2, and not to loss of mTOR itself.

By crossing the mTOR KD mice with mice that have T-cell specific hyperactivation of the PI3K/AKT/mTOR pathway, we were able to determine how cell signaling differed in T-cell acute lymphoblastic leukemias/lymphomas (T-ALL/LBL) with decreased mTOR

signaling, and use this information to identify a possible target for chemotherapy in combination with mTOR inhibitors. The identification of possible combination therapies is crucial because of the resistance developed by many cells treated with targeted therapies, which can be lessened by targeting multiple pathways or steps in the same pathway. Combination therapies are also useful because lower doses of individual drugs can be given to patients, often with the benefit of lessening side effects. The cooperative combination of a dual mTOR kinase inhibitor and a CDK4/6 inhibitor that we found in this study has been shown to be effective in other tumors with hyperactive PI3K/AKT/mTOR signaling, such as breast cancers with PI3K mutations (Vora, Juric et al. 2014). However, this combination has not yet been evaluated clinically in T-ALL/LBL.

Future directions for this arm of the project are many fold. An in vivo experiment, whereby nude mice that received subcutaneous pre-T LBL transplants from WT and KD mice are being treated with single agents and the combination of an mTOR inhibitor with a CDK4/6 inhibitor is in progress. Tumors from these mice will be assessed for apoptosis (by flow cytometry), cell cycle arrest (by flow cytometry), and proliferation (by immunohistochemistry for KI67 or BRDU). Cell signaling will also be evaluated in these tumors by immunoblots. Additional steps would include testing this combination on additional tumor types, both human cell lines and mouse models, and especially those with hyperactive PI3K/AKT/mTOR pathway signaling to better understand the spectrum of activity of the combination. Finally, evaluating the biologic effects (apoptosis and proliferation) of CDK6 knock out and over expression would help elucidate the mechanism of delayed tumor formation in the mTOR KD mice, which also had decreased CDK6 levels.

To evaluate the role of a naturally-occurring single nucleotide polymorphism in mTOR (C1977T) that leads to an amino acid substitution in the protein (R628C), we used a mouse engineered to carry the BALB/c variant on a B6;129 mixed genetic background. This SNP was originally identified in BALB/c mice as one susceptibility allele for peritoneal plasma cell tumor formation after intraperitoneal injection with the oil, pristane (Bliskovsky, Ramsay et al. 2003). mTOR mutations were initially thought to be rare in human cancers, but more mutations have been reported as a result of the current TCGA projects to sequence collections of different types of tumors. In addition, mutations in upstream effectors of the mTOR pathway are quite common. Thus, a better understanding of mTOR mutations and their effects on the protein may shed light on mTOR's role in tumorigenesis. In addition, the 628C amino acid alteration occurs in a HEAT domain of the mTOR protein, a region near the N-terminus that is not well studied. Further understanding of the function of this region will help us better understand mTOR's role in protein interactions.

To emphasize the importance of exploring the role of the SNP in *Mtor*, we found that DNA damage response (DDR) genes were down regulated in the bone marrow cells from pristane-treated 628C KI mice. mTOR has previously been described as having roles in DDR, though the exact connections are unclear, often through signaling interactions with the p53 signaling pathway or through specific DDR proteins. We have found that decreased DDRs in cells with the 628C allelic variant of mTOR is likely multifactorial, with decreases in DDR proteins such as FANCD2 and ATM, as well as downstream targets of mTOR such as phospho-PKC α . The combined effects from each alteration downstream of the 628C variant of mTOR add up to increased

sensitivity to irradiation, increased formation of thymic lymphomas following repeated exposure to low dose irradiation as well as larger skin papillomas from RAS-transformed keratinocytes.

Future directions for this project are to understand the connections between FANCD2 and the allelic variant of mTOR in our system. A likely starting point for this exploration is to examine the bone marrow hematopoietic stem cells from 628C KI mice and their response to inflammation and genotoxic stress. Also, because the heat domains are reported to be regions of protein-protein interaction, exploring the binding of mTOR partners with the allelic variant may open the door to understanding the mechanism of increased sensitivity to DNA damage. Finally, a more complete understanding of the biologic consequences of decreased PKC α under stress conditions would complete the picture of the allelic variant's effect.

Mtor's role in numerous pathways, the dysregulation of the PI3K/AKT/mTOR pathway in numerous cancers, and its ability to be targeted by specific compounds, such as rapamycin, clearly highlight the importance of understanding the protein and its roles. Herein, we have evaluated mTOR's signaling in T-cell acute lymphoblastic leukemia, and the effects of downregulating mTOR in this setting. Through this study, we were able to identify CDK6, a crucial cell cycle signaling protein, as an indirect target of mTOR signaling in this cancer, and as a target for combined therapy. In a separate, but related, study we also explored the role of a naturally-occurring single nucleotide polymorphism (SNP) in mTOR. We identified the DDR pathway as down regulated in cells with this SNP, and explored the mechanism and consequences of this down regulation both in cells and mice. Because of mTOR's dysregulation in cancer, its role in

the DDR is crucial, as many cancer therapies induce DNA damage in rapidly dividing cells. In all of these studies, we used mouse models with altered mTOR, allowing us to assess the consequences of mTOR at both the cellular and organismal level.

APPENDICES

APPENDIX A: Additional results from mTOR WT and 628C KI mice that are not significantly different by genotype

Inflammatory response by complete blood count (CBC)

mTOR WT and 628C KI mice are phenotypically normal when not perturbed. Seven days after intraperitoneal pristane injection, WT and 628C KI mice have similar neutrophil (PMN) and lymphocyte counts by CBC (Figure 47). Neutrophil counts were increased in both pristane-treated groups.

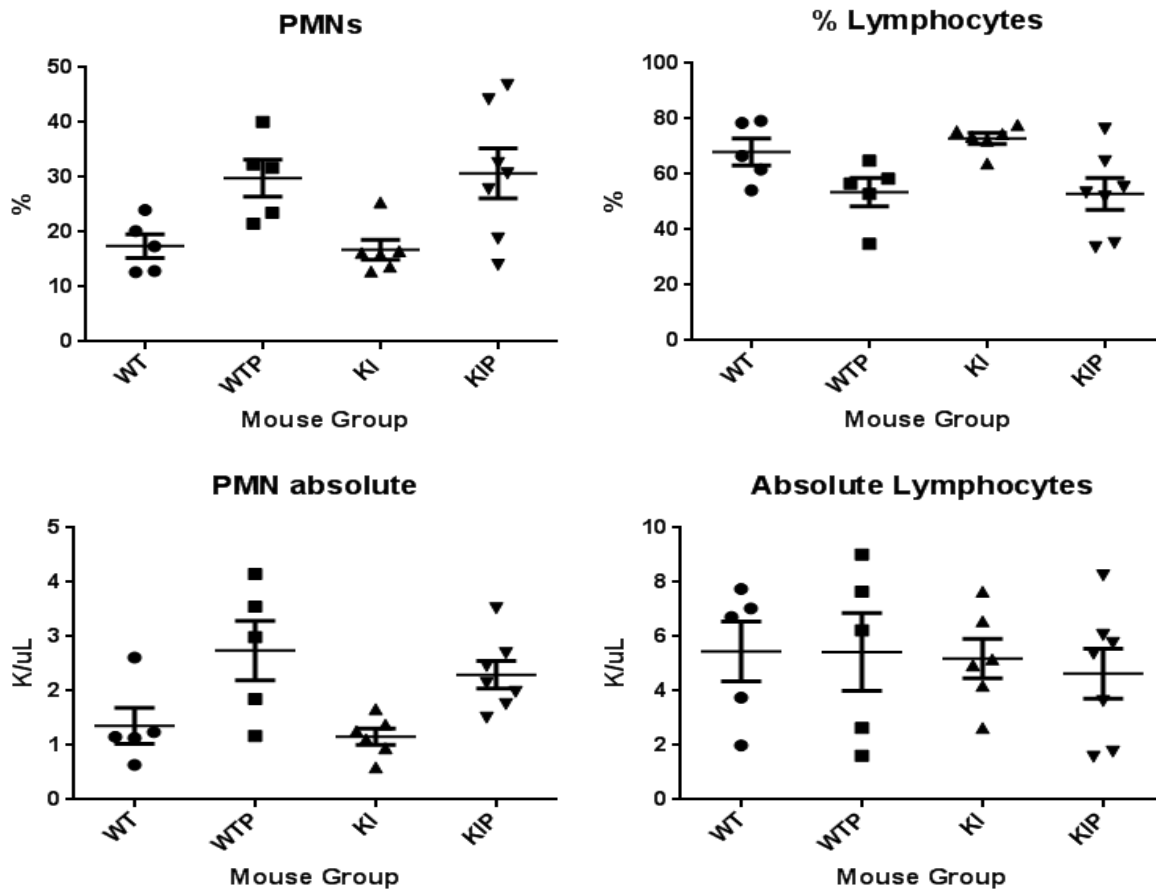


Figure 47: Polymorphonuclear cells (PMNs) and lymphocytes from untreated (WT and KI) and pristane-treated (designated WTP and KIP) mTOR WT

Figure 47 (cont'd). and 628C KI mice by CBC. Each point represents a value for an individual mouse. Included are both percent and absolute values.

Downstream protein phosphorylation

The phosphorylation of the main downstream targets of mTOR, 4E-BP1, S6, and AKT, shown as a ratio of phospho – to total protein by immunoblot or size-based capillary electrophoresis [(Peggy, Protein Simple; (Chen, Heldman et al. 2013)] showed variable differences based on tissue and with or without pristane-treatment (Figure 48). The biggest differences in phospho/total ratios between WT and KI were in untreated tissues, but these differences were not statistically significant (Student T-test, n per group =3). Differences were apparent between B220+ (splenic B-cell) and B220- populations in spleens from pristane-treated mice, indicating different phosphorylation patterns in different cell subtypes within a tissue (Figure 48).

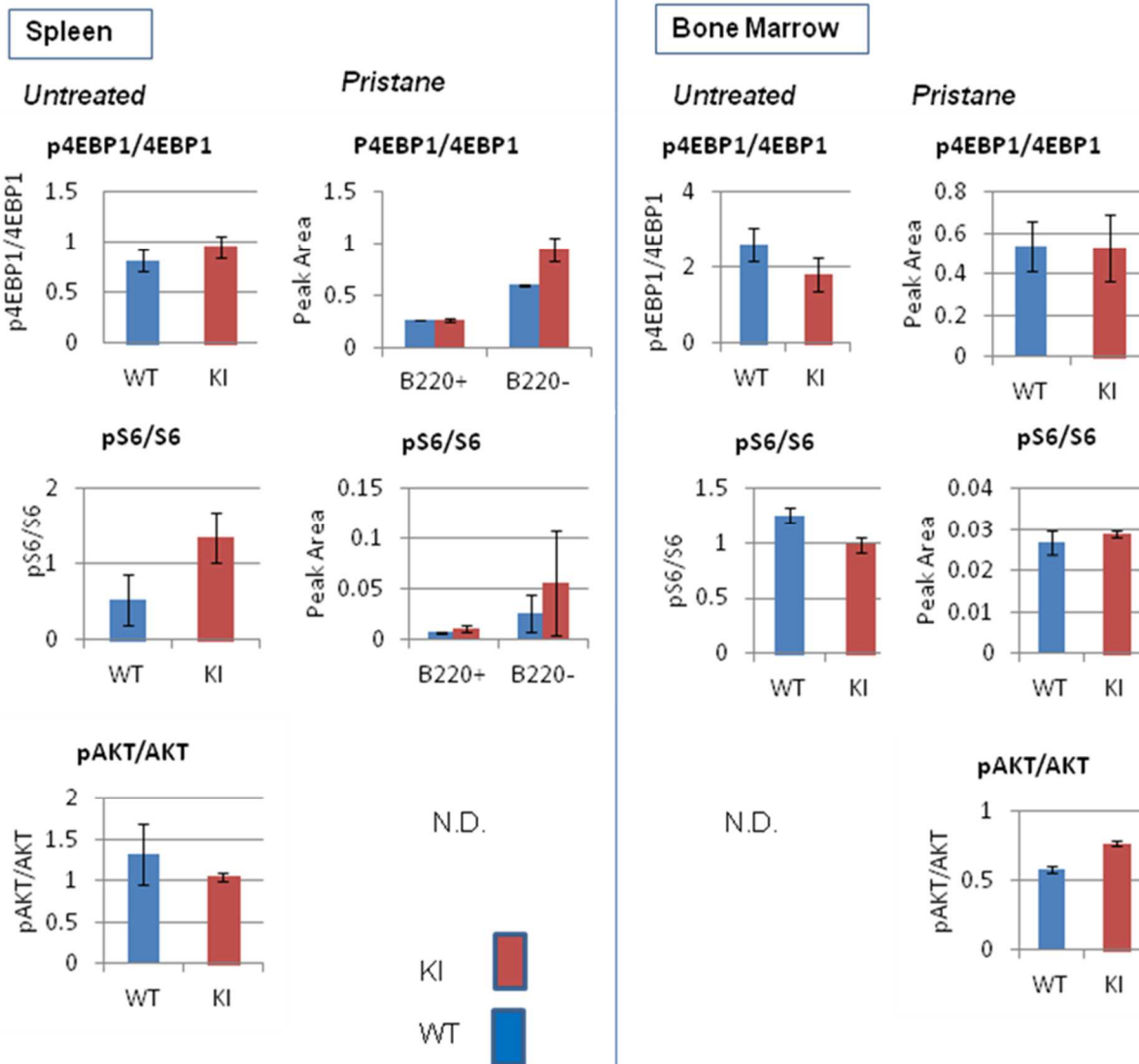


Figure 48: Average protein expression levels by quantification of western blot bands or by size-based, automated, capillary immunoassay system (peak area), showing levels of downstream targets of mTOR. Levels of phospho-4E-BP1, phospho-S6, and phospho-AKT in the bone marrow and spleen from untreated and pristane-treated mice. Error bars represent standard error of the mean from three animals. N.D. signifies that indicated ratios were not tested for this cell/treatment type.

APPENDIX B: Levels of three miRNAs are differentially expressed between WT and 628C KI B220+ splenocytes by Nanostring; the magnitude of the differences by Real Time PCR were not significant

Nanostring arrays (Nanostring, Seattle, WA) were performed on B220+ splenocytes (B-cells) isolated from untreated mice or mice 7 days after pristane treatment. Analysis of the Nanostring results indicated that three microRNAs were significantly different between untreated WT and KI cells: miR30a, mir101, mir423-5p (no microRNAs were different in cells from pristane-treated mice, Figure 49). However, there was no significant difference between WT and 628C KI cell miR expression levels by real time PCR (RT-PCR).

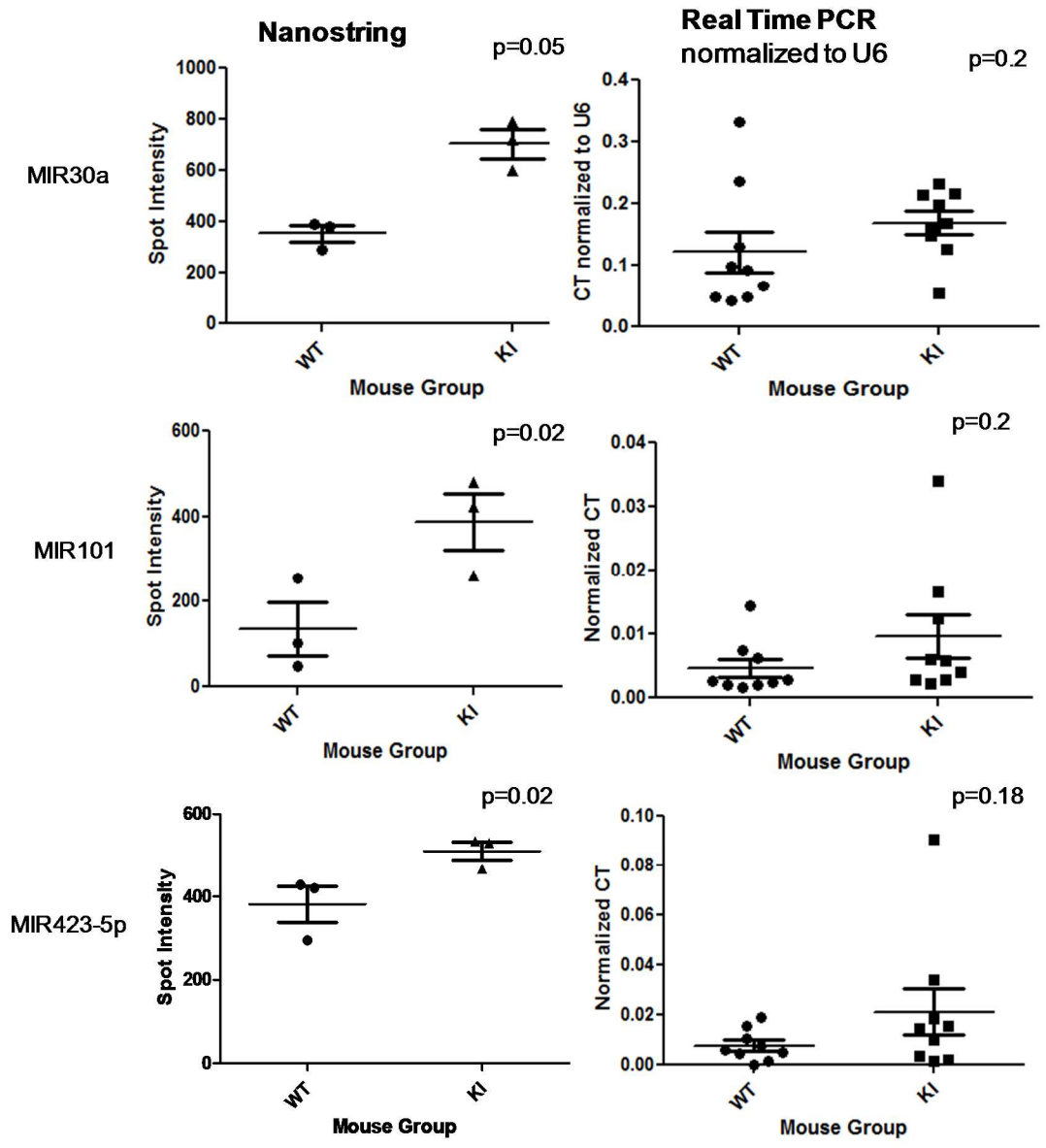
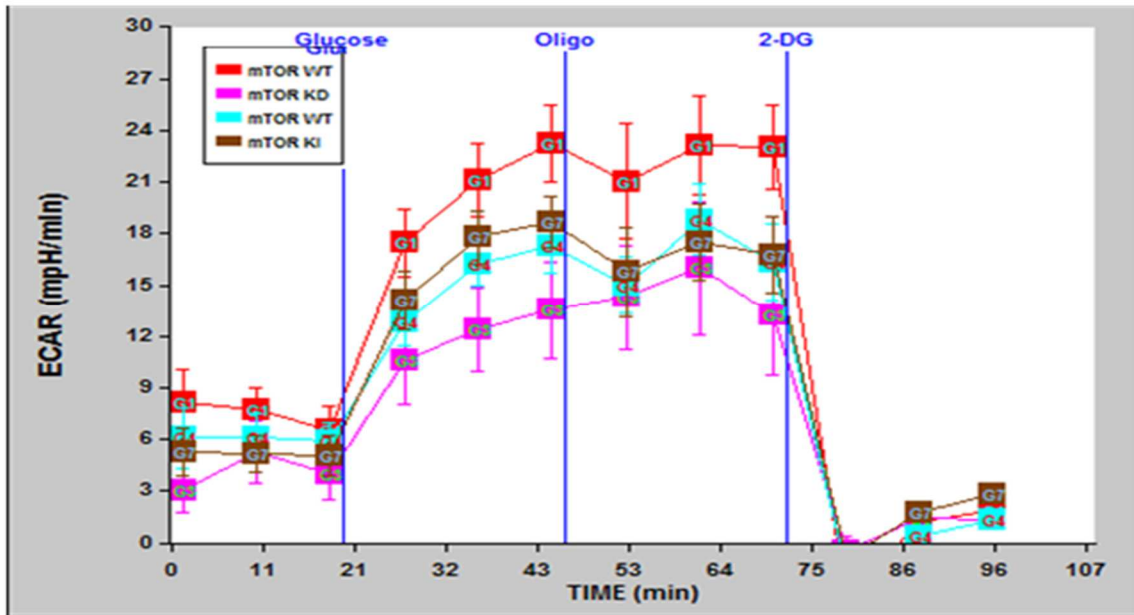


Figure 49: Spot intensity by Nanostring array for miR30a, miR101, and mir423-5P, and transcript levels by RT-PCR for each miR in WT and KI bone marrow cells. All miRs were significantly up regulated in the KI cells by Nanostring array. However, by RT-PCR (reported as $2^{-\Delta CT}$) in additional animals, none of the miRs had differential expression between WT and KI mice; although for each miR, the trend was similar.

APPENDIX C: Glycolysis is similar in primary and transformed mTOR WT and 628C KI, and mTOR WT and KD mouse embryonic fibroblasts

Glycolysis was measured in transformed (by SV40 Large T antigen) and primary WT, KI, and KD mouse embryonic fibroblasts (MEFs) by the XF Glycolysis stress test on the Seahorse XF (Seahorse Bioscience, MA). In this test, baseline pH, (measured by ECAR: mpH/min), glycolysis after glucose introduction, and glycolytic capacity and reserve after oligomycin (ATP Synthase inhibitor) and then 2 Deoxy-D-glucose (glycolysis inhibitor) was measured. Glycolytic capacity, which is the area under the curve from 50 minutes to 75 minutes was compared between groups by ANOVA. Experiments were repeated in triplicate. Transformed KD MEFs had significantly lower glycolytic capacity than transformed WT MEFs, though WT and 628C KI transformed MEFs had similar glycolytic capacity. There was no significant difference in glycolytic capacity between primary WT, KI, and KD MEFs, indicating that glycolysis was not different between WT and KI MEFs under these conditions (Figure 50, representative experiment).

Transformed Mouse Embryonic Fibroblasts



Primary Mouse Embryonic Fibroblasts

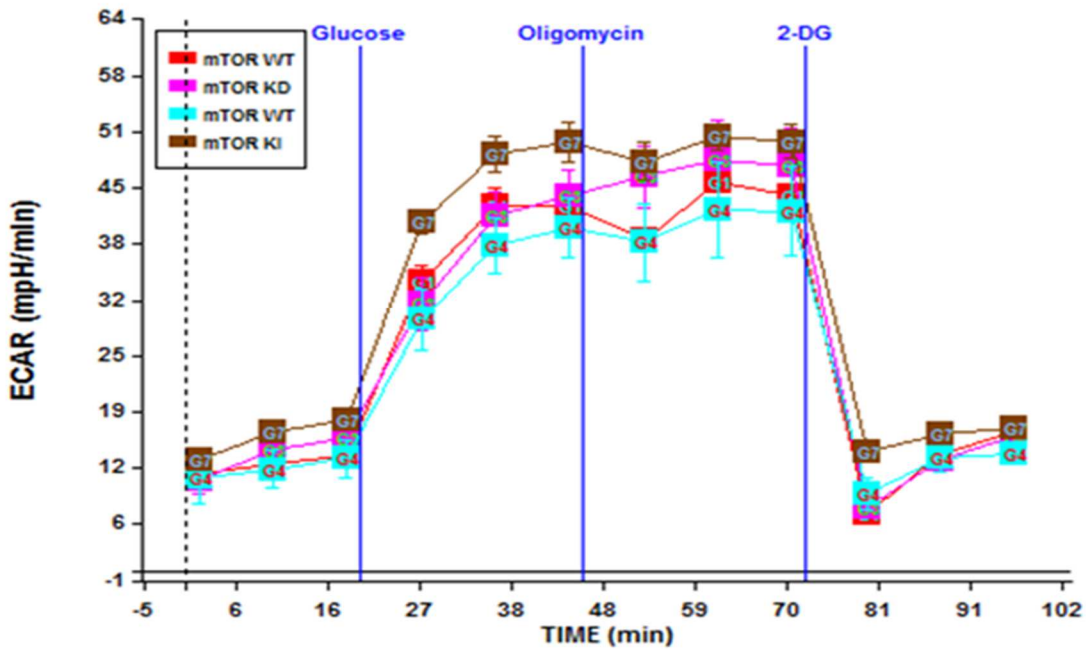


Figure 50: Curves representing glycolytic function in SV40-transformed and primary mTOR WT, KI, and KD mouse embryonic fibroblasts. Each line represents a different cell line. Error bars represent standard error of the mean of 4 technical replicates. Glucose, oligomycin (ATP Synthase inhibitor), and then 2 Deoxy-D-glucose (glycolysis inhibitor) are added to the cells as pH (a measure of glycolytic byproducts) is measured in the media adjacent to the cells.

APPENDIX D: Top Molecular and Cellular Functions identified by Ingenuity Pathway Analysis in genes from bone marrow of pristane- treated animals

Table 4: Cell morphology-associated top molecular functions as identified by Ingenuity Pathway Analysis. Sub-category of Disease or Functions Annotation, p-value, activation z-score, molecules involved, and numbers of molecules are included.

Diseases or Functions Annotation	p-Value	Activation z-score	Molecules	# Molecules
morphology of red blood cells	2.09E-08		ADD1,ADD2,Ahsp,ARHGEF12,BNIP3L,EIF2AK1,EPB41,EPB42,EPOR,GATA1,GFI1B,Gypa,HBA1/HBA2,Hbb-b2, IREB2, KLF1, MPP1, PRDX2, RB1, SCARB1, SIN3B, SLC11A2, SLC4A1, SPI1, STEAP3, TFRC, THBS1, TSPAN33	28
abnormal morphology of red blood cells	4.29E-08		ADD1,ADD2,Ahsp,ARHGEF12,BNIP3L,EIF2AK1,EPB42,EPOR,GATA1,GFI1B,Gypa,HBA1/HBA2,Hbb-b2, IREB2, KLF1, PRDX2, RB1, SCARB1, SIN3B, SLC11A2, SLC4A1, SPI1, STEAP3,TFRC,TSPAN33	25
morphology of blood cells	3.56E-06		ABHD5,ADD1,ADD2,Ahsp,ANO6,ARHGEF12,ARID3A,ATF2,BAD,BCL11B,BCL2L1,BNIP3L,CCDC86,CCND2,CD36,CD8A,CP,CSF1,CTSZ,DCK,EBI3,EIF2AK1,EPB41,EPB42,EPOR,EPH2,EPX,FANCC,FCGR2B,FLT3LG,FOXO3,GATA1,GBA,GFI1B,Gypa,HBA1/HBA2,Hbb-b2, ICAM2, ID1, IKBKG, IL5RA, IL7R, IREB2, KLF1, KLF13, LIPA, MAPKAPK2, MCL1, MPP1, MST1, Mt1, MXD1,MYB,NFKBIZ,PARL,PIK3CD,PPM1D,PPP3CB,PRDX2,PRG2,PSMB10,PSMB9,RB1,RBL1,RC3H1,S1PR4,SCARB1,SELP,SENP1,SIN3B,SLA,SLC11A2,SLC4A1,SOX4,SPI1,STEAP3,TAL1,TAP1,TFRC,THBS1,TLR4,TNFAIP8L2,TNFSF14,TRIB1,TSPAN33,TSTA3,ZBTB46,ZFP M1	88
volume of blood cells	1.29E-05		ADD1,ADD2,GATA1,GP1BA,Hbb-b2, SLC12A4, SPTA1, SPTB,ST3GAL6	9
volume of cells	2.32E-05		ADD1,ADD2,ADRB2,AQP1,BCL2L1,COL18A1,GATA1,GP1BA,Hbb-b2, IL1RL1, KCNN4, SLC12A4, SLC6A9, SPTA1,SPTB,ST3GAL6	16
morphology of bone marrow cells	1.52E-04		ANO6,ARID3A,ATF2,CCND2,CSNK2A1,FANCC,FLT3LG,GATA1,ICAM2,IKBKG,MXD1,RBL1,S1PR4,SELP,SENP1,SPI1,TAL1,TRIB1,TSTA3,ZFPM1	20
morphology of hematopoietic progenitor cells	3.60E-04		ANO6,ARID3A,ATF2,CCND2,CD8A,DCK,EPB41,EPOR,FANCC,FLT3LG,FOXO3,GATA1,ICAM2,IKBKG,KLF1,MCL1,MXD1,MYB,PRDX2,RBL1,S1PR4,SELP,SENP1,SLA,SLC4A1,SOX4,SPI1,STEAP3,TAL1,TRIB1,TSTA3,ZFPM1	32

Table 4 (cont'd)

morphology of lymphatic system cells	6.27E-04		ANO6,ARID3A,ATF2,CCND2,CSNK2A1,EPS15,FANCC,FLT3LG,GATA1,ICAM2,IKBKG,MXD1,RBL1,S1PR4,SELP,SENP1,SPI1,TAL1,TRIB1,TSTA3,ZFPM1	21
volume of red blood cells	6.75E-04		ADD2,Hbb-b2,SLC12A4,SPTA1,SPTB	5
shape change of tumor cell lines	2.57E-03	-2.584	AKAP12,ANXA5,BCL10,CCNE1,CDH11,CLIP1,CSF1,EDNRA,FERMT3,GFAP,HOOK1,ITGA4,ITGB1,PARVB,PIP5K1A,PPFIA1,PRNP,RAP1B,RB1,RBL1,SDC2,SRC,TAOK1,THBS1,TIAM1,TMBIM4,TNC	27
cell spreading of tumor cell lines	2.91E-03	-2.081	BCL10,CDH11,CLIP1,FERMT3,GFAP,HOOK1,ITGA4,ITGB1,PARVB,PPFIA1,PRNP,RAP1B,RB1,SDC2,SRC,THBS1,TIAM1,TMBIM4,TNC	19
abnormal morphology of hematopoietic progenitor cells	3.46E-03		ANO6,ARID3A,ATF2,CCND2,CD8A,DCK,FANCC,FLT3LG,FOXO3,GATA1,ICAM2,MCL1,MXD1,MYB,PRDX2,RBL1,S1PR4,SELP,SENP1,SLA,SLC4A1,SPI1,STEAP3,TRIB1,TSTA3,ZFPM1	26
morphology of nucleus	3.47E-03		AIFM1,BRCA1,BUB3,CHEK1,EIF4E,EP300,GADD45A,GMCL1,KIF22,LMNA,LMNB1,MAP4,MCPH1,MST1,NCAPG,NET1,PLSCR1,SIRT2,SMC2,SRC,TOR1A,VIM	22
initiation of autophagy of cells	4.89E-03		BECN1,SH3GLB1,WIP1	3
cell spreading of leukemia cell lines	6.54E-03	0.152	BCL10,FERMT3,ITGA4,ITGB1,TNC	5
autophagy of neuroblastoma cell lines	7.10E-03	-0.655	DNM1L,PRNP,ROCK1,SNCA	4
volume of blood platelets	7.10E-03		ADD1,GATA1,GP1BA,ST3GAL6	4
abnormal morphology of myeloid progenitor cells	8.10E-03		ATF2,CCND2,FLT3LG,GATA1,MXD1,RBL1,SELP,SPI1,TRIB1,TSTA3	10
shape change of vascular endothelial cells	1.11E-02	-1.6	ANG,ANGPT1,CRK,CTBP2,CTTN,DICER1,DROSHA,GP1BA,HS6ST1,ITGB1,SRC,TNC	12
abnormal morphology of dopaminergic neurons	1.12E-02		SLC18A2,SNCA,SPR	3
cell flattening of bone cancer cell lines	1.12E-02		CCNE1,RB1,RBL1	3
cellularity of bone marrow	1.12E-02		CLEC11A,CSF1,RNF2	3
abnormal morphology of megakaryocyte/erythrocyte lineage-restricted progenitor cells	1.17E-02		GATA1,ICAM2,SENP1,ZFPM1	4
cell spreading of colon cancer cell lines	1.17E-02	-2	PPFIA1,RAP1B,SDC2,SRC	4

Table 4 (cont'd)

abnormal morphology of eosinophils	1.21E-02		EPX,PRG2	2
osmotic water permeability of red blood cells	1.21E-02		AQP1,SLC14A1	2
ruffling of endothelial cell lines	1.21E-02		SRC,TIAM1	2
transmembrane potential of epithelial cells	1.21E-02		CASP9,KCNN4	2
volume of nucleus	1.21E-02		TMPO,TOP1	2
formation of invadopodia	1.24E-02	-0.896	ARF6,BTG2,CTTN,DIAPH3,ITGB1,RELN, SRC	7
cell spreading of kidney cell lines	1.35E-02	-0.254	ANTXR1,CRK,ITGB1,SORBS1,THBS1,VIM	6
morphology of erythroid progenitor cells	1.35E-02		EPB41,EPOR,GATA1,KLF1,PRDX2,SLC4A1,SPI1,STEAP3	8
permeability of mitochondrial membrane	1.37E-02		ATF2,BAD,BCL2L1,BNIP3L,PLEKHF1	5
cell rounding of tumor cell lines	1.56E-02	-2	AKAP12,EDNRA,PARVB,PIP5K1A,TAOK1,TIAM1,TNC	7
morphology of cerebral cortex cells	1.66E-02		ACHE,CLCN3,CPEB3,DYRK1A,FMR1,KALRN, KLK8,PAFAH1B1,SYNCRIP	9
shape change of bone cancer cell lines	1.78E-02	0	CCNE1,RB1,RBL1,TMBIM4	4
permeabilization of mitochondria	1.91E-02	0.549	AIFM1,BAD,BCL2L1,CLIC4,DNM1L,ITSN1,MC L1,PLEKHF1,RB1,SMPD4	10

Table 5: Small Molecule Biochemistry-associated top molecular functions as identified by Ingenuity Pathway Analysis. Sub-category of Disease or Function Annotation, p-value, activation z-score, molecules involved, and numbers of molecules are included.

Diseases or Functions Annotation	p-Value	Activation z-score	Molecules	# Molecules
metabolism of porphyrin	5.35E-07	-0.97	ABCB6,ALAD,ALAS2,ANK1,BCL2L1,BLVRB,EI F2AK1,FECH,IREB2,PPOX,PRDX2,SLC11A2,SLC25A38,SPTA1,SPTB,UROD,UROS	17
synthesis of porphyrin	9.55E-07	-1.432	ABCB6,ALAD,ALAS2,ANK1,BCL2L1,FECH,IREB2,PPOX,SLC11A2,SLC25A38,SPTA1,SPTB,UROD,UROS	14
synthesis of heme	2.56E-04	-1.387	ABCB6,ALAD,ALAS2,BCL2L1,FECH,PPOX,SLC11A2,SLC25A38,UROD,UROS	10
metabolism of phosphatidic acid	4.06E-04	-0.921	ABHD5,ADRB2,AGPAT2,ALOX15,ARF6,CHPT1,CTBP2,DPM1,DPM2,FABP5,FCGR2B,GPAA1,INPP5E,ITGB1,PCYT1A,PIGA,PIGQ,PIK3CD,PIK3R1,PIP5K1A,PIP5K1B,PLA1A,PLA2G4C,PLEK,PLSCR1,PNPLA6,PRDX2,PTDSS2,SH3GLB1,SH3YL1,SMPD4,SPI1	32

Table 5 (cont'd)

homeostasis of transition metal ion	8.20E-04		ABCB7,ALAS2,APLP2,ATOX1,ATP7B,COMMD1,IREB2,Mt1,NUBP1,PRNP,SLC30A5,TFR2,TFRC	13
incorporation of sphingomyelin	1.33E-03		GBA,SCARB1,SGMS1	3
metabolism of protoporphyrin	1.33E-03		EIF2AK1,FECH,IREB2	3
uptake of arachidonic acid	1.33E-03		APOD,FAT1,SCARB1	3
synthesis of phosphatidic acid	1.61E-03	-1.618	ABHD5,ADRB2,AGPAT2,ALOX15,ARF6,CHPT1,CTBP2,DPM1,DPM2,FABP5,GPAA1,INPP5E,ITGB1,PCYT1A,PIGA,PIGQ,PIK3CD,PIK3R1,PIP5K1A,PIP5K1B,PLSCR1,PNPLA6,PRDX2,PTDSS2,SH3GLB1,SH3YL1	26
metabolism of phospholipid	2.12E-03	-0.872	ABHD5,ADRB2,AGPAT2,ALOX15,ARF6,CHPT1,CLN8,CTBP2,DPM1,DPM2,FABP5,FCGR2B,GPAA1,INPP5E,ITGB1,LPCAT1,PCYT1A,PIGA,PIGQ,PIK3CD,PIK3R1,PIP5K1A,PIP5K1B,PLA1A,PLA2G16,PLA2G4C,PLEK,PLSCR1,PNPLA6,PRDX2,PTDSS2,PTGS2,PTPMT1,SGMS1,SH3GLB1,SH3YL1,SMPD4,SNCA,SPI1	39
transport of phospholipid	2.22E-03		ABCB4,ABCG4,ANO6,ATP11C,ATP8A1,ATP8A2,KCNN4,OSM,PLSCR1,PRELID1,SCARB1,TMEM30A	12
translocation of phospholipid	2.94E-03		ABCB4,ATP11C,ATP8A1,ATP8A2,KCNN4,PLSCR1,TMEM30A	7
synthesis of phospholipid	2.94E-03	-1.517	ABHD5,ADRB2,AGPAT2,ALOX15,ARF6,CHPT1,CTBP2,DPM1,DPM2,FABP5,GPAA1,INPP5E,ITGB1,LPCAT1,PCYT1A,PIGA,PIGQ,PIK3CD,PIK3R1,PIP5K1A,PIP5K1B,PLA2G16,PLSCR1,PNPLA6,PRDX2,PTDSS2,PTGS2,PTPMT1,SGMS1,SH3GLB1,SH3YL1	31
homeostasis of Cu²⁺	4.19E-03		APLP2,ATOX1,ATP7B,COMMD1,PRNP	5
synthesis of polyamines	4.19E-03		AMD1,AZIN1,ODC1,SMOX,SRM	5
metabolism of dolichol	4.89E-03		DPM1,DPM2,SRD5A3	3
synthesis of spermidine	4.89E-03		AMD1,ODC1,SRM	3
catabolism of hydrogen peroxide	7.46E-03	-2	ABCG2,CAT,HBA1/HBA2,PRDX2,PRDX3,PTGS2	6
metabolism of glutamine	9.68E-03		GLS,GLUL,ME1,NIT2,PHGDH	5
accumulation of porphyrin	1.21E-02		UROD,UROS	2
catabolism of glycerophospholipid	1.21E-02		PLA2G4C,SMPD4	2
formation of farnesyl pyrophosphate	1.21E-02		FDPS,GGPS1	2
hydrolysis of 1-oleoyl-2-acetyl glycerol	1.21E-02		PAFAH1B1,PAFAH1B2	2

Table 5 (cont'd)

hydrolysis of 1-palmitoyl-2-arachidonoyl-sn-glycero-3-phosphorylcholine	1.21E-02		PLA2G16,PNPLA6	2
hydrolysis of 1-palmitoyl-2-linoleoyl-sn-glycero-3-phosphocholine	1.21E-02		PLA2G16,PNPLA6	2
quantity of vinblastine	1.21E-02		ABCB4,UGCG	2
uptake of myristic acid	1.21E-02		CD36,THBS1	2
quantity of bilirubin	1.38E-02	2.121	ABCB4,ABCG2,ADD2,GFER,Hbb-b2,PFKM,RDX,SLC51A,SPTA1,SPTB	10
reduction of hydrogen peroxide	1.78E-02	-1.732	CAT,PRDX2,PRDX3,PTGS2	4

Table 6: DNA Replication, Recombination, and Repair-associated top molecular functions as identified by Ingenuity Pathway Analysis. Sub-category of Disease or Function Annotation, p-value, activation z-score, molecules involved, and numbers of molecules are included.

Diseases or Functions Annotation	p-Value	Activation z-score	Molecules	# Molecules
initiation of replication of DNA	2.31E-06	0	CCNE1,CCNE2,CDC6,CDC7,CDK2AP1,CHEK1,EP300,ORC1,ORC2,ORC4,ORC5,PURA	12
DNA replication	9.73E-06	-0.582	ABCB6,ABCB7,ACHE,BECN1,BRCA1,CCDC88A,CCNA2,CCNE1,CCNE2,CDC6,CDC7,CDK2AP1,CHEK1,CUL4A,CUL4B,DBF4,E2F2,E4F1,ENDOG,EP300,ESCO2,HELB,ID1,IGHMBP2,KIN,MAPKAPK2,NAP1L1,NASP,NRF1,OBFC1,ORC1,ORC2,ORC4,ORC5,Paxip1,PLK1,POLH,PTGS2,PURA,RB1,RNF2,SLA,SRC,SSBP1,SUPT16H,THRA,TMPO,TPX2,WAPAL,WRN	50
segregation of chromosomes	5.25E-05	-0.181	ATRX,BRCA1,BUB3,CCNA2,CDC6,CENPE,CENPH,CENPH,EBNA1BP2,ECT2,ESCO2,FAM96B,GPSM2,KIF2C,KNSTRN,LMNA,NCAPG,NEK2,NINL,NUSAP1,PLK1,RIOK3,SKA2,SMC2,SMC4,STAG1,TLK2,TPX2,WAPAL	29
metabolism of DNA	6.19E-05	0.382	ABCB6,ABCB7,ACHE,AGTR1,AIFM1,ANTXR1,BCL2L1,BECN1,BRCA1,CASP9,CCDC88A,CCNA2,CCNE1,CCNE2,CDC6,CDC7,CDK2AP1,CHEK1,CSF1,CUL4A,CUL4B,DBF4,DHX9,DUSP1,E2F2,E4F1,ENDOG,EP300,ESCO2,EXO5,HELB,HSD17B10,ID1,IGHMBP2,ISG20,JUN,KIN,LMNA,MAPKAPK2,MCL1,NAP1L1,NASP,NRF1,OBFC1,ORC1,ORC2,ORC4,ORC5,Paxip1,PIK3R1,PLK1,POLH,PPIB,PRNP,PTGS2,PURA,RB1,RNF2,SERINC3,SLA,SNCA,SRC,SSBP1,SUPT16H,THRA,TIAM1,TMPO,TNFRSF19,TPX2,TREX1,WAPAL,WRN	72

Table 6 (cont'd)

conformational modification of DNA	1.39E-02	-2.418	DNAJB1,GATA1,JUN,MCM4,MYB,PURA,TOP1,WRN,YY1	9
spindle checkpoint of cervical cancer cell lines	1.78E-02	-0.152	CENPI,DLGAP5,ERCC6L,NET1	4
catabolism of DNA	1.87E-02		AIFM1,ENDO G,EXO5,ISG20,TREX1	5

Table 7: Molecular Transport-associated top molecular functions as identified by Ingenuity Pathway Analysis. Sub-category of Disease or Function Annotation, p-value, activation z-score, molecules involved, and numbers of molecules are included.

Diseases or Functions Annotation	p-Value	Activation z-score	Molecules	# Molecules
quantity of heavy metal	8.39E-06	3.004	ADD2,ALAS2,APLP2,ATP7B,COMMD1,CP,EIF2AK1,EPB42,Hbb-b2,HMOX2,IREB2,KCNN4,Mt1,OSM,PRNP,RHAG,RHCE/RHD,SLC11A2,STEAP3,TFR2,TFRC,TRIB1,UROD	23
import of heavy metal	2.50E-04		ABCB10,ATP7B,SLC11A2,SLC25A37,STEAP3,TFRC	6
uptake of arachidonic acid	1.33E-03		APOD,FAT1,SCARB1	3
transport of heavy metal	1.38E-03	-1.976	ABCB10,ATOX1,ATP7B,COMMD1,CP,IREB2,Mgmt2,SLC11A2,SLC25A37,SLC30A5,SLC39A8,STEAP3,TFRC,TRPM7	14
transport of phospholipid	2.22E-03		ABCB4,ABCG4,ANO6,ATP11C,ATP8A1,ATP8A2,KCNN4,OSM,PLSCR1,PRELID1,SCARB1,TMEM30A	12
import of metal	2.94E-03		ABCB10,ATP1B2,ATP7B,SLC11A2,SLC25A37,STEAP3,TFRC	7
translocation of phospholipid	2.94E-03		ABCB4,ATP11C,ATP8A1,ATP8A2,KCNN4,PLSCR1,TMEM30A	7
transport of Co ²⁺	4.89E-03		Mgmt2,SLC11A2,SLC30A5	3
transport of carbon dioxide	4.89E-03		AQP1,CA2,RHAG	3
transport of polysaccharide	4.89E-03		ABCC5,CD14,SCARB1	3
transport of Cu ²⁺	6.54E-03		ATOX1,ATP7B,Mgmt2,SLC11A2,STEAP3	5
accumulation of porphyrin	1.21E-02		UROD,UROS	2
exocytosis of L-glutamic acid	1.21E-02		PRNP,SNCA	2
quantity of vinblastine	1.21E-02		ABCB4,UGCG	2
uptake of myristic acid	1.21E-02		CD36,THBS1	2
quantity of bilirubin	1.38E-02	2.121	ABCB4,ABCG2,ADD2,GFER,Hbb-b2,PFKM,RDX,SLC51A,SPTA1,SPTB	10

Table 8: Gene Expression-associated top molecular functions as identified by Ingenuity Pathway Analysis. Sub-category of Disease or Function Annotation, p-value, activation z-score, molecules involved, and numbers of molecules are included.

Diseases or Functions Annotation	p-Value	Activation z-score	Molecules	# Molecules
translation of mRNA	1.02E-05	1.289	AGO2,BTG2,CPEB3,EIF2AK1,EIF2S3,EIF3G,EIF4B,EIF4E,EIF4EBP1,EIF4G2,EIF5,ELAVL1,FARSB,FMR1,FOXO3,GAPDH,HBS1L,IREB2,KLHL25,MRPL15,MRPL17,MRPL19,MRPL39,MTIF3,PABPC4,PRG3,PURA,RPL23,RPL30,RPL39,RPS17,RPS9,SAMD4A,SYNCRIP	34
expression of mRNA	1.97E-03	0.379	AGO2,ATF2,BTG2,CPEB3,EIF2AK1,EIF2S3,EIF3G,EIF4B,EIF4E,EIF4EBP1,EIF4G2,EIF5,ELAVL1,FARSB,FMR1,FOXO3,GAPDH,HBS1L,IREB2,IRF3,JUN,KLHL25,MRPL15,MRPL17,MRPL19,MRPL39,MTIF3,PABPC4,PRG3,PURA,RPL23,RPL30,RPL39,RPS17,RPS9,SAMD4A,SYNCRIP,TIMP3	38
initiation of expression of RNA	3.55E-03	-1.269	AGO2,BRCA1,CDK7,E2F2,EIF2S3,EIF3G,EIF4B,EIF4E,EIF4EBP1,EIF4G2,EIF5,EP300,FMR1,KLHL25,MED13,MTIF3,NCOA4,PTRF,SRC,YY1	20
activation of chromosome components	4.89E-03		ATF2,NCAPG,SMC2	3
initiation of translation of mRNA	1.15E-02		AGO2,EIF2S3,EIF3G,EIF4B,EIF4E,EIF4EBP1,EIF4G2,EIF5,FMR1,KLHL25,MTIF3	11

APPENDIX E: Apoptosis and cell cycle in WT and 628C KI MEFs 3 hours and 18 hours post irradiation

WT and 628C KI mouse embryonic fibroblasts (MEFs) were irradiated at 4 Gy, and were collected at 3 hours and 18 hours post irradiation. Flow cytometry was used to assess apoptosis and cell cycle in these MEFs. A similar increase in % apoptotic cells (both early and late apoptosis) was seen in WT and KI MEFs post irradiation (Figure 51). The cell cycle in WT and KI MEFs was not altered at 3 hours post 4 Gy irradiation. A slight G1 arrest was present in both WT and KI MEFs 18 hours post 4 Gy irradiation (Figure 52).

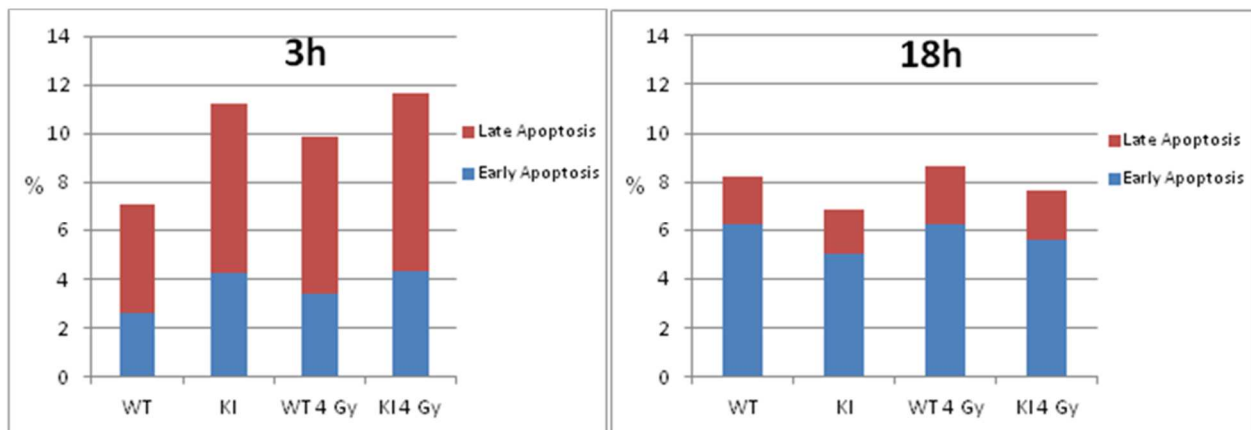
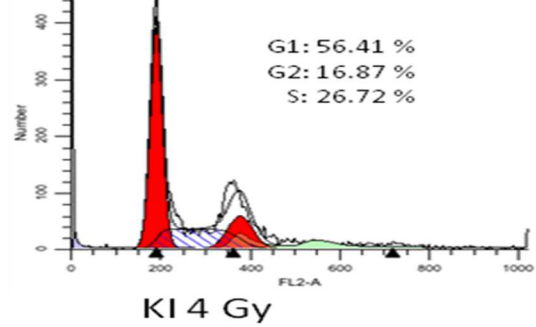
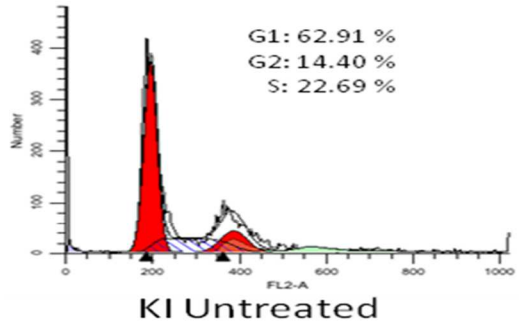
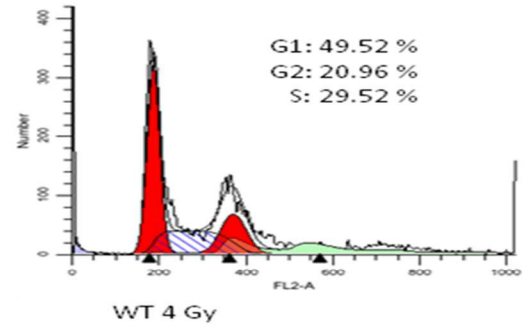
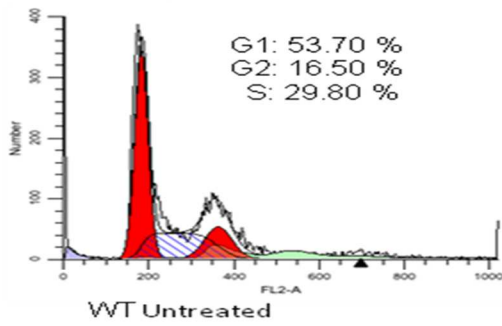


Figure 51: Percent cells in early and late apoptosis 3 hours and 18 hours post 4 Gy irradiation in WT and KI MEFs by flow cytometry.

Cell Cycle 3 hours post irradiation



Cell Cycle 18 hours post irradiation

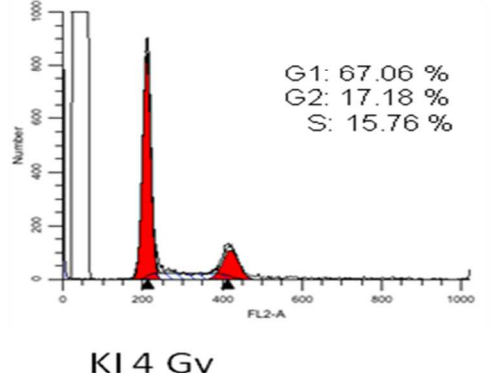
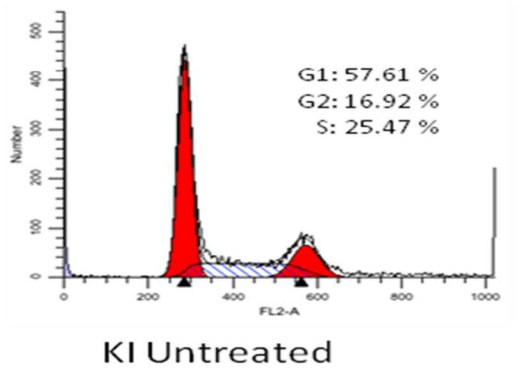
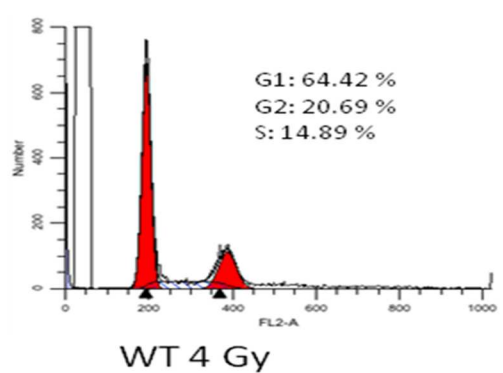
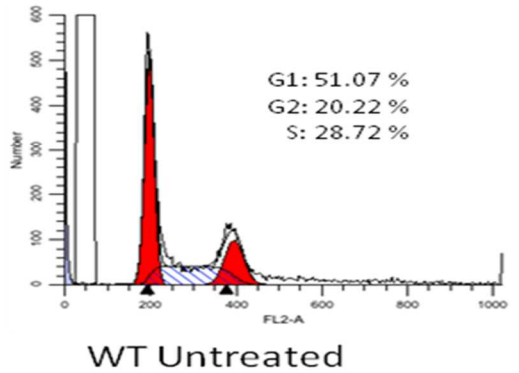


Figure 52: Cell cycle by flow cytometry in WT and KI MEFs 3 hours and 18 hours post 4 Gy irradiation.

REFERENCES

REFERENCES

- Adzhubei, I. A., S. Schmidt, L. Peshkin, V. E. Ramensky, A. Gerasimova, P. Bork, A. S. Kondrashov and S. R. Sunyaev (2010). "A method and server for predicting damaging missense mutations." Nature Methods **7**(4): 248-249.
- Ahmed, N. N., T. F. Franke, A. Bellacosa, K. Datta, M. E. Gonzalez-Portal, T. Taguchi, J. R. Testa and P. N. Tsichlis (1993). "The proteins encoded by c-akt and v-akt differ in post-translational modification, subcellular localization and oncogenic potential." Oncogene **8**(7): 1957-1963.
- Akeno, N., A. L. Miller, X. Ma and K. A. Wikenheiser-Brokamp (2015). "p53 suppresses carcinoma progression by inhibiting mTOR pathway activation." Oncogene **34**(5): 589-599.
- Alarcon, C. M., M. E. Cardenas and J. Heitman (1996). "Mammalian RAFT1 kinase domain provides rapamycin-sensitive TOR function in yeast." Genes & Development **10**(3): 279-288.
- Albert, J. M., K. W. Kim, C. Cao and B. Lu (2006). "Targeting the Akt/mammalian target of rapamycin pathway for radiosensitization of breast cancer." Molecular Cancer Therapeutics **5**(5): 1183-1189.
- Altomare, D. A. and J. R. Testa (2005). "Perturbations of the AKT signaling pathway in human cancer." Oncogene **24**(50): 7455-7464.
- Batista, A., J. T. Barata, E. Raderschall, S. E. Sallan, N. Carlesso, L. M. Nadler and A. A. Cardoso (2011). "Targeting of active mTOR inhibits primary leukemia T cells and synergizes with cytotoxic drugs and signaling inhibitors." Experimental Hematology **39**(4): 457-472 e453.
- Bliskovsky, V., E. S. Ramsay, J. Scott, W. DuBois, W. Shi, S. Zhang, X. Qian, D. R. Lowy and B. A. Mock (2003). "Frap, FKBP12 rapamycin-associated protein, is a candidate gene for the plasmacytoma resistance locus Pctr2 and can act as a tumor suppressor gene." Proceedings of the National Academy of Sciences **100**(25): 14982-14987.
- Borisy, A. A., P. J. Elliott, N. W. Hurst, M. S. Lee, J. Lehar, E. R. Price, G. Serbedzija, G. R. Zimmermann, M. A. Foley, B. R. Stockwell and C. T. Keith (2003). "Systematic discovery of multicomponent therapeutics." Proceedings of the National Academy of Sciences of the United States of America **100**(13): 7977-7982.
- Bressanin, D., C. Evangelisti, F. Ricci, G. Tabellini, F. Chiarini, P. L. Tazzari, F. Melchionda, F. Buontempo, P. Pagliaro, A. Pession, J. A. McCubrey and A. M. Martelli (2012). "Harnessing the PI3K/Akt/mTOR pathway in T-cell acute lymphoblastic leukemia: Eliminating activity by targeting at different levels." Oncotarget **3**(8).
- Brown, E. J., M. W. Albers, T. Bum Shin, K. Ichikawa, C. T. Keith, W. S. Lane and S. L. Schreiber (1994). "A mammalian protein targeted by G1-arresting rapamycin-receptor complex." Nature **369**(6483): 756-758.

Brunn, G. J., P. Fadden, T. A. J. Haystead and J. C. Lawrence (1997). "The Mammalian Target of Rapamycin Phosphorylates Sites Having a (Ser/Thr)-Pro Motif and Is Activated by Antibodies to a Region near Its COOH Terminus." Journal of Biological Chemistry **272**(51): 32547-32550.

Burnett, P. E., R. K. Barrow, N. A. Cohen, S. H. Snyder and D. M. Sabatini (1998). "RAFT1 phosphorylation of the translational regulators p70 S6 kinase and 4E-BP1." Proceedings of the National Academy of Sciences **95**(4): 1432-1437.

Byrd, L. G., A. H. McDonald, L. G. Gold and M. Potter (1991). "Specific pathogen-free BALB/cAn mice are refractory to plasmacytoma induction by pristane." The Journal of Immunology **147**(10): 3632-3637.

Cafferkey, R., P. R. Young, M. M. McLaughlin, D. J. Bergsma, Y. Koltin, G. M. Sathe, L. Faucette, W. K. Eng, R. K. Johnson and G. P. Livi (1993). "Dominant missense mutations in a novel yeast protein related to mammalian phosphatidylinositol 3-kinase and VPS34 abrogate rapamycin cytotoxicity." Molecular and Cellular Biology **13**(10): 6012-6023.

Cam, M., H. K. Bid, L. Xiao, G. P. Zambetti, P. J. Houghton and H. Cam (2014). "p53/TAp63 and AKT Regulate Mammalian Target of Rapamycin Complex 1 (mTORC1) Signaling through Two Independent Parallel Pathways in the Presence of DNA Damage." Journal of Biological Chemistry **289**(7): 4083-4094.

Carew, J. S., K. R. Kelly and S. T. Nawrocki (2011). "Mechanisms of mTOR inhibitor resistance in cancer therapy." Targeted Oncology **6**(1): 17-27.

Caron, E., S. Ghosh, Y. Matsuoka, D. Ashton-Beaucage, M. Therrien, S. Lemieux, C. Perreault, P. P. Roux and H. Kitano (2010). "A comprehensive map of the mTOR signaling network." Molecular Systems Biology **6**: 453-453.

Chan, S. M., A. P. Weng, R. Tibshirani, J. C. Aster and P. J. Utz (2007). "Notch signals positively regulate activity of the mTOR pathway in T-cell acute lymphoblastic leukemia." Blood **110**(1): 278-286.

Chen, J.-Q., M. R. Heldman, M. A. Herrmann, N. Kedei, W. Woo, P. M. Blumberg and P. K. Goldsmith (2013). "Absolute quantitation of endogenous proteins with precision and accuracy using a capillary Western system." Analytical Biochemistry **442**(1): 97-103.

Chen, J., X. F. Zheng, E. J. Brown and S. L. Schreiber (1995). "Identification of an 11-kDa FKBP12-rapamycin-binding domain within the 289-kDa FKBP12-rapamycin-associated protein and characterization of a critical serine residue." Proceedings of the National Academy of Sciences of the United States of America **92**(11): 4947-4951.

Chen, J. Q., M. R. Heldman, M. A. Herrmann, N. Kedei, W. Woo, P. M. Blumberg and P. K. Goldsmith (2013). "Absolute quantitation of endogenous proteins with precision and accuracy using a capillary Western system." Analytical Biochemistry **442**(1): 97-103.

Chen JQ, H. M., Herrmann MA, Kedei N, Woo W, Blumberg PM, Goldsmith PK (2013). "Absolute quantitation of endogenous proteins with precision and accuracy using a capillary Western system." Analytical Biochemistry **442**(1): 97-103.

Chilosi, M., C. Doglioni, Z. Yan, M. Lestani, F. Menestrina, C. Sorio, A. Benedetti, F. Vinante, G. Pizzolo and G. Inghirami (1998). "Differential expression of cyclin-dependent kinase 6 in cortical thymocytes and T-cell lymphoblastic lymphoma/leukemia." American Journal of Pathology **152**(1): 209-217.

Choi, Y. J. and L. Anders (2014). "Signaling through cyclin D-dependent kinases." Oncogene **33**(15): 1890-1903.

Chou, T.-C. a. M., N. (2005). "PC Software for quantization of synergism and antagonism and determination of IC50, ED50 and LD50. ." CompuSyn for Drug Combinations and for General Dose-Effect Analysis.

Chou, T. C. (2006). "Theoretical basis, experimental design, and computerized simulation of synergism and antagonism in drug combination studies." Pharmacology Reviews **58**(3): 621-681.

Chou, T. C. (2010). "Drug combination studies and their synergy quantification using the Chou-Talalay method." Cancer Research **70**(2): 440-446.

Dao, V., S. Pandeswara, Y. Liu, V. Hurez, S. Dodds, D. Callaway, A.-J. Liu, P. Hasty, Z. D. Sharp and T. J. Curiel (2015). "Prevention of carcinogen and inflammation-induced dermal cancer by oral rapamycin includes reducing genetic damage." Cancer Prevention Research.

Dean, J. L., C. Thangavel, A. K. McClendon, C. A. Reed and E. S. Knudsen (2010). "Therapeutic CDK4/6 inhibition in breast cancer: key mechanisms of response and failure." Oncogene **29**(28): 4018-4032.

Eng, C., S. Sehgal and C. Vezina (1984). "Activity of rapamycin (AY-22,989) against transplanted tumors." The Journal of Antibiotics **37**(10): 1231-1237.

Feldman, M. E., B. Apsel, A. Uotila, R. Loewith, Z. Knight, D. Ruggero and K. Shokat (2009). "Active-Site Inhibitors of mTOR Target Rapamycin-Resistant Outputs of mTORC1 and mTORC2." PLoS Biology **7**(2).

Fenech, M., M. Kirsch-Volders, A. T. Natarajan, J. Surralles, J. W. Crott, J. Parry, H. Norppa, D. A. Eastmond, J. D. Tucker and P. Thomas (2011). "Molecular mechanisms of micronucleus, nucleoplasmic bridge and nuclear bud formation in mammalian and human cells." Mutagenesis **26**(1): 125-132.

Feng, Z. (2010). "p53 Regulation of the IGF-1/AKT/mTOR Pathways and the Endosomal Compartment." Cold Spring Harbor Perspectives in Biology **2**(2): a001057.

Feng, Z., H. Zhang, A. J. Levine and S. Jin (2005). "The coordinate regulation of the p53 and mTOR pathways in cells." Proceedings of the National Academy of Sciences of the United States of America **102**(23): 8204-8209.

Forbes, S. A., N. Bindal, S. Bamford, C. Cole, C. Y. Kok, D. Beare, M. Jia, R. Shepherd, K. Leung, A. Menzies, J. W. Teague, P. J. Campbell, M. R. Stratton and P. A. Futreal (2011). "COSMIC: mining complete cancer genomes in the Catalogue of Somatic Mutations in Cancer." Nucleic Acids Research **39**(suppl 1): D945-D950.

Ford, D., D. F. Easton, D. T. Bishop, S. A. Narod and D. E. Goldgar (1994). "Risks of cancer in BRCA1-mutation carriers." The Lancet **343**(8899): 692-695.

Fry, D. W., P. J. Harvey, P. R. Keller, W. L. Elliott, M. Meade, E. Trachet, M. Albassam, X. Zheng, W. R. Leopold, N. K. Pryer and P. L. Toogood (2004). "Specific inhibition of cyclin-dependent kinase 4/6 by PD 0332991 and associated antitumor activity in human tumor xenografts." Molecular Cancer Therapeutics **3**(11): 1427-1438.

Gangloff, Y.-G., M. Mueller, S. G. Dann, P. Svoboda, M. Sticker, J.-F. Spetz, S. H. Um, E. J. Brown, S. Cereghini, G. Thomas and S. C. Kozma (2004). "Disruption of the Mouse mTOR Gene Leads to Early Postimplantation Lethality and Prohibits Embryonic Stem Cell Development." Molecular and Cellular Biology **24**(21): 9508-9516.

Garami, A., F. J. T. Zwartkuis, T. Nobukuni, M. Joaquin, M. Rocco, H. Stocker, S. C. Kozma, E. Hafen, J. L. Bos and G. Thomas (2003). "Insulin Activation of Rheb, a Mediator of mTOR/S6K/4E-BP Signaling, Is Inhibited by TSC1 and 2." Molecular Cell **11**(6): 1457-1466.

García-Morales, P., E. Hernando, E. Carrasco-García, M. P. Menéndez-Gutierrez, M. Saceda and I. Martínez-Lacaci (2006). "Cyclin D3 is down-regulated by rapamycin in HER-2-overexpressing breast cancer cells." Molecular Cancer Therapeutics **5**(9): 2172-2181.

Grabiner, B. C., V. Nardi, K. Birsoy, R. Possemato, K. Shen, S. Sinha, A. Jordan, A. H. Beck and D. M. Sabatini (2014). "A Diverse Array of Cancer-Associated MTOR Mutations Are Hyperactivating and Can Predict Rapamycin Sensitivity." Cancer Discovery **4**(5): 554-563.

Guertin, D. A. and D. M. Sabatini (2009). "The Pharmacology of mTOR Inhibition." Science Signaling **2**(67): pe24-pe24.

Guertin, D. A., D. M. Stevens, M. Saitoh, S. Kinkel, K. Crosby, J.-H. Sheen, D. J. Mullholland, M. A. Magnuson, H. Wu and D. M. Sabatini (2009). "The mTOR complex 2 is required for the development of prostate cancer induced by Pten loss in mice." Cancer Cell **15**(2): 148-159.

Guo, F., J. Li, S. Zhang, W. Du, S. Amarachintha, J. Sipple, J. Phelan, H. L. Grimes, Y. Zheng and Q. Pang (2014). "mTOR kinase inhibitor sensitizes T-cell lymphoblastic leukemia for chemotherapy-induced DNA damage via suppressing FANCD2 expression." Leukemia **28**(1): 203-206.

Gutierrez, A., T. Sanda, R. Grebliunaite, A. Carracedo, L. Salmena, Y. Ahn, S. Dahlberg, D. Neuberg, L. A. Moreau, S. S. Winter, R. Larson, J. Zhang, A. Protopopov, L. Chin, P. P. Pandolfi, L. B. Silverman, S. P. Hunger, S. E. Sallan and A. T. Look (2009). "High frequency of PTEN, PI3K, and AKT abnormalities in T-cell acute lymphoblastic leukemia." Blood **114**(3): 647-650.

Hall, M. N. (2008). "mTOR—What Does It Do?" Transplantation Proceedings **40**(10, Supplement): S5-S8.

Hardt, M., N. Chantaravisoot and F. Tamanoi (2011). "Activating mutations of TOR (target of rapamycin)." Genes to Cells **16**(2): 141-151.

Hardt, M., N. Chantaravisoot and F. Tamanoi (2011). "Activating mutations of TOR (target of rapamycin)." Genes to cells : devoted to molecular & cellular mechanisms **16**(2): 141-151.

- Haughian, J. M. and A. P. Bradford (2009). "Protein kinase C alpha (PKC α) regulates growth and invasion of endometrial cancer cells." Journal of Cellular Physiology **220**(1): 112-118.
- Hay, N. and N. Sonenberg (2004). "Upstream and downstream of mTOR." Genes & Development **18**(16): 1926-1945.
- Hilbret, D. M., M. Kopf, B. Mock, G. Kohler, and S. Rudikoff (1995). "Interleukin 6 is essential for in vivo development of B lineage neoplasms." The Journal of Experimental Medicine **182**: 243-248.
- Hildebrandt, M. A. T., H. Yang, M.-C. Hung, J. G. Izzo, M. Huang, J. Lin, J. A. Ajani and X. Wu (2009). "Genetic Variations in the PI3K/PTEN/AKT/mTOR Pathway Are Associated With Clinical Outcomes in Esophageal Cancer Patients Treated With Chemoradiotherapy." Journal of Clinical Oncology **27**(6): 857-871.
- Hoelzer, D. and N. Gökbüget (2009). "T-Cell Lymphoblastic Lymphoma and T-Cell Acute Lymphoblastic Leukemia: A Separate Entity?" Clinical Lymphoma and Myeloma **9, Supplement 3**(0): S214-S221.
- Hollander, M. C., G. M. Blumenthal and P. A. Dennis (2011). "PTEN loss in the continuum of common cancers, rare syndromes and mouse models." Nature Reviews Cancer **11**(4): 289-301.
- Hong, F., M. D. Larrea, C. Doughty, D. J. Kwiatkowski, R. Squillace and J. M. Slingerland (2008). "mTOR-Raptor Binds and Activates SGK1 to Regulate p27 Phosphorylation." Molecular Cell **30**(6): 701-711.
- Hoshii, T., A. Kasada, T. Hatakeyama, M. Ohtani, Y. Tadokoro, K. Naka, T. Ikenoue, T. Ikawa, H. Kawamoto, H. J. Fehling, K. Araki, K. Yamamura, S. Matsuda and A. Hirao (2014). "Loss of mTOR complex 1 induces developmental blockage in early T-lymphopoiesis and eradicates T-cell acute lymphoblastic leukemia cells." Proceedings of the National Academy of Science of United States of America **111**(10): 3805-3810.
- Hsieh, A. C., Y. Liu, M. P. Edlind, N. T. Ingolia, M. R. Janes, A. Sher, E. Y. Shi, C. R. Stumpf, C. Christensen, M. J. Bonham, S. Wang, P. Ren, M. Martin, K. Jessen, M. E. Feldman, J. S. Weissman, K. M. Shokat, C. Rommel and D. Ruggero (2012). "The translational landscape of mTOR signalling steers cancer initiation and metastasis." Nature **485**(7396): 55-61.
- Hu, M. G., A. Deshpande, N. Schlichting, E. A. Hinds, C. Mao, M. Dose, G. F. Hu, R. A. Van Etten, F. Gounari and P. W. Hinds (2011). "CDK6 kinase activity is required for thymocyte development." Blood **117**(23): 6120-6131.
- Huaiyu Mi, A. M. a. P. D. T. (2012). "PANTHER in 2013: modeling the evolution of gene function, and other gene attributes, in the context fo phylogenetic trees." Nucleic Acids Research.
- Hudson, C. C., M. Liu, G. G. Chiang, D. M. Otterness, D. C. Loomis, F. Kaper, A. J. Giaccia and R. T. Abraham (2002). "Regulation of Hypoxia-Inducible Factor 1 α Expression and Function by the Mammalian Target of Rapamycin." Molecular and Cellular Biology **22**(20): 7004-7014.

- Jacinto, E., R. Loewith, A. Schmidt, S. Lin, M. A. Ruegg, A. Hall and M. N. Hall (2004). "Mammalian TOR complex 2 controls the actin cytoskeleton and is rapamycin insensitive." Nature Cell Biology **6**(11): 1122-1128.
- Jackson, S. P. and J. Bartek (2009). "The DNA-damage response in human biology and disease." Nature **461**(7267): 1071-1078.
- Jewell, J. L., R. C. Russell and K. L. Guan (2013). "Amino acid signalling upstream of mTOR." Nature Reviews Molecular Cell Biology **14**(3): 133-139.
- Knapp, G. W. S., R.W.; Fuscoe, J.C. (2003). "Quantitation of aberrant interlocus T-cell receptor rearrangements in mouse thymocytes and the effect of the herbicide 2,4-dichlorophenoxyacetic acid." Environmental and Molecular Mutagenesis **42**(1): 37-43.
- Knutson, B. A. (2010). "Insights into the domain and repeat architecture of target of rapamycin." Journal of Structural Biology **170**(2): 354-363.
- Kominami, R. and O. Niwa (2006). "Radiation carcinogenesis in mouse thymic lymphomas." Cancer Science **97**(7): 575-581.
- Kroemer, G., G. Mariño and B. Levine (2010). "Autophagy and the integrated stress response." Molecular Cell **40**(2): 280-293.
- Lampasso, J. D., N. Marzec, J. Margarone and R. Dziak (2002). "Role of Protein Kinase C α in Primary Human Osteoblast Proliferation." Journal of Bone and Mineral Research **17**(11): 1968-1976.
- Laplante, M. and D. M. Sabatini (2009). "mTOR signaling at a glance." Journal of Cell Science **122**(20): 3589-3594.
- Laplante, M. and D. M. Sabatini (2012). "mTOR signaling in growth control and disease." Cell **149**(2): 274-293.
- Lempiainen, H. and T. D. Halazonetis (2009). "Emerging common themes in regulation of PIKKs and PI3Ks." EMBO Journal **28**(20): 3067-3073.
- Lichti, U., J. Anders and S. H. Yuspa (2008). "Isolation and short-term culture of primary keratinocytes, hair follicle populations and dermal cells from newborn mice and keratinocytes from adult mice for in vitro analysis and for grafting to immunodeficient mice." Nature Protocols **3**(5): 799-810.
- Lista, F., V. Bertness, C. Guidos, J. Danska and K. IR (1997). "The absolute number of trans-rearrangements between the TCRG and TCRB loci is predictive of lymphoma risk: a severe combined immune deficiency (SCID) murine model." Cancer Research **57**(19): 4408-4413.
- Loewith, R., E. Jacinto, S. Wullschleger, A. Lorberg, J. L. Crespo, D. Bonenfant, W. Oppliger, P. Jenoe and M. N. Hall (2002). "Two TOR Complexes, Only One of which Is Rapamycin Sensitive, Have Distinct Roles in Cell Growth Control." Molecular Cell **10**(3): 457-468.
- Ma, X. M. and J. Blenis (2009). "Molecular mechanisms of mTOR-mediated translational control." Nature Reviews Molecular Cell Biology **10**(5): 307-318.

- Malstrom, S., E. Tili, D. Kappes, J. D. Ceci and P. N. Tsihchlis (2001). "Tumor induction by an Lck-MyrAkt transgene is delayed by mechanisms controlling the size of the thymus." Proceedings of the National Academy of Science of United States of America **98**(26): 14967-14972.
- McClive, P. J. and A. H. Sinclair (2001). "Rapid DNA extraction and PCR-sexing of mouse embryos." Molecular Reproduction and Development **60**(2): 225-226.
- McIntire, K. R. and G. L. Princler (1969). "Prolonged adjuvant stimulation in germ-free BALB/c mice: development of plasma cell neoplasia." Immunology **17**(3): 481-487.
- Menon, S. and B. D. Manning (2009). "Common corruption of the mTOR signaling network in human tumors." Oncogene **27**(S2): S43-S51.
- Mock, B. A., J. Hartley, P. Le Tissier, J. S. Wax and M. Potter (1997). "The Plasmacytoma Resistance Gene, Pctr2, Delays the Onset of Tumorigenesis and Resides in the Telomeric Region of Chromosome 4." Blood **90**(10): 4092-4098.
- Mock, B. A., M. M. Krall and J. K. Dosik (1993). "Genetic mapping of tumor susceptibility genes involved in mouse plasmacytomagenesis." Proceedings of the National Academy of Sciences of the United States of America **90**(20): 9499-9503.
- Morse, H. C., III, Hartley, J. W. & Potter, M. (1980). Genetic considerations in plasmacytomas of BALB/c NZB and (BALB/c x NZB)F1 mice. Progress in Myeloma. Amsterdam, Elsevier: 263–279.
- Murphy, J. D., A. C. Spalding, Y. R. Somnay, S. Markwart, M. E. Ray and D. A. Hamstra (2009). "Inhibition of mTOR Radiosensitizes Soft Tissue Sarcoma and Tumor Vasculature." Clinical Cancer Research **15**(2): 589-596.
- Niedernhofer, L. J., A. S. Lalai and J. H. Hoeijmakers (2005). "Fanconi anemia (cross)linked to DNA repair." Cell **123**(7): 1191-1198.
- Okayasu, R., K. Suetomi, Y. Yu, A. Silver, J. S. Bedford, R. Cox and R. L. Ullrich (2000). "A Deficiency in DNA Repair and DNA-PKcs Expression in the Radiosensitive BALB/c Mouse." Cancer Research **60**(16): 4342-4345.
- Patnot, S., B. Colleoni, X. Bisteau and P. P. Roger (2014). "The CDK4/CDK6 inhibitor PD0332991 paradoxically stabilizes activated cyclin D3-CDK4/6 complexes." Cell Cycle **13**(18): 2879-2888.
- Perry, J. and N. Kleckner (2003). "The ATRs, ATMs, and TORs are giant HEAT repeat proteins." Cell **112**(2): 151-155.
- Peterson, T. R., M. Laplante, C. C. Thoreen, Y. Sancak, S. A. Kang, W. M. Kuehl, N. S. Gray and D. M. Sabatini (2009). "DEPTOR is an mTOR Inhibitor Whose Frequent Overexpression in Multiple Myeloma Cells Promotes their Survival." Cell **137**(5): 873-886.
- Ponnaiya, B., M. N. Cornforth and R. L. Ullrich (1997). "Radiation-Induced Chromosomal Instability in BALB/c and C57BL/6 Mice: The Difference Is as Clear as Black and White." Radiation Research **147**(2): 121-125.

Porstmann, T., C. R. Santos, B. Griffiths, M. Cully, M. Wu, S. Leever, J. R. Griffiths, Y. L. Chung and A. Schulze (2008). "SREBP activity is regulated by mTORC1 and contributes to Akt-dependent cell growth." Cell Metab **8**(3): 224-236.

Potter, M., K. K. Sanford, R. Parshad, R. E. Tarone, F. M. Price, B. Mock and K. Huppi (1988). "Genes on chromosomes 1 and 4 in the mouse are associated with repair of radiation-induced chromatin damage." Genomics **2**(3): 257-262.

Potter, M. and F. Wiener (1992). "Plasmacytomagenesis in mice: model of neoplastic development dependent upon chromosomal translocations." Carcinogenesis **13**(10): 1681-1697.

Potter, m. W., JS (1983). "Peritoneal plasmacytomagenesis in mice: comparison of different pristane dose regimens." Journal of the National Cancer Institute **71**(2): 391-395.

Pui, C. H., M. V. Relling and J. R. Downing (2004). "Acute lymphoblastic leukemia." New England Journal of Medicine **350**(15): 1535-1548.

Qi, C.-F., J. X. Zhou, C. H. Lee, Z. Naghashfar, S. Xiang, A. L. Kovalchuk, T. N. Fredrickson, J. W. Hartley, D. C. Roopenian, W. F. Davidson, S. Janz and H. C. Morse (2007). "Anaplastic, Plasmablastic, and Plasmacytic Plasmacytomas of Mice: Relationships to Human Plasma Cell Neoplasms and Late-Stage Differentiation of Normal B Cells." Cancer Research **67**(6): 2439-2447.

Rathmell, J. C., R. L. Elstrom, R. M. Cinalli and C. B. Thompson (2003). "Activated Akt promotes increased resting T cell size, CD28-independent T cell growth, and development of autoimmunity and lymphoma." Eur J Immunol **33**(8): 2223-2232.

Richter, J. D. and N. Sonenberg (2005). "Regulation of cap-dependent translation by eIF4E inhibitory proteins." Nature **433**(7025): 477-480.

Roberto Zoncu, A. E., and David M. Sabatini (2011). "mTOR: from growth signal integration to cancer, diabetes, and ageing." Nature Reviews Molecular Cell Biology **12**(1): 21-35.

Roderick, T. (1963). "The Response of Twenty-Seven Inbred Strains of Mice to Daily Doses of Whole-Body X-Irradiation." Radiation Research **20**: 631-639.

Ruscetti, M. and H. Wu (2013). PTEN in Prostate Cancer. Prostate Cancer. D. J. Tindall, Springer New York. **16**: 87-137.

Sabatini, D. M., H. Erdjument-Bromage, M. Lui, P. Tempst and S. H. Snyder (1994). "RAFT1: A mammalian protein that binds to FKBP12 in a rapamycin-dependent fashion and is homologous to yeast TORs." Cell **78**(1): 35-43.

Samuels, Y., Z. Wang, A. Bardelli, N. Silliman, J. Ptak, S. Szabo, H. Yan, A. Gazdar, S. M. Powell, G. J. Riggins, J. K. V. Willson, S. Markowitz, K. W. Kinzler, B. Vogelstein and V. E. Velculescu (2004). "High Frequency of Mutations of the PIK3CA Gene in Human Cancers." Science **304**(5670): 554.

Sarbassov, D. D., S. M. Ali, D. H. Kim, D. A. Guertin, R. R. Latek, H. Erdjument-Bromage, P. Tempst and D. M. Sabatini (2004). "Rictor, a novel binding partner of mTOR, defines a rapamycin-insensitive and raptor-independent pathway that regulates the cytoskeleton." Current Biology **14**(14): 1296-1302.

Sarbassov, D. D., S. M. Ali, S. Sengupta, J. H. Sheen, P. P. Hsu, A. F. Bagley, A. L. Markhard and D. M. Sabatini (2006). "Prolonged rapamycin treatment inhibits mTORC2 assembly and Akt/PKB." Molecular Cell **22**(2): 159-168.

Sato, T., A. Nakashima, L. Guo, K. Coffman and F. Tamanoi (2010). "Single amino-acid changes that confer constitutive activation of mTOR are discovered in human cancer." Oncogene **29**(18): 2746-2752.

Sawai, C. M., J. Freund, P. Oh, D. Ndiaye-Lobry, J. C. Bretz, A. Strikoudis, L. Genesca, T. Trimarchi, M. A. Kelliher, M. Clark, J. Soulier, S. Chen-Kiang and I. Aifantis (2012). "Therapeutic targeting of the cyclin D3:CDK4/6 complex in T cell leukemia." Cancer Cell **22**(4): 452-465.

Scaglione-Sewell, B., C. Abraham, M. Bissonnette, S. F. Skarosi, J. Hart, N. O. Davidson, R. K. Wali, B. H. Davis, M. Sitrin and T. A. Brasitus (1998). "Decreased PKC- α Expression Increases Cellular Proliferation, Decreases Differentiation, and Enhances the Transformed Phenotype of CaCo-2 Cells." Cancer Research **58**(5): 1074-1081.

Searle, J. S., K. L. Schollaert, B. J. Wilkins and Y. Sanchez (2004). "The DNA damage checkpoint and PKA pathways converge on APC substrates and Cdc20 to regulate mitotic progression." Nature Cell Biology **6**(2): 138-145.

Sekulić, A., C. C. Hudson, J. L. Homme, P. Yin, D. M. Otterness, L. M. Karnitz and R. T. Abraham (2000). "A Direct Linkage between the Phosphoinositide 3-Kinase-AKT Signaling Pathway and the Mammalian Target of Rapamycin in Mitogen-stimulated and Transformed Cells." Cancer Research **60**(13): 3504-3513.

Sengupta, S., T. R. Peterson and D. M. Sabatini (2010). "Regulation of the mTOR Complex 1 Pathway by Nutrients, Growth Factors, and Stress." Molecular Cell **40**(2): 310-322.

Shacter, E., R. L. Lopez and S. Pati (1991). "Inhibition of the myeloperoxidase-H₂O₂-Cl⁻ system of neutrophils by indomethacin and other non-steroidal anti-inflammatory drugs." Biochemical Pharmacology **41**(6-7): 975-984.

Shen, C., C. S. Lancaster, B. Shi, H. Guo, P. Thimmaiah and M.-A. Bjornsti (2007). "TOR Signaling Is a Determinant of Cell Survival in Response to DNA Damage." Molecular and Cellular Biology **27**(20): 7007-7017.

Shen, C., D. Oswald, D. Phelps, H. Cam, C. E. Pelloski, Q. Pang and P. J. Houghton (2013). "Regulation of FANCD2 by the mTOR Pathway Contributes to the Resistance of Cancer Cells to DNA Double-Strand Breaks." Cancer Research **73**(11): 3393-3401.

Shimada, K., I. Filipuzzi, M. Stahl, S. B. Helliwell, C. Studer, D. Hoepfner, A. Seeber, R. Loewith, N. R. Movva and S. M. Gasser (2013). "TORC2 signaling pathway guarantees genome stability in the face of DNA strand breaks." Molecular Cell **51**(6): 829-839.

- Simmons, J. K., J. Patel, A. Michalowski, S. Zhang, B.-R. Wei, P. Sullivan, B. Gamache, K. Felsenstein, W. M. Kuehl, R. M. Simpson, A. Zingone, O. Landgren and B. A. Mock (2014). "TORC1 and class I HDAC inhibitors synergize to suppress mature B cell neoplasms." Molecular Oncology **8**(2): 261-272.
- Slattery, M. L., J. S. Herrick, A. Lundgreen, F. A. Fitzpatrick, K. Curtin and R. K. Wolff (2010). "Genetic variation in a metabolic signaling pathway and colon and rectal cancer risk: mTOR, PTEN, STK11, RPKAA1, PRKAG2, TSC1, TSC2, PI3K and Akt1." Carcinogenesis **31**(9): 1604-1611.
- Stambolic, V., D. MacPherson, D. Sas, Y. Lin, B. Snow, Y. Jang, S. Benchimol and T. W. Mak "Regulation of PTEN Transcription by p53." Molecular Cell **8**(2): 317-325.
- Tamburini, J., C. Elie, V. Bardet, N. Chapuis, S. Park, P. Broët, P. Cornillet-Lefebvre, B. Lioure, V. Ugo, O. Blanchet, N. Ifrah, F. Witz, F. Dreyfus, P. Mayeux, C. Lacombe and D. Bouscary (2007). "Constitutive phosphoinositide 3-kinase/Akt activation represents a favorable prognostic factor in de novo acute myelogenous leukemia patients." Blood **110**(3): 1025-1028.
- Tamburini, J., A. S. Green, V. Bardet, N. Chapuis, S. Park, L. Willems, M. Uzunov, N. Ifrah, F. Dreyfus, C. Lacombe, P. Mayeux and D. Bouscary (2009). "Protein synthesis is resistant to rapamycin and constitutes a promising therapeutic target in acute myeloid leukemia." Blood **114**(8): 1618-1627.
- Tan, Y., R. A. Timakhov, M. Rao, D. A. Altomare, J. Xu, Z. Liu, Q. Gao, S. C. Jhanwar, A. Di Cristofano, D. L. Wiest, J. E. Knepper and J. R. Testa (2008). "A Novel Recurrent Chromosomal Inversion Implicates the Homeobox Gene Dlx5 in T-Cell Lymphomas from Lck-Akt2 Transgenic Mice." Cancer Research **68**(5): 1296-1302.
- Tchevkina, E. and A. Komelkov (2012). Protein Phosphorylation as a Key Mechanism of mTORC1/2 Signaling Pathways. Protein Phosphorylation in Human Health. C. Huang, InTech.
- Team, R. D. C. (2011). "A Language and Environment for Statistical Computing." Vienna, Austria : the R Foundation for Statistical Computing.
- Thoreen, C. C., S. A. Kang, J. W. Chang, Q. Liu, J. Zhang, Y. Gao, L. J. Reichling, T. Sim, D. M. Sabatini and N. S. Gray (2009). "An ATP-competitive Mammalian Target of Rapamycin Inhibitor Reveals Rapamycin-resistant Functions of mTORC1." The Journal of Biological Chemistry **284**(12): 8023-8032.
- Timakhov, R. A., Y. Tan, M. Rao, Z. Liu, D. A. Altomare, J. Pei, D. L. Wiest, O. O. Favorova, J. E. Knepper and J. R. Testa (2009). "Recurrent chromosomal rearrangements implicate oncogenes contributing to T-cell lymphomagenesis in Lck-MyrAkt2 transgenic mice." Genes Chromosomes Cancer **48**(9): 786-794.
- Truett, G. (2000). "Preparation of PCR Quality Mouse Genomic DNA with Hot Sodium Hydroxide and Tris (HotSHOT)." BioTechniques **29**: 52-54.
- Vender, J., K. Dhandapani, N. Singh and S. Sukumari-Ramesh (2011). "mTOR inhibition reduces cellular proliferation and sensitizes pituitary adenoma cells to ionizing radiation." Surgical Neurology International **2**:22

Vezina, C., A. Kudelski and S. Sehgal (1975). "Rapamycin (AY-22,989), a new antifungal antibiotic. 1. Taxonomy of the producing streptomycete and isolation of the active principle." The Journal of Antibiotics **28**(10): 721-726.

Vora, S. R., D. Juric, N. Kim, M. Mino-Kenudson, T. Huynh, C. Costa, E. L. Lockerman, S. F. Pollack, M. Liu, X. Li, J. Lehar, M. Wiesmann, M. Wartmann, Y. Chen, Z. A. Cao, M. Pinzon-Ortiz, S. Kim, R. Schlegel, A. Huang and J. A. Engelman (2014). "CDK 4/6 inhibitors sensitize PIK3CA mutant breast cancer to PI3K inhibitors." Cancer Cell **26**(1): 136-149.

Wan, X., B. Harkavy, N. Shen, P. Grohar and L. J. Helman (2006). "Rapamycin induces feedback activation of Akt signaling through an IGF-1R-dependent mechanism." Oncogene **26**(13): 1932-1940.

Withers, D. J., D. M. Ouwens, B. T. Nave, G. C. M. van der Zon, C. M. Alarcon, M. E. Cardenas, J. Heitman, J. A. Maassen and P. R. Shepherd (1997). "Expression, Enzyme Activity, and Subcellular Localization of Mammalian Target of Rapamycin in Insulin-Responsive Cells." Biochemical and Biophysical Research Communications **241**(3): 704-709.

Wu, J. J., J. Liu, E. B. Chen, J. J. Wang, L. Cao, N. Narayan, M. M. Fergusson, Rovira, II, M. Allen, D. A. Springer, C. U. Lago, S. Zhang, W. DuBois, T. Ward, R. deCabo, O. GavriloVA, B. Mock and T. Finkel (2013). "Increased mammalian lifespan and a segmental and tissue-specific slowing of aging after genetic reduction of mTOR expression." Cell Reports **4**(5): 913-920.

Xu, Q., J. E. Thompson and M. Carroll (2005). "mTOR regulates cell survival after etoposide treatment in primary AML cells." Blood **106**(13): 4261-4268.

Yamada, Y., Y. Hatta, K. Murata, K. Sugawara, S. Ikeda, M. Mine, T. Maeda, Y. Hirakata, S. Kamihira, K. Tsukasaki, S. Ogawa, H. Hirai, H. P. Koeffler and M. Tomonaga (1997). "Deletions of p15 and/or p16 genes as a poor-prognosis factor in adult T-cell leukemia." Journal of Clinical Oncology **15**(5): 1778-1785.

Yu, Y., R. Okayasu, M. M. Weil, A. Silver, M. McCarthy, R. Zabriskie, S. Long, R. Cox and R. L. Ullrich (2001). "Elevated Breast Cancer Risk in Irradiated BALB/c Mice Associates with Unique Functional Polymorphism of the Prkdc (DNA-dependent Protein Kinase Catalytic Subunit) Gene." Cancer Research **61**(5): 1820-1824.

Zhang, K., D. Kagan, W. DuBois, R. Robinson, V. Bliskovsky, W. C. Vass, S. Zhang and B. A. Mock (2009). "Mndal, a new interferon-inducible family member, is highly polymorphic, suppresses cell growth, and may modify plasmacytoma susceptibility." Blood **114**(14): 2952-2960.

Zhang, S., W. DuBois, E. S. Ramsay, V. Bliskovski, H. C. Morse, L. Taddesse-Heath, W. C. Vass, R. A. DePinho and B. A. Mock (2001). "Efficiency Alleles of the Pctr1 Modifier Locus for Plasmacytoma Susceptibility." Molecular and Cellular Biology **21**(1): 310-318.

Zhang, S., M. Pruitt, D. Tran, W. Du Bois, K. Zhang, R. Patel, S. Hoover, R. M. Simpson, J. Simmons, J. Gary, C. M. Snapper, R. Casellas and B. A. Mock (2013). "B Cell-Specific Deficiencies in mTOR Limit Humoral Immune Responses." The Journal of Immunology **191**(4): 1692-1703.

Zhang, S., X. Qian, C. Redman, V. Bliskovski, E. S. Ramsay, D. R. Lowy and B. A. Mock (2003). "p16INK4a gene promoter variation and differential binding of a repressor, the ras-responsive zinc-finger transcription factor, RREB." Oncogene **22**(15): 2285-2295.

Zhang, S., E. S. Ramsay and B. A. Mock (1998). "Cdkn2a, the cyclin-dependent kinase inhibitor encoding p16(INK4a) and p19(ARF), is a candidate for the plasmacytoma susceptibility locus, Pctr1." Proceedings of the National Academy of Sciences of the United States of America **95**(5): 2429-2434.

Zhang, S., J. A. Readinger, W. DuBois, M. Janka-Junttila, R. Robinson, M. Pruitt, V. Bliskovsky, J. Z. Wu, K. Sakakibara, J. Patel, C. A. Parent, L. Tessarollo, P. L. Schwartzberg and B. A. Mock (2011). "Constitutive reductions in mTOR alter cell size, immune cell development, and antibody production." Blood **117**(4): 1228-1238.

Zhao, L., C. Zhou, J. Zhang, F. Gao, B. Li, Y. Chuai, C. Liu and J. Cai (2011). "Hydrogen Protects Mice from Radiation Induced Thymic Lymphoma in BALB/c Mice." International Journal of Biological Sciences **7**(3): 297-300.